Defining Roles of Metabolic Reprogramming in Pancreatic Tumorigenesis and Tumor Maintenance

by

Barbara S. Nelson

A dissertation submitted in partial fulfillment
of the requirements for the degree of
Doctor of Philosophy
(Cancer Biology)
in the University of Michigan
2020

Doctoral Committee:

Assistant Professor Costas A. Lyssiotis, Chair
Professor Howard Crawford
Professor Eric Fearon
Assistant Professor Sriram Venneti

Barbara S. Nelson
barbnels@umich.edu
ORCID iD:
0000-0001-9316-4482

DEDICATION

To my parents, for all the support, encouragement, and love you have selflessly given my entire life.

To my husband, for being by my side throughout this crazy journey.

ACKNOWLEDGEMENTS

To my mentors, Costas Lyssiotis and Howard Crawford, thank you for your unwavering support. I could not wish for better mentors to guide me through these past five years. Thank you for creating a supportive, engaging, and enjoyable work environment. Thank you for your patience and understanding through stressful moments. I am a better scientist because of you.

To my thesis committee members Eric Fearon and Sriram Venneti, thank you for your continued guidance and support. I truly value the help and advice you provided towards my research and career.

To the current and past members of the Lyssiotis lab, thank you for your assistance, advice, mentorship, and friendship. To Chris Halbrook, thank you for being my go-to with anything I ever needed in lab.

To the all the members of PanTERA, thank you for creating a collaborative and supportive environment—it is unlike any other I have experienced.

To David Lombard, thank you for providing opportunities I likely would not have experienced without your support and assistance in my career development

To the Cancer Biology Program faculty, students, and staff, thank you for all your help throughout these years. I am privileged to have learned from all of you.

To my family, this would not have been possible without you. I am forever grateful for your love and support.

Finally, to my husband, thank you all you have done for me. Thank you for providing love and laughter these past 10 years. Thank you for keeping me grounded during my most stressful times.

Table of Contents

LIST OF FIGURES

LIST OF TABLES

ABSTRACT

Pancreatic cancer is the third leading cause of cancer-related deaths in the United States. Nearly all pancreatic tumors harbor mutations in oncogenic KRAS. Unfortunately, KRAS is difficult to target therapeutically, despite decades of efforts. As such, KRAS-dependent pathways remain promising targets for the development of new therapeutics. Pancreatic cancer extensively reprograms cellular metabolism to support uncontrolled growth and proliferation. Mutations in oncogenic *KRAS* drive metabolic rewiring that PDA cells are dependent on to supply biosynthetic precursors and energy. Understanding the metabolic dependencies of tumorigenesis and tumor maintenance could reveal targetable vulnerabilities for disease detection and/or treatment.

Acinar cells can give rise to pancreatic tumors through acinar-to-ductal metaplasia (ADM), and inhibiting pathways that maintain acinar homeostasis can accelerate tumorigenesis. During ADM, acinar cells transdifferentiate to duct-like cells, a process driven by oncogenic KRAS, and one that we hypothesized was mediated by metabolic rewiring. Transcriptomic analysis revealed global enhancement of metabolic programs in acinar cells undergoing ADM. We previously demonstrated that pancreatic cancer cells rewire glucose and glutamine metabolism to support growth and survival. Using *in vitro* models of ADM, we found that glutamine availability is not required for ADM. In contrast, glucose availability and intact oxidative phosphorylation are required for ADM. A more detailed analysis of the pathways downstream of glucose metabolism revealed that disrupting the oxidative pentose phosphate pathway accelerates ADM *in vitro* and tumorigenesis *in vivo*, likely due to heightened oxidative stress. Changes in redox balance can attenuate or accelerate ADM *in vitro* and *in vivo*.

Redox homeostasis is also tightly regulated in pancreatic cancer cells by rewiring glutamine metabolism through a glutamate oxaloacetate transaminase 1 (GOT1)-dependent pathway. GOT1 inhibition disrupts redox homeostasis in pancreatic cancer cells. These insights were leveraged in PDA, where we demonstrate that radiotherapy

potently enhanced the effect of GOT1 inhibition on tumor growth. Understanding the metabolic pathways that contribute to pancreatic tumorigenesis and tumor maintenance, such as redox homeostasis, could provide biomarkers for diagnosis of early disease or development of better therapeutics for treating pancreatic cancer.

CHAPTER 1

Introduction: Pancreatic Cancer, Tumorigenesis, and Metabolic Adaptations

Pancreatic Ductal Adenocarcinoma

The pancreas—with both exocrine and endocrine functions—regulates digestion and glucose homeostasis[1,2]. Making up the exocrine compartment are acinar cells that produce and secrete digestive enzymes, ductal cells that transport the digestive enzymes to the gastrointestinal tract, and the centro-acinar cells that lie between acinar and ductal cells. The endocrine compartment is comprised of Islets of Langerhans that consists of hormone-secreting cells. The vast majority of pancreatic neoplasias arise from the exocrine compartment[1].

Pancreatic ductal adenocarcinoma (PDA), the most common form of pancreatic cancer, accounts for approximately 90% of all pancreatic neoplasms[1,3]. While PDA is the eleventh most commonly diagnosed cancer in the United states, it is the third leading cause of cancer-related deaths and projected to be the second within the next decade[4,5]. PDA has the lowest overall five-year survival at 10%; median survival is approximately nine months for patients diagnosed with late stage disease[4,6]. The extremely poor prognosis of PDA is attributed to no or nonspecific symptoms, difficulty imaging early stage tumors, and lack of diagnostic testing[1]. Diagnosis typically occurs at advanced stages—PDA is an aggressive tumor that metastasizes early[7]—making most patients ineligible for surgical resections. The standard of care for advanced and/or metastasized tumors is chemotherapy occasionally with radiotherapy; unfortunately, PDA is remarkably resistant to therapeutic options. Risk factors for PDA include age, chronic pancreatitis, tobacco smoking, heavy alcohol consumption, and obesity[1,3]. Long-term diabetes mellitus is a considerable risk factor, but it can also be a manifestation of PDA. Genetic syndromes and a familial history of pancreatic cancer account for 10% of PDA patients. Overall, risk factors are associated with approximately 25-35% of PDA cases[1].

Cell of Origin

Development of PDA is hypothesized to be a multistep process beginning with acinar-to-ductal metaplasia (ADM) progressing into pancreatic intraepithelial neoplasia (PanIN)—from low-grade dysplasia (PanIN1-2) to high-grade/carcinoma in situ (PanIN3)—then transforming into invasive carcinoma (**Fig. 1.1**)[2,8]. Mucinous cystic neoplasm (MCN) and intraductal papillary mucinous neoplasm (IPMN) are other PDA precursor lesions, however PanINs are the most common and well-studied. An oncogenic *KRAS* mutation, most commonly *KRAS*^{G12D}, is believed to be the initiating genetic alteration; over 90% of pancreatic cancers harbor *KRAS* mutations[9]. Additional molecular alterations are needed for PanIN progression and carcinoma[8]. Early genetic events include *KRAS* mutations and loss of tumor suppressor *CDKN2A* and late genetic events include mutation or loss of tumor suppressors *TP53* and *SMAD4/DPC4* (**Fig. 1.1**)[8].

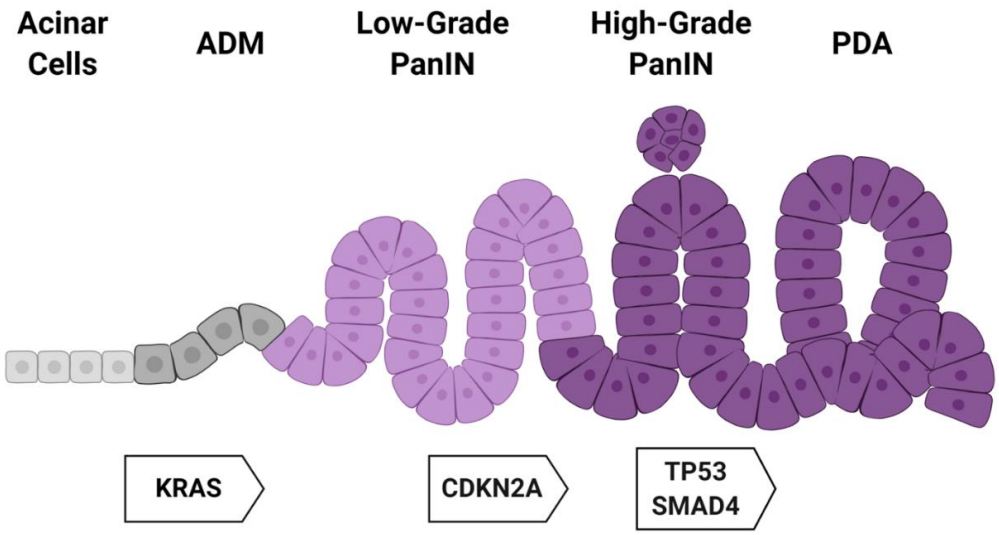

Figure 1.1 Development and progression of pancreatic cancer. Expression of oncogenic *KRAS* mutations in acinar cells initiates acinar-to-ductal metaplasia (ADM) and progression to low-grade pancreatic intraepithelial neoplasia (PanIN). Loss of tumor suppressor *CDKN2A* can induce progression to high-grade PanIN. Subsequent loss or mutation of tumor suppressors *TP53* or *SMAD4* promote progression to invasive pancreatic ductal adenocarcinoma (PDA). Created with BioRender.com

Genetically engineered mouse models (GEMM) of PDA have been instrumental in understanding the progression of the disease[10]. Generation of a *Kras*$^{LSL\text{-}G12D/+}$ mouse enabled tissue-specific, endogenous expression of mutant *Kras*[11,12]. Pancreas-specific expression of *Kras*^{G12D} is achieved by driving expression of Cre recombinase from pancreatic progenitor transcription factor promoters *Pdx1* (transgenic)[13,14] or *Ptf1a/p48*

(knock-in)[15]. *Kras*$^{LSL\text{-}G12D/+}$*; Pdx1-Cre* and *Kras*$^{LSL\text{-}G12D/+}$*; Ptf1a/p48*$^{Cre/+}$ mice, commonly referred to as KC, recapitulate the progression of PanINs seen in human disease[13]. Mutant KRAS is critical for driving PDA development and tumor maintenance, however it is not sufficient for development of invasive and metastatic cancer[13,16,17]. Crossing additional genetic alterations commonly found in human PDA into the KC model increases the penetrance and development of invasive and metastatic PDA: loss of *Cdkn2a*, mutation or heterozygous deletion of *Tp53* (referred to as the KPC model), or homozygous deletion of *Tgfbr2* (dysregulates SMAD signaling)[18-22]. Interestingly mice with loss of *SMAD4* in the context of *Kras*^{G12D} develop IPMN or MCN lesions[23,24].

Determining the PDA cell of origin with mouse models has been challenging[25]. The KC and KPC models, and others based off of them, reflect PanIN development and invasive/metastatic PDA seen in human disease[13,18]. However, because *Pdx1* and *Ptf1a* are expressed in pancreatic progenitor cells *in utero*, recombination of oncogenic *Kras* occurs in all pancreatic epithelial cells (acini, ducts, and islets). Inducible expression of Cre recombinase allows expression of mutant *Kras* in specific cell compartments in adult mice. Expression of *Kras*^{G12D} in adult pancreatic ductal cells (via *CK19*$^{CreERT/+}$) gives rise to occasional mucinous metaplasia resembling low-grade PanINs, indicating ductal cells have the potential to give rise to neoplasia[26]. Since PDA displays ductal morphology, ductal cells are an obvious cell of origin. However, adult acinar cells are highly plastic and can dedifferentiate/transdifferentiate into pancreatic progenitors through ADM and express ductal markers[27]. Analysis of KC pancreata show “biphenotypic” cells—expression of both acinar and ductal markers—are present in ADM and PanIN lesions, suggesting acinar cells transdifferentiate and give rise to metaplasia[28,29]. In addition, lineage-tracing and acinar cell specific recombination of *Kras*$^{LSL\text{-}G12D/+}$ in adult cells (via *Ela-CreERT2* or *Mist1*$^{CreERT2/+}$) show acinar cells are capable of transdifferentiating into hyperplastic ductal cells and giving rise to PanIN lesions[30-33].

A study that directly compared recombination of *Kras*$^{LSL\text{-}G12D/+}$ in adult acinar or ductal cells (*Ptf1a*$^{CreER/+}$ or *Sox9-CreER*, respectively) found acinar cells have a 112-fold greater propensity to form PanINs than ductal cells[34]. Morphologically normal *Kras*$^{LSL\text{-}G12D/+}$; *Ptf1a*$^{CreERT/+}$ acinar cells express Sox9 indicating activation of a duct-like state prior to

transdifferentiating[34]. PDA tumors arise from both cell types in the context of p53 loss (*Tp53*$^{f/f}$)[35]. However, ductal cells have more rapid tumorigenesis and progression to invasive PDA. While acinar cells give rise to low-grade PanINs that accumulate and progress to high-grade lesions as mice age, ductal cells develop only high-grade lesions that readily progress to invasive PDA. Another comparative study had similar findings with *Kras*$^{LSL\text{-}G12D}$ and *Tp53*$^{R172H/+}$ expression in adult acinar cells (*Mist1-CreERT2*) or ductal cells (*Hnf1b-CreERT2*)[36]. Again, acinar cells readily form PanINs and PDA while ductal cells are comparatively refractory to transformation. However, biallelic expression of mutant p53 (*Tp53*$^{R172H/R172H}$) in ductal cells rapidly forms PDA with virtually no evidence of PanIN lesions. Although *Kras*^{G12D} expressing acinar cells have a higher tendency to develop PanINs that progress histologically, duct cells with *Tp53* alterations more readily develop PDA without progression through early PanIN lesions. These studies provide evidence that the cell of origin can be both acinar and ductal cells, but acinar cell transformation progresses through PanIN stages seen in human PDA.

Modeling Acinar-to-Ductal Metaplasia

ADM is a normal response to pancreatic injury or inflammation[27,37]. Acinar cells dedifferentiate/transdifferentiate to proliferative ductal progenitors to regenerate depleted acinar tissue. ADM is observed in patients with chronic and acute pancreatitis, an inflammatory disease characterized by acinar cell atrophy and fibrosis[38-40]. Since chronic pancreatitis is a predisposing factor for PDA, this lends credence to PDA developing from ADM[27]. In wild-type cells, upon tissue repair, ductal progenitors redifferentiate to acinar cells where normal acinar function is resumed[41]. However, in the presence of oncogenic KRAS, ADM is irreversible and metaplasia can transition to PanIN lesions which can progress to PDA (**Fig. 1.2**).

ADM can be modeled and observed *in vivo* by inducing acute or chronic pancreatitis in mice[42,43]. A common method for inducing pancreatitis is repeated injections of cerulein, a cholecystokinin ortholog that promotes excessive acinar enzyme production and premature activation at supraphysiologic concentrations[44]. Modeling ADM *in vitro* is

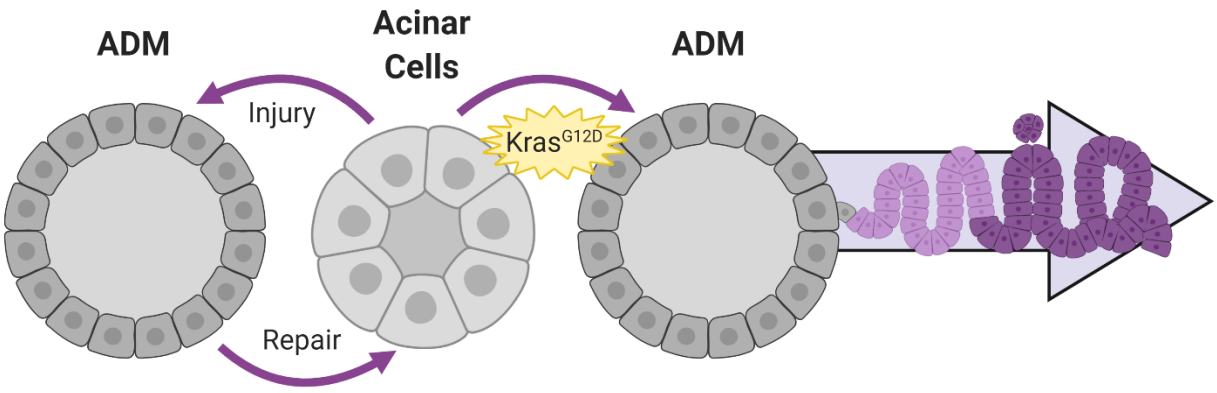

Figure 1.2 Differences in ADM in response to injury or mutant Kras expression. Acinar cells transdifferentiate into proliferative ductal progenitor cells (acinar-to-ductal metaplasia [ADM]) in response to pancreatic injury or inflammation. Upon tissue repair, ductal progenitors redifferentiate to acinar cells, restoring normal acinar function. In the presence of oncogenic KRAS, ADM is irreversible and metaplasia can transition to PanIN lesions which can progress to PDA. Created with BioRender.com

achieved by culturing primary acinar cell explants in suspension or a matrix. Lineage tracing of primary mouse and human cells under these conditions demonstrate acinar cells can transdifferentiate to form ductal structures, repress acinar genes, and express ductal genes[45-48]. To initiate ADM *in vitro*, wild-type acinar explants can be stimulated by TGFα, cerulein, and the milieu of growth factors in Matrigel[42,45,49]; *Kras* mutant acinar cells spontaneously transdifferentiate[49,50].

Constitutively activate Kras^{G12D} stimulates mitogenic signaling to drive persistent growth and proliferation[51]. Acquisition of oncogenic Kras, along with upregulation of EGFR and wild-type KRAS signaling and chronic inflammation, drives ADM and tumorigenesis in mouse models.[43,45,49,50,52-55]. Signaling pathways downstream of EGFR and KRAS required for mediating ADM are MAPK/ERK[42,49,56,57], PI3K[58,59], and RAC1 (ref:[60]). Understanding the pathways that drive ADM are important because 1) it is the first step to initiate tumorigenesis, 2) blocking ADM *in vitro* can translate to impeding ADM *in vivo* and preventing tissue transformation[49], and 3) early lesions can be reprogramed back to normal tissue by targeting ADM dependencies[57].

Metabolic Reprogramming in Cancer

Reprogramming metabolic pathways to support aberrant growth, proliferation, and survival is a hallmark of cancer cells[61]. The metabolic requirements of proliferating cells, including cancer cells, are vastly different than those of quiescent, differentiated cells[62].

While the need for ATP generation are relatively the same, cancer cells require a continuous supply of building blocks to generate macromolecules for growth and proliferation. Nutrients are used by cells for generation of biosynthetic precursors and the energy needed to make macromolecules. Glucose, a major fuel source, is broken down to pyruvate via glycolysis and, in normal cells, pyruvate fuels mitochondrial metabolism to generate ATP. When oxygen levels are insufficient to maintain oxidative phosphorylation, fermentation metabolizes pyruvate to lactate. Cancer cells, driven by oncogenes, convert glucose to lactate even in the presence of sufficient oxygen, a process known as aerobic glycolysis or the Warburg Effect[63]. Aerobic glycolysis allows cancer cells to divert glucose carbon into anabolic pathways—such as the pentose phosphate pathway (PPP), hexosamine biosynthetic pathway (HBP), and serine/glycine one-carbon metabolism—to produce precursors of ribose, lipids, and amino acids rather than supplying oxidative phosphorylation[64]. The tricarboxylic acid (TCA) cycle and oxidative phosphorylation (collectively, mitochondrial metabolism) is maintained by anaplerosis. Glutamine is the most abundant amino acid in circulation and is a primary anaplerotic substrate that replenishes the TCA cycle, a major biosynthetic hub[64]. Glutamine metabolism generates biosynthetic precursors used in protein, lipid, and nucleotide synthesis, energy production, and antioxidant defense. To meet the increased demand for nutrients to generate biosynthetic precursors and energy, cancer cells rewire nutrient acquisition pathways[64]. Metabolic reprogramming provides cancer cells with increased nutrient availability and promotes anabolic metabolism necessary for continuous growth.

Pancreatic Cancer Metabolism

Pancreatic tumors characteristically have a low percentage of neoplastic cells, with the bulk of the tumor consisting of fibroblasts and immune cells[65]. Activated fibroblasts deposit large amounts of extracellular matrix proteins that contribute to immense interstitial pressures[66]. This extreme pressure collapses vasculature, impairing perfusion and limiting oxygen (hypoxia) and nutrient availability[67-69]. PDA reprograms cellular metabolism through oncogenic KRAS to adapt to this harsh microenvironment (**Fig. 1.3**).

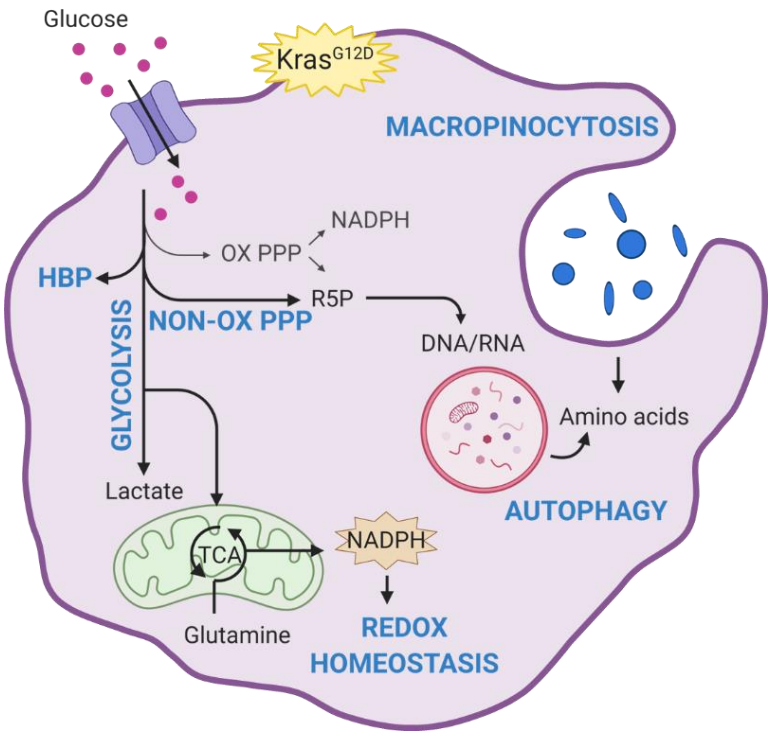

Figure 1.3 Pancreatic cancer rewires cell autonomous metabolism to support growth. Mutant KRAS increases glucose uptake and channels glycolytic intermediates into the hexosamine biosynthetic pathway (HBP) and the non-oxidative branch of the pentose phosphate pathway (non-ox PPP) to generate ribose-5-phosphate (R5P), a precursor molecule for DNA and RNA synthesis. $Kras^{G12D}$ reprograms glutamine metabolism to generate NADPH to maintain redox homeostasis. Unlike normal cells, PDA cells do not utilize the oxidative branch of the PPP (ox PPP) for NADPH generation. PDA cells activate macropinocytosis and autophagy for acquisition of amino acids. Created with BioRender.com

Since glucose is in high demand to support continuous growth, PDA cells upregulate expression of glucose transporter GLUT1 and hexokinase—mediated by oncogenic KRAS—to increase uptake and intercellular retention of glucose[16,69]. Mutant KRAS and hypoxia increase glycolytic gene expression to promote aerobic glycolysis and anabolic metabolism. Driven by mutant KRAS, glycolytic intermediates are shuttled into the non-oxidative branch of the PPP to generate nucleotide precursors and the HBP for protein glycosylation[16].

Glutamine plays an important role supporting redox balance in pancreatic cancer. Glutamine-derived glutamate is utilized for glutathione (GSH) generation[70]. Glutamine metabolism is also rewired in PDA to supply reducing equivalents in the form of NADPH[71]. Normal cells typically generate NADPH from the oxidative branch of the PPP[72]. PDA cells do not proportionally upregulate oxidative PPP to generate the quantity of NADPH

needed for redox homeostasis or fatty acid synthesis[16,63]. Demand for NADPH is met through oncogenic KRAS-mediated reprogramming of the malate-aspartate shuttle to generate NADPH via ME1 and maintain redox homeostais[71,73]. Disruption of redox balance by targeting this pathway represents a metabolic vulnerability in pancreatic cancer (**see Chapter 3**)[73].

PDA cells activate and depend on nutrient acquisition pathways, such as recycling and scavenging, to supplement cellular metabolism in a nutrient deprived micro-environment[67,69,74]. Macroautophagy, generally known as autophagy, is elevated in PDA cells to increase the availability of biomolecule nutrients generated from the lysosomal degradation of damaged or excessive cellular components[75]. Oncogenic KRAS induces macropinocytosis to engulf extracellular fluid and solutes, which increases intercellular nutrient concentrations following lysosomal degradation. In PDA, autophagy and macropinocytosis are a source of amino acids to fuel the TCA cycle and oxidative phosphorylation[67,74-76].

While metabolic rewiring and dependencies in PDA cells are extensively studied[69], much less is known about metabolic pathways that govern oncogenic KRAS-induced ADM. The following sections discuss metabolic pathways involved in acinar cell homeostasis and how manipulation of these pathways can regulate ADM (**Fig. 1.4**). These studies either provide context for my findings in metabolic regulation of ADM or provide hypotheses for future investigation (**see Chapters 2 and 5**).

Acetyl-CoA Metabolism

Acetyl-CoA is a central metabolite used as a key substrate for anabolic metabolism and the regulation of protein function[77]. Specifically, acetyl-CoA is involved in bioenergetic reactions, biosynthetic pathways, including fatty-acid and cholesterol synthesis, and serves as the acetyl donor for lysine acetylation[78]. Acetyl-CoA concentrations respond to different stimuli such as nutrient availability, oxygen availability, and PI3K-AKT signaling[79,80]. Two major enzymes produce acetyl-CoA in the cytosol and nucleus: ACLY from mitochondrial-derived citrate and ACSS2 from acetate[77]. Pancreatic cancer increases production of acetyl-CoA through AKT–ACLY signaling to activate gene

transcription via histone acetylation[79]. In human PDA, elevated expression of *ACLY* and *ACSS2* and high stroma content contributes to increased histone acetylation[81,82].

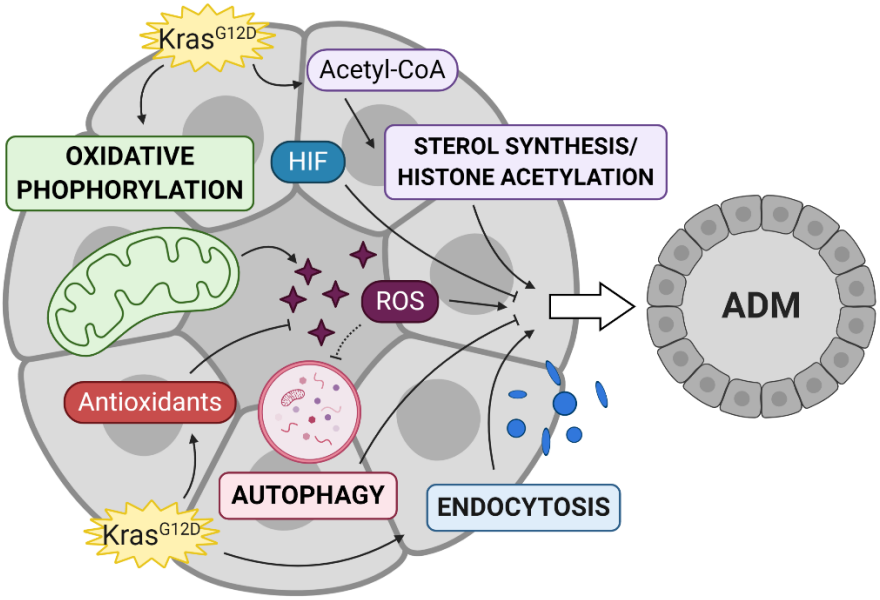

Figure 1.4 Metabolic regulation of ADM. Mutant KRAS increases acetyl-CoA generation for utilization in sterol synthesis and histone acetylation to drive ADM. Kras^{G12D} promotes the generation of oxidative phosphorylation-derived reactive oxygen species (ROS) necessary for ADM. Antioxidant pathways are activated by oncogenic KRAS and increased oxidative stress to maintain ROS at pro-tumorigenic levels and below those that induce senescence or cell death. Autophagy maintains acinar cell homeostasis. Inhibition of autophagic flux, possibly mediated by dysfunctional mitochondria, is necessary for tumorigenesis. Mutant KRAS-driven induction of endocytosis promotes ADM. Loss of HIF transcription factors promotes ADM. Created with BioRender.com

AKT–ACLY signaling drives pancreatic ADM and tumorigenesis in KC mice (**see Table 1.1**) by increasing levels of citrate-derived acetyl-CoA[81,83]. *Kras^{G12D}*-expressing acinar explants use acetyl-CoA to generate cholesterol through the mevalonate pathway and to promote expression of ductal genes through histone acetylation. Mutant KRAS reprograms metabolism to increase the availability of acetyl-CoA needed during ADM. Isotope-tracing of glucose, palmitate, and leucine revealed leucine is the major carbon source of acetyl-CoA in wild-type and KC acinar cells[81], consistent with high metabolism of branched-chain amino acids in mouse pancreas[84]. To meet the demand for acetyl-CoA during ADM, oncogenic Kras enhances acetyl-CoA generation from glucose and palmitate. *Acly* ablation in KC pancreas (**see Table 1.1**) impedes tumorigenesis and effectively prevents formation of high-grade PanINs[81]. Deletion of *Acly* decreases tumor burden and significantly extends survival in KPC mice (**see Table 1.1**). ACLY facilitates

but is not required for tumorigenesis *in vivo*. Since acetyl-CoA is needed for tumor progression and maintenance, *Acly*-deficient PanINs compensate by upregulating expression of *Acss2*.

This recently published study by Carrer et al was the first to demonstrate Kras-driven metabolic reprogramming and nutrient utilization driving ADM[81,83]. However, metabolic regulation of ADM is still largely unknown. Part of my thesis research was conducted to address this large gap in knowledge (**see Chapter 2**).

Redox Homeostasis

Reactive oxygen species (ROS) are a byproduct of metabolism typically associated with mutagenic and damaging properties on DNA, lipids, and proteins. However, ROS can function as signaling molecules to regulate proliferation, survival, and cell death[64,85]. At low concentrations, ROS promotes proliferation by inactivating phosphatases that counter the effects of mitogenic kinases. At moderate concentrations, ROS induces stress-response gene expression that provide pro-survival signals. At high concentrations, ROS can trigger senescence or cell death. Inducible antioxidant programs, for example those regulated by transcription factor NRF2 and its repressor protein KEAP1, are activated to maintain redox balance and repair oxidative damage due to high ROS levels[86]. NRF2 can be activated by oncogenes, ROS, and hypoxia to control the expression of over 200 genes involved in redox homeostasis, bioenergetics, metabolism, survival, proliferation, mitochondrial homeostasis, autophagy, and DNA repair.

In cancer, including PDA, ROS levels are elevated to support increased signaling through mitogenic pathways needed for metabolic reprogramming and continuous proliferation[50]. The heightened metabolism of cancer cells in turn generates more ROS which is accompanied by an increase in antioxidant activity[85,87]. Oncogenic KRAS, ROS, and hypoxia can induce expression of NRF2 and its target genes to aid sustained proliferation, biosynthetic metabolic reprogramming, and resistance to cell death[86,87].

ROS promotes *Kras*^{G12D}-driven tumorigenesis and proliferation[50,88]. KC mice (**see Table 1.1**) display high levels of oxidative stress in acinar cells which is further enhanced in ADM and PanIN lesions[50]. Oncogenic KRAS drives ADM in acinar explants by mediating

increased mitochondrial proton leak and elevating mitochondrial ROS (mROS) levels. In fact, treating primary wild-type acinar explants with hydrogen peroxide to increase ROS induces ADM—although not as strongly as mutant *Kras*. Cooperation between mutant KRAS and oxidative stress to initiate and promote pancreatic tumorigenesis is apparent in the absence of TP53INP1, an antioxidant target gene of p53 that promotes autophagy of damaged mitochondria (ref:[89]). The loss of *Tp53inp1* in KC mice (**see Table 1.1**) increases oxidative damage and accelerates ADM and PanIN initiation and progression of high-grade PanINs[90]. Antioxidant treatment dramatically reduces the number of ADM and PanIN lesions demonstrating increased ROS levels are necessary for efficient oncogenic *Kras*-induced tumorigenesis[50,90]. Ductal formation in acinar explants is also attenuated by decreasing ROS levels with antioxidants[50].

Oncogenic-driven increases in ROS must be balanced by induction of an antioxidant response to maintain ROS at pro-tumorigenic levels without surpassing the threshold to induce senescence or cell death[85]. *Kras^{G12D}* induces *Nrf2* expression, increases NRF2 target gene expression, and enhances GSH pools and the reduced to oxidized glutathione (GSSG) ratio (GSH/GSSH)[87]. Due to heightened ROS levels in KC mice (**see Table 1.1**), *Nrf2* expression is reciprocally increased in acinar cells, ADM, and PanIN lesions[50,87]; *Nrf2* expression is further increased under enhanced oxidative stress in the absence of *Tp53inp1*[90]. Ablation of *Nrf2* in the KC pancreas (**see Table 1.1**) results in fewer PanIN lesions which displayed increased oxidative stress[87]. Oxidative stress also induces expression of TIGAR, a p53 target gene, to reduce glycolytic flux and shuttle glycolytic intermediates into the PPP to generate NADPH[91-94]. TIGAR can also localize to the mitochondria to reduce mitochondrial membrane potential and decrease ROS production[95]. Given the ability to modulate ROS, TIGAR is often dysregulated in cancer[96]. In KC and KPC mouse models, loss of TIGAR in the pancreas (**see Table 1.1**) slows progression of PanIN lesions and increases mROS levels in PanIN lesions and PDA[97].

At first, these studies seem to be contradictory: the absence of an antioxidant should allow increased pancreatic tumorigenesis from the consequential increases in ROS. However, the levels of unbalanced KRAS-induced ROS from lack of an antioxidant response become detrimental and induce cellular senescence[87,98]. Indeed, *Nrf2* null KC

PanINs display increased senescence and a lower proliferative index; both are rescued by decreasing ROS levels with an antioxidant[87]. Also, despite slower tumorigenesis in the absence of TIGAR in KPC mice, there is accelerated tumor onset and increased metastatic disease[97]. Elevated ROS due to loss of TIGAR or NRF2 in KPC mice (**see Table 1.1**) promotes metastasis by inducing an epithelial-to-mesenchymal transition (EMT)[97,99]. Human and mouse PDA samples show dynamic fluctuations in TIGAR expression, demonstrating ROS and antioxidant programs are tightly regulated to promote different stages of disease progression[97].

Autophagy

Autophagy is a general term for pathways that deliver cellular materials to the lysosome for degradation[100]. There are three classes of autophagy: macroautophagy, microautophagy, and chaperone-mediated autophagy. Macroautophagy, usually referenced as autophagy, sequesters cytoplasmic materials in a double-membrane autophagosome that fuses with a lysosome for degradation. In microautophagy, the lysosome itself engulfs cytoplasmic components. Chaperone-mediated autophagy directly delivers proteins across the lysosomal membrane. These processes are essential for cellular homeostasis, survival, differentiation, and development.

Autophagy plays a dual role during cellular stress. Autophagy is elevated during nutrient deprivation, oxidative stress, hypoxia, and genotoxic stress to balance the cellular demands for energy and building blocks needed to sustain survival and to turn over damaged cellular components[101]. However, if attempts to promote survival fail, autophagy can lead to cell death. An important factor in mediating this balance is p62 (ref:[102]). p62 forms aggregates of damaged organelles and misfolded proteins and interacts with LC3. p62 along with its cargo becomes incorporated into the autophagosome and degraded. The level of p62 inversely correlates with autophagic flux, so the other roles of p62 can affect the survival-death balance: forming aggregates of proteins involved in survival or apoptotic signaling. p62 can also interact with KEAP1 to prevent sequestering NRF2 and tagging it for degradation[103].

Impaired autophagy is implicated in many human diseases[101], including pancreatitis[104]. The exocrine pancreas has one of the highest rates of autophagy to maintain proteostasis

under the high demands for protein synthesis, highlighting the importance of autophagy in preserving acinar cell homeostasis and function[104]. Characteristics of pancreatitis are accumulation of large vacuole formation and increased trypsinogen activation in acinar cells[104,105]. These vacuoles have a double membrane and contain partially degraded cellular material—both hallmarks of autophagic vacuoles[101]. Experimental models of acute pancreatitis in rodents show increased accumulation of large vacuoles in acinar cells[105,106]. Increased vacuolization could be the result of either enhanced autophagy or impaired autophagic flux. The observation that protein degradation is decreased demonstrates pancreatitis-induced vacuolization is a result of dysfunction in autophagic flux and not enhancement of autophagy[105]. Key characteristics of impaired autophagy are increased cytoplasmic vacuolization, improperly formed autophagosomes that contain undegraded cellular components, decreased protein degradation, increased expression of p62, accumulation of LC3-I, and decreased LC3-II expression[107-110]. Staining for the two forms of LC3, mammalian homolog of yeast Atg8, can indicate levels of autophagy. LC3-I is cytosolic whereas LC3-II is membrane bound and correlates with the extent of autophagosome formation[111]. Atg genes are key components of autophagic machinery and are essential for the formation of autophagosomes.

Since acinar cells depend on autophagy to maintain homeostasis, it is not surprising that autophagy impairment causes damage to the pancreas. Pancreas-specific loss of *Atg5* (ref:[107]) or *Atg7* (ref:[108,109]) via Cre expression from *Ptf1a* or *Pdx1* (**see Table 1.1**) causes, impaired autophagy. Ultimately, these mice develop chronic pancreatitis with features of severe acinar cell degeneration, ADM lesions, fibrosis, inflammation, necrosis/apoptosis with compensatory proliferation, and tissue atrophy. Pancreas tissue from these mice display increased ROS, ER stress, expression of p62, NRF2, and p53, and accumulation of damaged mitochondria. *Atg5*-deficient pancreata resemble human chronic pancreatitis patient samples[107]. A conflicting study where *Atg5* was deleted using Cre recombinase driven by the elastase promoter (*Ela-Cre; Atg5$^{f/f}$*) saw no pancreatic injury and concluded cerulein-induced pancreatitis was diminished[106]. This is surprising because experimental models of pancreatitis show impaired autophagic flux causes pancreatic damage[105]. The differences may be due to the recombination efficiency of the Cre-driver used[112].

Pancreata in *Ela-Cre; Atg5$^{f/f}$* mice were noted to have incomplete recombination[106]; lineage-tracing revealed Cre activity in about 70% of acinar cells[107].

Autophagy plays conflicting roles in tumor progression by suppressing tumorigenesis but supporting the metabolic needs of malignant tumors[113]. Impaired autophagy accelerates tumorigenesis but inhibits malignancy. In established tumors, autophagy promotes growth and survival by providing energy and nutrients[114]. Elevated autophagy is a feature of PDA and important for maintaining tumor viability and integrity[115,116]. A central mediator of metabolism, autophagy provides cells glucose, amino acids, and fatty acids; while this is certainly important in normal cells, PDA cells are dependent on autophagy to provide these substrates for growth and survival[117]. Interestingly, autophagy was recently shown to contribute to immune evasion in PDA[118].

Atg5 or *Atg7* deletions accelerate accumulation of low-grade PanIN lesions in KC pancreata (**see Table 1.1**). However, late-stage PanINs rarely manifest and progression to PDA does not occur[110]. PanIN lesions, regardless of autophagy status, have elevated p53 expression and stain strongly for senescence markers; those deficient for *Atg5* or *Atg7* have increased caspase-3 activation and growth arrest which impede PDA progression[119]. Wild-type p53 likely blocks PDA progression when autophagy is impaired. When p53 is concomitantly deleted (**see Table 1.1**), PDA tumors form in the context of impaired autophagy[110]. In this KPC model, impaired autophagy accelerates tumorigenesis and tumor onset and decreases survival, implying autophagy plays a tumor suppressive role throughout tumor development.

Another study utilized the p53 loss of heterozygosity (LOH) model to study the effect of autophagy during pancreatic tumorigenesis[75]. These mice (**see Table 1.1**) also have accelerated PanIN formation, but significantly less had invasive PDA which contributed to longer overall survival with significantly more long-term survivors[75]. These tumors show decreased proliferation with elevated apoptosis and DNA damage. In the context of *Tp53* LOH, autophagy is tumor suppressive during tumorigenesis but is needed in later stages in established tumors. This KPC model supports the dual roles of autophagy during tumor progression, likely because the *Tp53* LOH model closely resembles *Tp53* alterations that occur in human PDA: loss of function during tumor progression[18,75,113].

Defective lysosomal function is a possible mechanism of impaired autophagic flux[105,120]. Acinar cell trypsinogen activation is balanced by efficient lysosomal degradation during homeostasis. In pancreatitis, deficient protein degradation increases trypsinogen activation. Improper processing/maturation of lysosomal cathepsin enzymes that regulate trypsinogen activation and degradation promote intra-acinar accumulation of premature trypsinogen activation, causing pancreatic damage[105,120-122]. Mice deficient for LAMP-2 develop spontaneous pancreatitis with the characteristic features of impaired autophagy[120]. LAMP-2, a major component of lysosome membranes that facilitates fusion with autophagosomes, is downregulated in mouse and human pancreatitis[120,123].

Since all these studies genetically ablate autophagic or lysosomal machinery, it is difficult to determine how autophagy becomes dysregulated during natural disease progression. Recent evidence from experimental pancreatitis models indicate mitochondrial dysfunction causes autophagy impairment[124]. As a tumor suppressor, autophagy can mediate oncogenic-induced senescence, which may be bypassed in acinar cells via mutant Kras-driven mitochondrial dysfunction[50,125].

Endocytosis

Endocytosis consists of many different processes that internalize extracellular materials within endosomes[126]. Lysosomal degradation of endosomes and its cargo releases biosynthetic building blocks into the cell. Endosomes are also sites for signal transduction—activated EGFR can be internalized by endocytosis and Ras/MAPK signaling can occur on endosomes[127]. Dysregulated endocytosis has emerged as feature of malignant cells to support growth and survival[128].

Fluid-phase endocytosis (FPE) is distinguished by internalizing fluid phase markers, such as horseradish peroxidase and dextran[129]. FPE, in a manner dependent on EGFR and RAC1-driven actin polymerization, is required for ADM *in vitro* and *in vivo*[130]. FPE is elevated in KC pancreatic acinar cells prior to any histological changes[130]. Mouse and human acinar explants increase FPE as acinar cells undergo ADM. KC mice (**see Table 1.1**) with pancreas-specific deletion of *N-Wasp*—(the homolog of human *WASL*) a factor of F-actin that regulates endosomal internalization of EGFR—have dramatically reduced rates of FPE resulting in fewer ADM lesions, no PanIN lesions, and no ERK activation in

acinar cells[130,131]. Endocytosis, mediated by actin, may support ADM by enhancing ERK activity through internalization of EGFR and signal transduction on endosomes[42,49,56,57].

Macropinocytosis is an endocytic pathway where large volumes of extracellular fluid and solutes are internalized into vesicles called macropinosomes. Macropinocytosis is a method for cells to obtain nutrients to support cellular metabolism and growth[130]. Many different types of cancer cells upregulate macropinocytosis—typically by oncogene activation—as a means to scavenge nutrients from the microenvironment to support growth. Human PDA samples and mouse PDA models display robust mutant KRAS-driven activation of macropinocytosis in order to scavenge proteins and maintain intercellular amino acid levels, importantly glutamine[67,74,132]. KPC mice (**see Table 1.1**) display elevated macropinocytic uptake in mid- to late-stage PanIN lesions[74]. Acinar cells or ADM lesions were not analyzed in this KPC model to determine macropinocytosis status. However, it is possible that the FPE that drives ADM is macropinocytosis[130]. Oncogenic KRAS-induced FPE depends on EGFR, RAC1, and N-WASP, all of which are represented in a classic example of macropinocytosis[126]. Also, FPE in acinar cells and ADM was measured with dextran which is also used in macropinocytosis assays[74,130]. Activation of macropinocytosis may support ADM by scavenging extra nutrients to support metabolic reprogramming, by increasing endosomes to support mitogenic signaling, or by assisting Rac1-dependent actin reorganization to support morphological changes[60].

HIF Signaling

Hypoxia, the state of low oxygen tension, occurs in both physiological and pathophysiological conditions[133]. Hypoxia inducible factors (HIFs) are the major players involved in the hypoxic response. The HIF transcription factors—HIF1α, HIF2α, and HIF3α—are activated in low cellular oxygen levels. Upon activation, HIFs can no longer associate with their negative repressor VHL, which would otherwise target these proteins for proteasomal degradation. Over 100 target genes are controlled by HIFs, most regulating oxygen and energy homeostasis[134]. Not only do HIFs participate in embryonic development and normal cellular proliferation and differentiation, they are important factors in cancer[133,135]. Solid tumors, including PDA, contain hypoxic environments due to decreased vascularity[68,69]. Expression of HIF1α and HIF2α in tumors support growth

by regulating cellular metabolism, the inflammatory response, angiogenesis, and metastasis[69,135,136] .

Basal levels of HIF1α are very low while HIF2α is undetectable in human and mouse exocrine pancreas[137-140]. Mice with pancreas-specific deletion of HIF1α or HIF2α (**see Table 1.1**) develop histologically normal pancreata[137,138]. Expression of an oxygen-stable form of HIF1α in acinar cells (**see Table 1.1**) has no effect on pancreas morphology or function[139]. However, expression of an oxygen-stable form of HIF2α in acinar cells (**see Table 1.1**) causes spontaneous pancreatitis manifested by decreased acinar cell numbers, increased ADM, loss of amylase expression, exocrine cell atrophy, increased ER stress, and fibrosis[139,140]. This phenotype correlates with overexpression of HIF2α seen in chronic pancreatitis patient samples[139].

In PDA, hypoxia and HIF1α stabilization are detected early in ADM and PanIN stages of PDA development and persist throughout carcinogenesis[137]. Loss of HIF1α in KC mice (**see Table 1.1**) accelerates pancreatic tumorigenesis, demonstrating a tumor suppressive role for HIF1α[137]. Deletion of HIF1α augments PanIN number and grade, however, there is no difference in survival or tumor incidence[137]. Tumor progression may decelerate due to impaired metabolic reprogramming of glycolysis via expression of HIF1α target genes.

HIF2α expression is high in human and mouse ADM and low-grade PanIN lesions and gradually declines during PDA progression[138]. Like HIF1α deletion, loss of HIF2α in KC mice (**see Table 1.1**) accelerates pancreatic tumorigenesis[137]. However, HIF2α-deficient PanIN lesions fail to progress to more advanced PanIN stages and PDA[138]. Interestingly, concurrent expression of oncogenic *Kras*^{G12D} and HIF2α stabilization drives formation of MCN lesions rather than PanINs[139]. PanIN lesions in the HIF2α knockout model and MCN lesions in the HIF2α stabilization model display dysregulated Wnt signaling. Although β-catenin/Wnt signaling is restrained during Kras-induced ADM reprogramming, it is reactivated during PanIN progression[41] and MCN formation[141]. Both studies indicate a role for HIF2α modulating Wnt signaling during tumorigenesis.

Conclusions

In addition to the work described above, important interactions among these pathways are also likely to impact pancreas ADM and tumorigenesis. Oncogenic KRAS orchestrates metabolic reprogramming to drive ADM in a currently under-appreciated manner. Characterizing transforming, enabling, or neutral metabolic activities[142] involved in KRAS-induced ADM could lead to the development of early detection methods or targeted therapies to treat PDA, both of which are desperately needed. This concept was demonstrated by Carrer et al with treatment of acinar explants or PDA xenografts with atorvastatin and JQ1 to inhibit the mevalonate pathway and histone acetylation, respectively, effectively blocked ADM *in vitro* and suppressed tumor growth in immune competent mice[81]. Similarly, redox homeostasis plays an important role during pancreatic tumorigenesis[50,87,97] (**see Chapter 2**) and in tumor maintenance (**see Chapter 3**). Disrupting redox balance in PDA tumors is a promising target for the development of new therapeutics that could improve standard of care therapies. Characterizing the metabolic dependences for ADM could reveal metabolic vulnerabilities in PDA tumors for therapeutic targeting or early disease detection.

Table 1.1: Variations of mouse models

Study	Ref.	*Kras* status	Cre driver	*Tp53* status	Study specific gene
Acetyl-CoA Metabolism					
Carrer, et al. (2019)	81	*Kras*$^{LSL\text{-}G12D/+}$	*Pdx1*		
		Kras$^{LSL\text{-}G12D/+}$	*Pdx1*		*Acly*$^{f/f}$
		Kras$^{LSL\text{-}G12D/+}$	*Pdx1*	*Tp53*$^{f/+}$	*Acly*$^{f/f}$
ROS					
Liou, et al. (2016)	50	*Kras*$^{LSL\text{-}G12D/+}$	*Ptf1a/p48*		
DeNicola, et al. (2011)	87	*Kras*$^{LSL\text{-}G12D/+}$	*Ptf1a/p48*		
		Kras$^{LSL\text{-}G12D/+}$	*Ptf1a/p48*		*Nrf2*$^{-/-}$
Al Saati, et al. (2013)	90	*Kras*$^{LSL\text{-}G12D/+}$	*Pdx1*		*Tp53inp1*$^{-/-}$
Cheung, et al. (2020)	97	*Kras*$^{LSL\text{-}G12D/+}$	*Pdx1*		*Tigar*$^{f/f}$
		Kras$^{LSL\text{-}G12D/+}$	*Pdx1*	*Tp53*$^{f/+}$	*Tigar*$^{f/f}$
		Kras$^{LSL\text{-}G12D/+}$	*Pdx1*	*Tp53*$^{R172H/+}$	*Tigar*$^{f/f}$
		Kras$^{LSL\text{-}G12D/+}$	*Pdx1*	*Tp53*$^{R270H/+}$	*Nrf2*$^{-/-}$
Autophagy					
Diakopoulos, et al. (2015)	107		*Ptf1a/p48*		*Atg5*$^{f/f}$
Antonucci, et al. (2015)	108		*Pdx1*		*Atg7*$^{f/f}$
Iwahashi, et al. (2018)	109		*Pdx1*		*Atg7*$^{f/f}$
Rosenfeldt, et al. (2013)	110	*Kras*$^{LSL\text{-}G12D/+}$	*Pdx1*		*Atg5*$^{f/f}$ or *Atg7*$^{f/f}$
		Kras$^{LSL\text{-}G12D/+}$	*Pdx1*	*Tp53*$^{f/f}$	*Atg5*$^{f/f}$ or *Atg7*$^{f/f}$
Yang, et al. (2014)	75	*Kras*$^{LSL\text{-}G12D/+}$	*Pdx1*	*Tp53*$^{f/+}$	*Atg5*$^{f/f}$
Endocytosis					
Commisso, et al. (2013)	74	*Kras*$^{LSL\text{-}G12D/+}$	*Ptf1a/p48*	*Tp53*$^{f/+}$	
Lubeseder-Martellato, et al. (2017)	130	*Kras*$^{LSL\text{-}G12D/+}$	*Ptf1a/p48*		*N-Wasp*$^{f/f}$
HIF					
Lee, et al (2016)	137		*Ptf1a/p48*		*Hif1α*$^{f/f}$
		Kras$^{LSL\text{-}G12D/+}$	*Ptf1a/p48*		*Hif1α*$^{f/f}$
Criscimanna, et al. (2013)	138		*Ptf1a/p48*		*Hif2α*$^{f/f}$
		Kras$^{LSL\text{-}G12D/+}$	*Ptf1a/p48*		*Hif2α*$^{f/f}$
Schofield, et al (2018)	139		*Pdx1* or *Ptf1a/p48*		*Rosa26*$^{LSL\text{-}HIF1α/+}$ (stable)
			Pdx1 or *Ptf1a/p48*		*Rosa26*$^{LSL\text{-}HIF2α/+}$ (stable)
		Kras$^{LSL\text{-}G12D/+}$	*Pdx1* or *Ptf1a/p48*		*Rosa26*$^{LSL\text{-}HIF2α/+}$ (stable)
Flores-Martínez, et al. (2018)	140		*Pdx1*		*HIF2dPA* (stable)

References

1 Kleeff, J. *et al.* Pancreatic cancer. *Nature reviews. Disease primers* **2**, 16022, doi:10.1038/nrdp.2016.22 (2016).

2 Hezel, A. F., Kimmelman, A. C., Stanger, B. Z., Bardeesy, N. & Depinho, R. A. Genetics and biology of pancreatic ductal adenocarcinoma. *Genes Dev* **20**, 1218-1249, doi:10.1101/gad.1415606 (2006).

3 Midha, S., Chawla, S. & Garg, P. K. Modifiable and non-modifiable risk factors for pancreatic cancer: A review. *Cancer letters* **381**, 269-277, doi:10.1016/j.canlet.2016.07.022 (2016).

4 Siegel, R. L., Miller, K. D. & Jemal, A. Cancer statistics, 2020. *CA: a cancer journal for clinicians* **70**, 7-30, doi:10.3322/caac.21590 (2020).

5 Rahib, L. *et al.* Projecting cancer incidence and deaths to 2030: the unexpected burden of thyroid, liver, and pancreas cancers in the United States. *Cancer research* **74**, 2913-2921, doi:10.1158/0008-5472.can-14-0155 (2014).

6 Huang, L. *et al.* Stratified survival of resected and overall pancreatic cancer patients in Europe and the USA in the early twenty-first century: a large, international population-based study. *BMC medicine* **16**, 125, doi:10.1186/s12916-018-1120-9 (2018).

7 Rhim, A. D. *et al.* EMT and dissemination precede pancreatic tumor formation. *Cell* **148**, 349-361, doi:10.1016/j.cell.2011.11.025 (2012).

8 Feldmann, G., Beaty, R., Hruban, R. H. & Maitra, A. Molecular genetics of pancreatic intraepithelial neoplasia. *Journal of hepato-biliary-pancreatic surgery* **14**, 224-232, doi:10.1007/s00534-006-1166-5 (2007).

9 Shi, C. *et al.* KRAS2 mutations in human pancreatic acinar-ductal metaplastic lesions are limited to those with PanIN: implications for the human pancreatic cancer cell of origin. *Molecular cancer research : MCR* **7**, 230-236, doi:10.1158/1541-7786.mcr-08-0206 (2009).

10 Westphalen, C. B. & Olive, K. P. Genetically engineered mouse models of pancreatic cancer. *Cancer journal (Sudbury, Mass.)* **18**, 502-510, doi:10.1097/PPO.0b013e31827ab4c4 (2012).

11 Johnson, L. *et al.* Somatic activation of the K-ras oncogene causes early onset lung cancer in mice. *Nature* **410**, 1111-1116, doi:10.1038/35074129 (2001).

12 Jackson, E. L. *et al.* Analysis of lung tumor initiation and progression using conditional expression of oncogenic K-ras. *Genes Dev* **15**, 3243-3248, doi:10.1101/gad.943001 (2001).

13 Hingorani, S. R. *et al.* Preinvasive and invasive ductal pancreatic cancer and its early detection in the mouse. *Cancer cell* **4**, 437-450, doi:10.1016/s1535-6108(03)00309-x (2003).

14 Gu, G., Dubauskaite, J. & Melton, D. A. Direct evidence for the pancreatic lineage: NGN3+ cells are islet progenitors and are distinct from duct progenitors. *Development (Cambridge, England)* **129**, 2447-2457 (2002).

15 Kawaguchi, Y. *et al.* The role of the transcriptional regulator Ptf1a in converting intestinal to pancreatic progenitors. *Nat Genet* **32**, 128-134, doi:10.1038/ng959 (2002).

16 Ying, H. *et al.* Oncogenic Kras maintains pancreatic tumors through regulation of anabolic glucose metabolism. *Cell* **149**, 656-670, doi:10.1016/j.cell.2012.01.058 (2012).
17 Collins, M. A. *et al.* Oncogenic Kras is required for both the initiation and maintenance of pancreatic cancer in mice. *J Clin Invest* **122**, 639-653, doi:10.1172/jci59227 (2012).
18 Hingorani, S. R. *et al.* Trp53R172H and KrasG12D cooperate to promote chromosomal instability and widely metastatic pancreatic ductal adenocarcinoma in mice. *Cancer cell* **7**, 469-483, doi:10.1016/j.ccr.2005.04.023 (2005).
19 Olive, K. P. *et al.* Mutant p53 gain of function in two mouse models of Li-Fraumeni syndrome. *Cell* **119**, 847-860, doi:10.1016/j.cell.2004.11.004 (2004).
20 Bardeesy, N. *et al.* Both p16(Ink4a) and the p19(Arf)-p53 pathway constrain progression of pancreatic adenocarcinoma in the mouse. *Proc Natl Acad Sci U S A* **103**, 5947-5952, doi:10.1073/pnas.0601273103 (2006).
21 Aguirre, A. J. *et al.* Activated Kras and Ink4a/Arf deficiency cooperate to produce metastatic pancreatic ductal adenocarcinoma. *Genes Dev* **17**, 3112-3126, doi:10.1101/gad.1158703 (2003).
22 Ijichi, H. *et al.* Aggressive pancreatic ductal adenocarcinoma in mice caused by pancreas-specific blockade of transforming growth factor-beta signaling in cooperation with active Kras expression. *Genes Dev* **20**, 3147-3160, doi:10.1101/gad.1475506 (2006).
23 Bardeesy, N. *et al.* Smad4 is dispensable for normal pancreas development yet critical in progression and tumor biology of pancreas cancer. *Genes Dev* **20**, 3130-3146, doi:10.1101/gad.1478706 (2006).
24 Izeradjene, K. *et al.* Kras(G12D) and Smad4/Dpc4 haploinsufficiency cooperate to induce mucinous cystic neoplasms and invasive adenocarcinoma of the pancreas. *Cancer cell* **11**, 229-243, doi:10.1016/j.ccr.2007.01.017 (2007).
25 Bailey, J. M., DelGiorno, K. E. & Crawford, H. C. The secret origins and surprising fates of pancreas tumors. *Carcinogenesis* **35**, 1436-1440, doi:10.1093/carcin/bgu056 (2014).
26 Ray, K. C. *et al.* Epithelial tissues have varying degrees of susceptibility to Kras(G12D)-initiated tumorigenesis in a mouse model. *PLoS One* **6**, e16786, doi:10.1371/journal.pone.0016786 (2011).
27 Storz, P. Acinar cell plasticity and development of pancreatic ductal adenocarcinoma. *Nature reviews. Gastroenterology & hepatology* **14**, 296-304, doi:10.1038/nrgastro.2017.12 (2017).
28 Zhu, L., Shi, G., Schmidt, C. M., Hruban, R. H. & Konieczny, S. F. Acinar cells contribute to the molecular heterogeneity of pancreatic intraepithelial neoplasia. *Am J Pathol* **171**, 263-273, doi:10.2353/ajpath.2007.061176 (2007).
29 Aichler, M. *et al.* Origin of pancreatic ductal adenocarcinoma from atypical flat lesions: a comparative study in transgenic mice and human tissues. *The Journal of pathology* **226**, 723-734, doi:10.1002/path.3017 (2012).
30 Desai, B. M. *et al.* Preexisting pancreatic acinar cells contribute to acinar cell, but not islet beta cell, regeneration. *J Clin Invest* **117**, 971-977, doi:10.1172/jci29988 (2007).

31 Habbe, N. *et al.* Spontaneous induction of murine pancreatic intraepithelial neoplasia (mPanIN) by acinar cell targeting of oncogenic Kras in adult mice. *Proc Natl Acad Sci U S A* **105**, 18913-18918, doi:10.1073/pnas.0810097105 (2008).
32 Strobel, O. *et al.* In vivo lineage tracing defines the role of acinar-to-ductal transdifferentiation in inflammatory ductal metaplasia. *Gastroenterology* **133**, 1999-2009, doi:10.1053/j.gastro.2007.09.009 (2007).
33 De La, O. J. *et al.* Notch and Kras reprogram pancreatic acinar cells to ductal intraepithelial neoplasia. *Proc Natl Acad Sci U S A* **105**, 18907-18912, doi:10.1073/pnas.0810111105 (2008).
34 Kopp, J. L. *et al.* Identification of Sox9-dependent acinar-to-ductal reprogramming as the principal mechanism for initiation of pancreatic ductal adenocarcinoma. *Cancer cell* **22**, 737-750, doi:10.1016/j.ccr.2012.10.025 (2012).
35 Lee, A. Y. L. *et al.* Cell of origin affects tumour development and phenotype in pancreatic ductal adenocarcinoma. *Gut* **68**, 487-498, doi:10.1136/gutjnl-2017-314426 (2019).
36 Bailey, J. M. *et al.* p53 mutations cooperate with oncogenic Kras to promote adenocarcinoma from pancreatic ductal cells. *Oncogene* **35**, 4282-4288, doi:10.1038/onc.2015.441 (2016).
37 Murtaugh, L. C. & Keefe, M. D. Regeneration and repair of the exocrine pancreas. *Annual review of physiology* **77**, 229-249, doi:10.1146/annurev-physiol-021014-071727 (2015).
38 Yadav, D. & Lowenfels, A. B. The epidemiology of pancreatitis and pancreatic cancer. *Gastroenterology* **144**, 1252-1261, doi:10.1053/j.gastro.2013.01.068 (2013).
39 Bockman, D. E., Boydston, W. R. & Anderson, M. C. Origin of tubular complexes in human chronic pancreatitis. *American journal of surgery* **144**, 243-249, doi:10.1016/0002-9610(82)90518-9 (1982).
40 Willemer, S. & Adler, G. Histochemical and ultrastructural characteristics of tubular complexes in human acute pancreatitis. *Digestive diseases and sciences* **34**, 46-55, doi:10.1007/bf01536153 (1989).
41 Morris, J. P. t., Cano, D. A., Sekine, S., Wang, S. C. & Hebrok, M. Beta-catenin blocks Kras-dependent reprogramming of acini into pancreatic cancer precursor lesions in mice. *J Clin Invest* **120**, 508-520, doi:10.1172/jci40045 (2010).
42 Halbrook, C. J. *et al.* Mitogen-activated Protein Kinase Kinase Activity Maintains Acinar-to-Ductal Metaplasia and Is Required for Organ Regeneration in Pancreatitis. *Cellular and molecular gastroenterology and hepatology* **3**, 99-118, doi:10.1016/j.jcmgh.2016.09.009 (2017).
43 Guerra, C. *et al.* Chronic pancreatitis is essential for induction of pancreatic ductal adenocarcinoma by K-Ras oncogenes in adult mice. *Cancer cell* **11**, 291-302, doi:10.1016/j.ccr.2007.01.012 (2007).
44 Lerch, M. M. & Gorelick, F. S. Models of acute and chronic pancreatitis. *Gastroenterology* **144**, 1180-1193, doi:10.1053/j.gastro.2012.12.043 (2013).
45 Means, A. L. & Leach, S. D. Lineage commitment and cellular differentiation in exocrine pancreas. *Pancreatology : official journal of the International Association of Pancreatology (IAP) ... [et al.]* **1**, 587-596, doi:10.1159/000055868 (2001).

46 Houbracken, I. *et al.* Lineage tracing evidence for transdifferentiation of acinar to duct cells and plasticity of human pancreas. *Gastroenterology* **141**, 731-741, 741.e731-734, doi:10.1053/j.gastro.2011.04.050 (2011).
47 Pinho, A. V. *et al.* Adult pancreatic acinar cells dedifferentiate to an embryonic progenitor phenotype with concomitant activation of a senescence programme that is present in chronic pancreatitis. *Gut* **60**, 958-966, doi:10.1136/gut.2010.225920 (2011).
48 Baldan, J., Houbracken, I., Rooman, I. & Bouwens, L. Adult human pancreatic acinar cells dedifferentiate into an embryonic progenitor-like state in 3D suspension culture. *Sci Rep* **9**, 4040, doi:10.1038/s41598-019-40481-1 (2019).
49 Ardito, C. M. *et al.* EGF receptor is required for KRAS-induced pancreatic tumorigenesis. *Cancer cell* **22**, 304-317, doi:10.1016/j.ccr.2012.07.024 (2012).
50 Liou, G. Y. *et al.* Mutant KRas-Induced Mitochondrial Oxidative Stress in Acinar Cells Upregulates EGFR Signaling to Drive Formation of Pancreatic Precancerous Lesions. *Cell reports* **14**, 2325-2336, doi:10.1016/j.celrep.2016.02.029 (2016).
51 Buscail, L., Bournet, B. & Cordelier, P. Role of oncogenic KRAS in the diagnosis, prognosis and treatment of pancreatic cancer. *Nature reviews. Gastroenterology & hepatology* **17**, 153-168, doi:10.1038/s41575-019-0245-4 (2020).
52 Storz, P. & Crawford, H. C. Carcinogenesis of Pancreatic Ductal Adenocarcinoma. *Gastroenterology* **158**, 2072-2081, doi:10.1053/j.gastro.2020.02.059 (2020).
53 Navas, C. *et al.* EGF receptor signaling is essential for k-ras oncogene-driven pancreatic ductal adenocarcinoma. *Cancer cell* **22**, 318-330, doi:10.1016/j.ccr.2012.08.001 (2012).
54 Ji, B. *et al.* Ras activity levels control the development of pancreatic diseases. *Gastroenterology* **137**, 1072-1082, 1082.e1071-1076, doi:10.1053/j.gastro.2009.05.052 (2009).
55 Daniluk, J. *et al.* An NF-κB pathway-mediated positive feedback loop amplifies Ras activity to pathological levels in mice. *J Clin Invest* **122**, 1519-1528, doi:10.1172/jci59743 (2012).
56 Shi, G. *et al.* Maintenance of acinar cell organization is critical to preventing Kras-induced acinar-ductal metaplasia. *Oncogene* **32**, 1950-1958, doi:10.1038/onc.2012.210 (2013).
57 Collins, M. A., Yan, W., Sebolt-Leopold, J. S. & Pasca di Magliano, M. MAPK signaling is required for dedifferentiation of acinar cells and development of pancreatic intraepithelial neoplasia in mice. *Gastroenterology* **146**, 822-834.e827, doi:10.1053/j.gastro.2013.11.052 (2014).
58 Eser, S. *et al.* Selective requirement of PI3K/PDK1 signaling for Kras oncogene-driven pancreatic cell plasticity and cancer. *Cancer cell* **23**, 406-420, doi:10.1016/j.ccr.2013.01.023 (2013).
59 Wu, C. Y. *et al.* PI3K regulation of RAC1 is required for KRAS-induced pancreatic tumorigenesis in mice. *Gastroenterology* **147**, 1405-1416.e1407, doi:10.1053/j.gastro.2014.08.032 (2014).

60 Heid, I. *et al.* Early requirement of Rac1 in a mouse model of pancreatic cancer. *Gastroenterology* **141**, 719-730, 730.e711-717, doi:10.1053/j.gastro.2011.04.043 (2011).
61 Hanahan, D. & Weinberg, R. A. Hallmarks of cancer: the next generation. *Cell* **144**, 646-674, doi:10.1016/j.cell.2011.02.013 (2011).
62 Vander Heiden, M. G. Targeting cancer metabolism: a therapeutic window opens. *Nature reviews. Drug discovery* **10**, 671-684, doi:10.1038/nrd3504 (2011).
63 Lunt, S. Y. & Vander Heiden, M. G. Aerobic glycolysis: meeting the metabolic requirements of cell proliferation. *Annual review of cell and developmental biology* **27**, 441-464, doi:10.1146/annurev-cellbio-092910-154237 (2011).
64 Pavlova, N. N. & Thompson, C. B. The Emerging Hallmarks of Cancer Metabolism. *Cell Metab* **23**, 27-47, doi:10.1016/j.cmet.2015.12.006 (2016).
65 Chu, G. C., Kimmelman, A. C., Hezel, A. F. & DePinho, R. A. Stromal biology of pancreatic cancer. *Journal of cellular biochemistry* **101**, 887-907, doi:10.1002/jcb.21209 (2007).
66 Provenzano, P. P. *et al.* Enzymatic targeting of the stroma ablates physical barriers to treatment of pancreatic ductal adenocarcinoma. *Cancer cell* **21**, 418-429, doi:10.1016/j.ccr.2012.01.007 (2012).
67 Kamphorst, J. J. *et al.* Human pancreatic cancer tumors are nutrient poor and tumor cells actively scavenge extracellular protein. *Cancer research* **75**, 544-553, doi:10.1158/0008-5472.can-14-2211 (2015).
68 Koong, A. C. *et al.* Pancreatic tumors show high levels of hypoxia. *International journal of radiation oncology, biology, physics* **48**, 919-922, doi:10.1016/s0360-3016(00)00803-8 (2000).
69 Halbrook, C. J. & Lyssiotis, C. A. Employing Metabolism to Improve the Diagnosis and Treatment of Pancreatic Cancer. *Cancer cell* **31**, 5-19, doi:10.1016/j.ccell.2016.12.006 (2017).
70 DeBerardinis, R. J. *et al.* Beyond aerobic glycolysis: transformed cells can engage in glutamine metabolism that exceeds the requirement for protein and nucleotide synthesis. *Proc Natl Acad Sci U S A* **104**, 19345-19350, doi:10.1073/pnas.0709747104 (2007).
71 Son, J. *et al.* Glutamine supports pancreatic cancer growth through a KRAS-regulated metabolic pathway. *Nature* **496**, 101-105, doi:10.1038/nature12040 (2013).
72 Stanton, R. C. Glucose-6-phosphate dehydrogenase, NADPH, and cell survival. *IUBMB life* **64**, 362-369, doi:10.1002/iub.1017 (2012).
73 Nelson, B. S. *et al.* Tissue of origin dictates GOT1 dependence and confers synthetic lethality to radiotherapy. *Cancer & metabolism* **8**, 1, doi:10.1186/s40170-019-0202-2 (2020).
74 Commisso, C. *et al.* Macropinocytosis of protein is an amino acid supply route in Ras-transformed cells. *Nature* **497**, 633-637, doi:10.1038/nature12138 (2013).
75 Yang, A. *et al.* Autophagy is critical for pancreatic tumor growth and progression in tumors with p53 alterations. *Cancer discovery* **4**, 905-913, doi:10.1158/2159-8290.cd-14-0362 (2014).

76 Palm, W. *et al.* The Utilization of Extracellular Proteins as Nutrients Is Suppressed by mTORC1. *Cell* **162**, 259-270, doi:10.1016/j.cell.2015.06.017 (2015).
77 Pietrocola, F., Galluzzi, L., Bravo-San Pedro, J. M., Madeo, F. & Kroemer, G. Acetyl coenzyme A: a central metabolite and second messenger. *Cell Metab* **21**, 805-821, doi:10.1016/j.cmet.2015.05.014 (2015).
78 Carrer, A. & Wellen, K. E. Metabolism and epigenetics: a link cancer cells exploit. *Current opinion in biotechnology* **34**, 23-29, doi:10.1016/j.copbio.2014.11.012 (2015).
79 Lee, J. V. *et al.* Akt-dependent metabolic reprogramming regulates tumor cell histone acetylation. *Cell Metab* **20**, 306-319, doi:10.1016/j.cmet.2014.06.004 (2014).
80 Schug, Z. T. *et al.* Acetyl-CoA synthetase 2 promotes acetate utilization and maintains cancer cell growth under metabolic stress. *Cancer cell* **27**, 57-71, doi:10.1016/j.ccell.2014.12.002 (2015).
81 Carrer, A. *et al.* Acetyl-CoA Metabolism Supports Multistep Pancreatic Tumorigenesis. *Cancer discovery* **9**, 416-435, doi:10.1158/2159-8290.cd-18-0567 (2019).
82 Sherman, M. H. *et al.* Stromal cues regulate the pancreatic cancer epigenome and metabolome. *Proc Natl Acad Sci U S A* **114**, 1129-1134, doi:10.1073/pnas.1620164114 (2017).
83 Halbrook, C. J., Nelson, B. S. & Lysstiotis, C. A. Metabolism Drives Carcinogenesis and Maintenance of Pancreatic Tumors. *Cancer discovery* **9**, 326-328, doi:10.1158/2159-8290.cd-19-0034 (2019).
84 Neinast, M. D. *et al.* Quantitative Analysis of the Whole-Body Metabolic Fate of Branched-Chain Amino Acids. *Cell Metab* **29**, 417-429.e414, doi:10.1016/j.cmet.2018.10.013 (2019).
85 Schieber, M. & Chandel, N. S. ROS function in redox signaling and oxidative stress. *Curr Biol* **24**, R453-462, doi:10.1016/j.cub.2014.03.034 (2014).
86 Rojo de la Vega, M., Chapman, E. & Zhang, D. D. NRF2 and the Hallmarks of Cancer. *Cancer cell* **34**, 21-43, doi:10.1016/j.ccell.2018.03.022 (2018).
87 DeNicola, G. M. *et al.* Oncogene-induced Nrf2 transcription promotes ROS detoxification and tumorigenesis. *Nature* **475**, 106-109, doi:10.1038/nature10189 (2011).
88 Weinberg, F. *et al.* Mitochondrial metabolism and ROS generation are essential for Kras-mediated tumorigenicity. *Proc Natl Acad Sci U S A* **107**, 8788-8793, doi:10.1073/pnas.1003428107 (2010).
89 Saadi, H., Seillier, M. & Carrier, A. The stress protein TP53INP1 plays a tumor suppressive role by regulating metabolic homeostasis. *Biochimie* **118**, 44-50, doi:10.1016/j.biochi.2015.07.024 (2015).
90 Al Saati, T. *et al.* Oxidative stress induced by inactivation of TP53INP1 cooperates with KrasG12D to initiate and promote pancreatic carcinogenesis in the murine pancreas. *Am J Pathol* **182**, 1996-2004, doi:10.1016/j.ajpath.2013.02.034 (2013).
91 Bensaad, K. *et al.* TIGAR, a p53-inducible regulator of glycolysis and apoptosis. *Cell* **126**, 107-120, doi:10.1016/j.cell.2006.05.036 (2006).

92 Bensaad, K., Cheung, E. C. & Vousden, K. H. Modulation of intracellular ROS levels by TIGAR controls autophagy. *The EMBO journal* **28**, 3015-3026, doi:10.1038/emboj.2009.242 (2009).
93 Lui, V. W. *et al.* Inhibition of c-Met downregulates TIGAR expression and reduces NADPH production leading to cell death. *Oncogene* **30**, 1127-1134, doi:10.1038/onc.2010.490 (2011).
94 Yin, L., Kosugi, M. & Kufe, D. Inhibition of the MUC1-C oncoprotein induces multiple myeloma cell death by down-regulating TIGAR expression and depleting NADPH. *Blood* **119**, 810-816, doi:10.1182/blood-2011-07-369686 (2012).
95 Cheung, E. C., Ludwig, R. L. & Vousden, K. H. Mitochondrial localization of TIGAR under hypoxia stimulates HK2 and lowers ROS and cell death. *Proc Natl Acad Sci U S A* **109**, 20491-20496, doi:10.1073/pnas.1206530109 (2012).
96 Lee, P., Vousden, K. H. & Cheung, E. C. TIGAR, TIGAR, burning bright. *Cancer & metabolism* **2**, 1, doi:10.1186/2049-3002-2-1 (2014).
97 Cheung, E. C. *et al.* Dynamic ROS Control by TIGAR Regulates the Initiation and Progression of Pancreatic Cancer. *Cancer cell* **37**, 168-182.e164, doi:10.1016/j.ccell.2019.12.012 (2020).
98 Lee, A. C. *et al.* Ras proteins induce senescence by altering the intracellular levels of reactive oxygen species. *J Biol Chem* **274**, 7936-7940, doi:10.1074/jbc.274.12.7936 (1999).
99 Aiello, N. M. *et al.* Upholding a role for EMT in pancreatic cancer metastasis. *Nature* **547**, E7-e8, doi:10.1038/nature22963 (2017).
100 Mizushima, N. & Komatsu, M. Autophagy: renovation of cells and tissues. *Cell* **147**, 728-741, doi:10.1016/j.cell.2011.10.026 (2011).
101 Mizushima, N., Levine, B., Cuervo, A. M. & Klionsky, D. J. Autophagy fights disease through cellular self-digestion. *Nature* **451**, 1069-1075, doi:10.1038/nature06639 (2008).
102 Moscat, J. & Diaz-Meco, M. T. p62 at the crossroads of autophagy, apoptosis, and cancer. *Cell* **137**, 1001-1004, doi:10.1016/j.cell.2009.05.023 (2009).
103 Jiang, T. *et al.* p62 links autophagy and Nrf2 signaling. *Free radical biology & medicine* **88**, 199-204, doi:10.1016/j.freeradbiomed.2015.06.014 (2015).
104 Gukovskaya, A. S. & Gukovsky, I. Autophagy and pancreatitis. *American journal of physiology. Gastrointestinal and liver physiology* **303**, G993-g1003, doi:10.1152/ajpgi.00122.2012 (2012).
105 Mareninova, O. A. *et al.* Impaired autophagic flux mediates acinar cell vacuole formation and trypsinogen activation in rodent models of acute pancreatitis. *J Clin Invest* **119**, 3340-3355, doi:10.1172/jci38674 (2009).
106 Hashimoto, D. *et al.* Involvement of autophagy in trypsinogen activation within the pancreatic acinar cells. *The Journal of cell biology* **181**, 1065-1072, doi:10.1083/jcb.200712156 (2008).
107 Diakopoulos, K. N. *et al.* Impaired autophagy induces chronic atrophic pancreatitis in mice via sex- and nutrition-dependent processes. *Gastroenterology* **148**, 626-638.e617, doi:10.1053/j.gastro.2014.12.003 (2015).
108 Antonucci, L. *et al.* Basal autophagy maintains pancreatic acinar cell homeostasis and protein synthesis and prevents ER stress. *Proc Natl Acad Sci U S A* **112**, E6166-6174, doi:10.1073/pnas.1519384112 (2015).

109 Iwahashi, K. *et al.* Autophagy impairment in pancreatic acinar cells causes zymogen granule accumulation and pancreatitis. *Biochemical and biophysical research communications* **503**, 2576-2582, doi:10.1016/j.bbrc.2018.07.018 (2018).
110 Rosenfeldt, M. T. *et al.* p53 status determines the role of autophagy in pancreatic tumour development. *Nature* **504**, 296-300, doi:10.1038/nature12865 (2013).
111 Mizushima, N., Yoshimori, T. & Ohsumi, Y. The role of Atg proteins in autophagosome formation. *Annual review of cell and developmental biology* **27**, 107-132, doi:10.1146/annurev-cellbio-092910-154005 (2011).
112 Magnuson, M. A. & Osipovich, A. B. Pancreas-specific Cre driver lines and considerations for their prudent use. *Cell Metab* **18**, 9-20, doi:10.1016/j.cmet.2013.06.011 (2013).
113 Sun, K. *et al.* Paradoxical roles of autophagy in different stages of tumorigenesis: protector for normal or cancer cells. *Cell & bioscience* **3**, 35, doi:10.1186/2045-3701-3-35 (2013).
114 Kimmelman, A. C. The dynamic nature of autophagy in cancer. *Genes Dev* **25**, 1999-2010, doi:10.1101/gad.17558811 (2011).
115 Yang, S. *et al.* Pancreatic cancers require autophagy for tumor growth. *Genes Dev* **25**, 717-729, doi:10.1101/gad.2016111 (2011).
116 Yang, A. *et al.* Autophagy Sustains Pancreatic Cancer Growth through Both Cell-Autonomous and Nonautonomous Mechanisms. *Cancer discovery* **8**, 276-287, doi:10.1158/2159-8290.cd-17-0952 (2018).
117 Kimmelman, A. C. & White, E. Autophagy and Tumor Metabolism. *Cell Metab* **25**, 1037-1043, doi:10.1016/j.cmet.2017.04.004 (2017).
118 Yamamoto, K. *et al.* Autophagy promotes immune evasion of pancreatic cancer by degrading MHC-I. *Nature* **581**, 100-105, doi:10.1038/s41586-020-2229-5 (2020).
119 Caldwell, M. E. *et al.* Cellular features of senescence during the evolution of human and murine ductal pancreatic cancer. *Oncogene* **31**, 1599-1608, doi:10.1038/onc.2011.350 (2012).
120 Mareninova, O. A. *et al.* Lysosome associated membrane proteins maintain pancreatic acinar cell homeostasis: LAMP-2 deficient mice develop pancreatitis. *Cellular and molecular gastroenterology and hepatology* **1**, 678-694, doi:10.1016/j.jcmgh.2015.07.006 (2015).
121 Halangk, W. *et al.* Role of cathepsin B in intracellular trypsinogen activation and the onset of acute pancreatitis. *J Clin Invest* **106**, 773-781, doi:10.1172/jci9411 (2000).
122 Wartmann, T. *et al.* Cathepsin L inactivates human trypsinogen, whereas cathepsin L-deletion reduces the severity of pancreatitis in mice. *Gastroenterology* **138**, 726-737, doi:10.1053/j.gastro.2009.10.048 (2010).
123 Huynh, K. K. *et al.* LAMP proteins are required for fusion of lysosomes with phagosomes. *The EMBO journal* **26**, 313-324, doi:10.1038/sj.emboj.7601511 (2007).
124 Biczo, G. *et al.* Mitochondrial Dysfunction, Through Impaired Autophagy, Leads to Endoplasmic Reticulum Stress, Deregulated Lipid Metabolism, and

Pancreatitis in Animal Models. *Gastroenterology* **154**, 689-703, doi:10.1053/j.gastro.2017.10.012 (2018).
125 Young, A. R. *et al.* Autophagy mediates the mitotic senescence transition. *Genes Dev* **23**, 798-803, doi:10.1101/gad.519709 (2009).
126 Kumari, S., Mg, S. & Mayor, S. Endocytosis unplugged: multiple ways to enter the cell. *Cell research* **20**, 256-275, doi:10.1038/cr.2010.19 (2010).
127 Fehrenbacher, N., Bar-Sagi, D. & Philips, M. Ras/MAPK signaling from endomembranes. *Molecular oncology* **3**, 297-307, doi:10.1016/j.molonc.2009.06.004 (2009).
128 Mosesson, Y., Mills, G. B. & Yarden, Y. Derailed endocytosis: an emerging feature of cancer. *Nature reviews. Cancer* **8**, 835-850, doi:10.1038/nrc2521 (2008).
129 Shurety, W., Stewart, N. L. & Stow, J. L. Fluid-phase markers in the basolateral endocytic pathway accumulate in response to the actin assembly-promoting drug Jasplakinolide. *Molecular biology of the cell* **9**, 957-975, doi:10.1091/mbc.9.4.957 (1998).
130 Lubeseder-Martellato, C. *et al.* Oncogenic KRas-induced Increase in Fluid-phase Endocytosis is Dependent on N-WASP and is Required for the Formation of Pancreatic Preneoplastic Lesions. *EBioMedicine* **15**, 90-99, doi:10.1016/j.ebiom.2016.12.013 (2017).
131 Benesch, S. *et al.* N-WASP deficiency impairs EGF internalization and actin assembly at clathrin-coated pits. *Journal of cell science* **118**, 3103-3115, doi:10.1242/jcs.02444 (2005).
132 Davidson, S. M. *et al.* Direct evidence for cancer-cell-autonomous extracellular protein catabolism in pancreatic tumors. *Nature medicine* **23**, 235-241, doi:10.1038/nm.4256 (2017).
133 Brahimi-Horn, M. C. & Pouysségur, J. HIF at a glance. *Journal of cell science* **122**, 1055-1057, doi:10.1242/jcs.035022 (2009).
134 Wenger, R. H., Stiehl, D. P. & Camenisch, G. Integration of oxygen signaling at the consensus HRE. *Science's STKE : signal transduction knowledge environment* **2005**, re12, doi:10.1126/stke.3062005re12 (2005).
135 Schito, L. & Semenza, G. L. Hypoxia-Inducible Factors: Master Regulators of Cancer Progression. *Trends in cancer* **2**, 758-770, doi:10.1016/j.trecan.2016.10.016 (2016).
136 Talks, K. L. *et al.* The expression and distribution of the hypoxia-inducible factors HIF-1alpha and HIF-2alpha in normal human tissues, cancers, and tumor-associated macrophages. *Am J Pathol* **157**, 411-421, doi:10.1016/s0002-9440(10)64554-3 (2000).
137 Lee, K. E. *et al.* Hif1a Deletion Reveals Pro-Neoplastic Function of B Cells in Pancreatic Neoplasia. *Cancer discovery* **6**, 256-269, doi:10.1158/2159-8290.cd-15-0822 (2016).
138 Criscimanna, A. *et al.* PanIN-specific regulation of Wnt signaling by HIF2α during early pancreatic tumorigenesis. *Cancer research* **73**, 4781-4790, doi:10.1158/0008-5472.can-13-0566 (2013).
139 Schofield, H. K. *et al.* Pancreatic HIF2α Stabilization Leads to Chronic Pancreatitis and Predisposes to Mucinous Cystic Neoplasm. *Cellular and*

molecular gastroenterology and hepatology **5**, 169-185.e162, doi:10.1016/j.jcmgh.2017.10.008 (2018).
140 Flores-Martínez, A., García-Núñez, A., Rojas, A. & Cano, D. A. Stabilization of HIF-2α impacts pancreas growth. *Sci Rep* **8**, 13713, doi:10.1038/s41598-018-32054-5 (2018).
141 Sano, M., Driscoll, D. R., De Jesus-Monge, W. E., Klimstra, D. S. & Lewis, B. C. Activated wnt signaling in stroma contributes to development of pancreatic mucinous cystic neoplasms. *Gastroenterology* **146**, 257-267, doi:10.1053/j.gastro.2013.09.044 (2014).
142 Vander Heiden, M. G. & DeBerardinis, R. J. Understanding the Intersections between Metabolism and Cancer Biology. *Cell* **168**, 657-669, doi:10.1016/j.cell.2016.12.039 (2017).

CHAPTER 2

Metabolic Regulation of Acinar-to-Ductal Metaplasia

Summary

Activating mutations in *KRAS* extensively reprogram cellular metabolism to support the continuous growth, proliferation, and survival of pancreatic tumors. These metabolic dependencies are attractive targets for treating established tumors. However, metabolic reprogramming begins during tumorigenesis to provide transforming cells selective advantage towards malignancy. Acinar cells can give rise to pancreatic tumors through acinar-to-ductal metaplasia (ADM), and inhibiting pathways that maintain acinar homeostasis can accelerate tumorigenesis. During ADM, acinar cells transdifferentiate to duct-like cells, a process driven by oncogenic KRAS, and one that we hypothesized was mediated by metabolic rewiring. We performed transcriptomic analysis on acinar cells undergoing ADM and found metabolic programs are globally enhanced. Indeed, we and others have recently demonstrated how inhibiting metabolic pathways necessary for ADM can prevent transdifferentiation and tumorigenesis. We previously demonstrated that PDA cells rewire glucose and glutamine metabolism to support growth and survival. Using *in vitro* models of ADM, we found that glutamine availability is dispensable for ADM. In contrast, glucose availability and intact oxidative phosphorylation are required for ADM. A more detailed analysis of the pathways downstream of glucose metabolism revealed that disrupting the oxidative pentose phosphate pathway accelerates ADM *in vitro* and tumorigenesis *in vivo*. Together, this work demonstrates metabolic dependencies can differ during tumorigenesis and tumor maintenance.

Introduction

The majority of patients with pancreatic ductal adenocarcinoma (PDA) are diagnosed with advanced or metastasized disease[1]. Lack of early detection methods and effective therapies contributes to a dismal 10% five-year survival rate[2]. Oncogenic *KRAS* mutation is the initiating event in PDA and found in over 90% of pancreatic tumors[3]. Tumorigenesis

is hypothesized to progress stepwise from acinar-to-ductal metaplasia (ADM) to pancreatic intraepithelial neoplasia (PanIN) to invasive carcinoma. Lineage tracing studies of pancreatic cancer mouse models demonstrate PDA can arise from mutant KRAS-expressing acinar cells that undergo ADM[4,5]. ADM is a normal wound healing response to pancreatic injury or inflammation where acinar cells transdifferentiate to ductal progenitor cells and repopulate tissue lost due to injury[6]. Upon healing, ductal progenitor cells redifferentiate to acinar cells and resume normal acinar function. Oncogenic *Kras* mutations hijack the healing process to where ADM can progress into neoplastic lesions and PDA. Previous studies have demonstrated ADM can be blocked by inhibiting signaling pathways necessary for transdifferentiation[7-10]. In fact, targeting pathways that drive tumorigenesis can revert ADM and PanIN lesions back to normal tissue[7,9].

Cancer cells, including PDA, require a continuous supply of biosynthetic precursors and energy to generate macromolecules necessary for growth and proliferation[11,12]. To meet this demand, oncogenic KRAS reprograms cellular metabolism to promote aerobic glycolysis (the Warburg Effect) where glucose is diverted into anabolic pathways to generate biosynthetic precursors and energy[13]. Glutamine metabolism is rewired to maintain anaplerosis and redox homeostasis[14,15]. We hypothesized global shifts in metabolism occur during ADM that reflect metabolic reprogramming required for PDA maintenance. However, metabolic changes that drive ADM are not well characterized. Using well established *in vitro* models of ADM, we demonstrate dependencies of ADM on different nutrients and metabolic pathways that could be leveraged as therapeutic targets.

Results

Broad changes in metabolic programs during ADM

Oncogenic KRAS regulates metabolic reprogramming in PDA cells[13,14]. To investigate KRAS-driven changes that occur during tumorigenesis, we performed transcriptomics on acinar cells undergoing ADM. Since mutant KRAS elicits an inflammatory response in pancreatic tissue[16], we activated oncogenic *Kras ex vivo* as to identify *Kras*-driven changes and control for differences in inflammation between mutant Kras-expressing and wild-type pancreas. As such, we isolated acinar cells from *Kras*$^{LSL\text{-}G12D/+}$ mice and infected

the cells with either control adenovirus (ad-GFP) or adenovirus that expresses Cre recombinase (ad-CRE) to induce expression of mutant *Kras*^{G12D}. RNA was isolated 24 hours after plating ad-GFP infected acinar cells (ad-GFP day 1) and 24, 48, and 72 hours after plating ad-CRE infected cells (ad-CRE day 1/2/3, respectively). Gene Set Enrichment Analysis (GSEA)[17,18] demonstrated signatures known to be enhanced during ADM are present in our transcriptome data from ad-GFP day 1 and ad-CRE day 2 acinar cells—prior to ductal formation (**Fig. 2.1a**). Genes upregulated by KRAS signaling are enriched in *Kras*^{G12D}-expressing acinar cells and genes downregulated by KRAS signaling are enriched in control cells. In addition, epithelial-to-mesenchymal transition (EMT), hypoxia, p53 activity, and inflammation signatures are consistent with previous studies showing these pathways are involved in ADM[19-24]. GSEA revealed metabolic signatures are highly enriched in *Kras*^{G12D}-expressing acinar explants (**Fig. 2.1b, Tables 2.1, 2.2**). Our transcriptomics data is consistent with studies demonstrating elevations in cholesterol metabolism, reactive oxygen species (ROS), and antioxidant programs during mutant *Kras*-driven ADM[25-27]. However, the regulation of other metabolic pathways during ADM is uncharacterized.

Acinar cell survival and ADM is dependent on glucose

Based on the upregulation of glycolysis and pathways that utilize glycolytic intermediates—including the pentose phosphate pathway (PPP), serine metabolism, pyruvate metabolism, and the tricarboxylic acid (TCA) cycle—in our GSEA analysis (**Table 2.2**), we first focused on the role of glucose during ADM. Glucose is a major fuel source for cancer cells, and in previous work we reported PDA cell lines are dependent on glucose for proliferation[13]. We also wanted to determine the dependence of ADM on glucose. Primary acinar cells were isolated from wild-type mice, embedded in a collagen matrix, and treated with TGFα to induce ADM. Acinar explants were sensitive to the absence of glucose in the culture media. Not only did acinar cells not undergo ADM without glucose supplementation, but they died within two days of plating (**Fig. 2.2a**). We next tested if a lower concentration of glucose was sufficient to support ADM. Surprisingly, glucose supplementation at 1:100 the concentration used in culture media—and approximately 1:20 to 1:30 the concentration found in plasma[28,29]—was adequate for

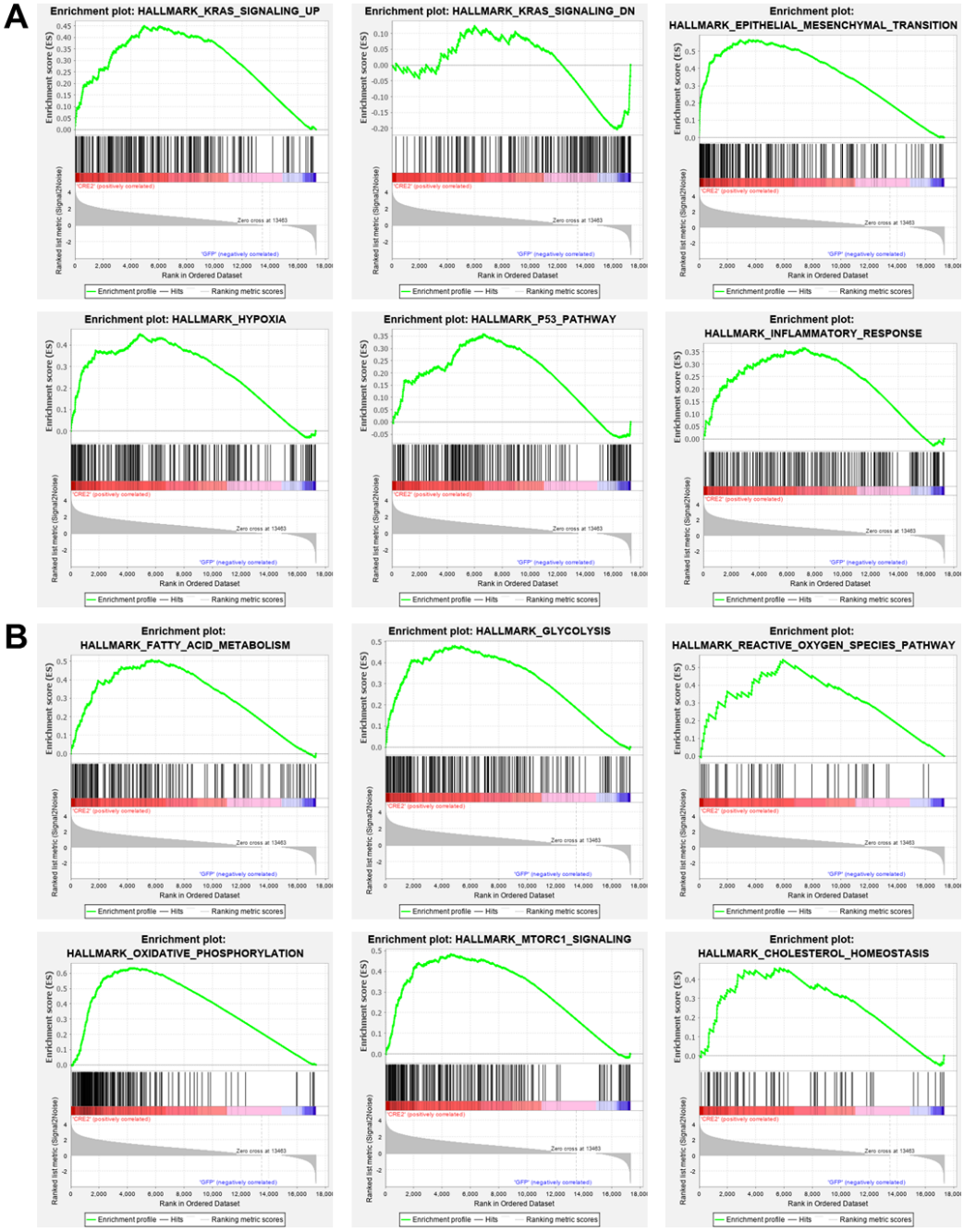

Figure 2.1 Metabolic signatures are enriched in *Kras*^{G12D}-expressing acinar cells undergoing ADM. GSEA analysis of transcriptomics from ad-GFP day 1 and ad-CRE day 2 acinar explants. **(A)** Selected confidence building enrichment plots of GSEA Hallmark signatures enriched in *Kras*^{G12D}-expressing acinar cells. Genes upregulated by KRAS signaling are enriched in *Kras*^{G12D}-expressing acinar cells (CRE2) while genes downregulated by KRAS signaling are enriched in control acinar cells (GFP). The other enrichment plots demonstrate signatures found in our system are consistent with previously reported data of ADM. **(B)** Selected enrichment plots of metabolic signatures enriched in *Kras*^{G12D}-expressing acinar cells from GSEA Hallmark signatures listed in **Table 2.1**. Enrichment score (ES) signifies the degree a gene set is overrepresented at the top or bottom of a ranked list of genes. The black vertical bars show where genes within the signature appear in the ranked list of genes. The waterfall plot represents a gene's correlation with a phenotype[17,18].

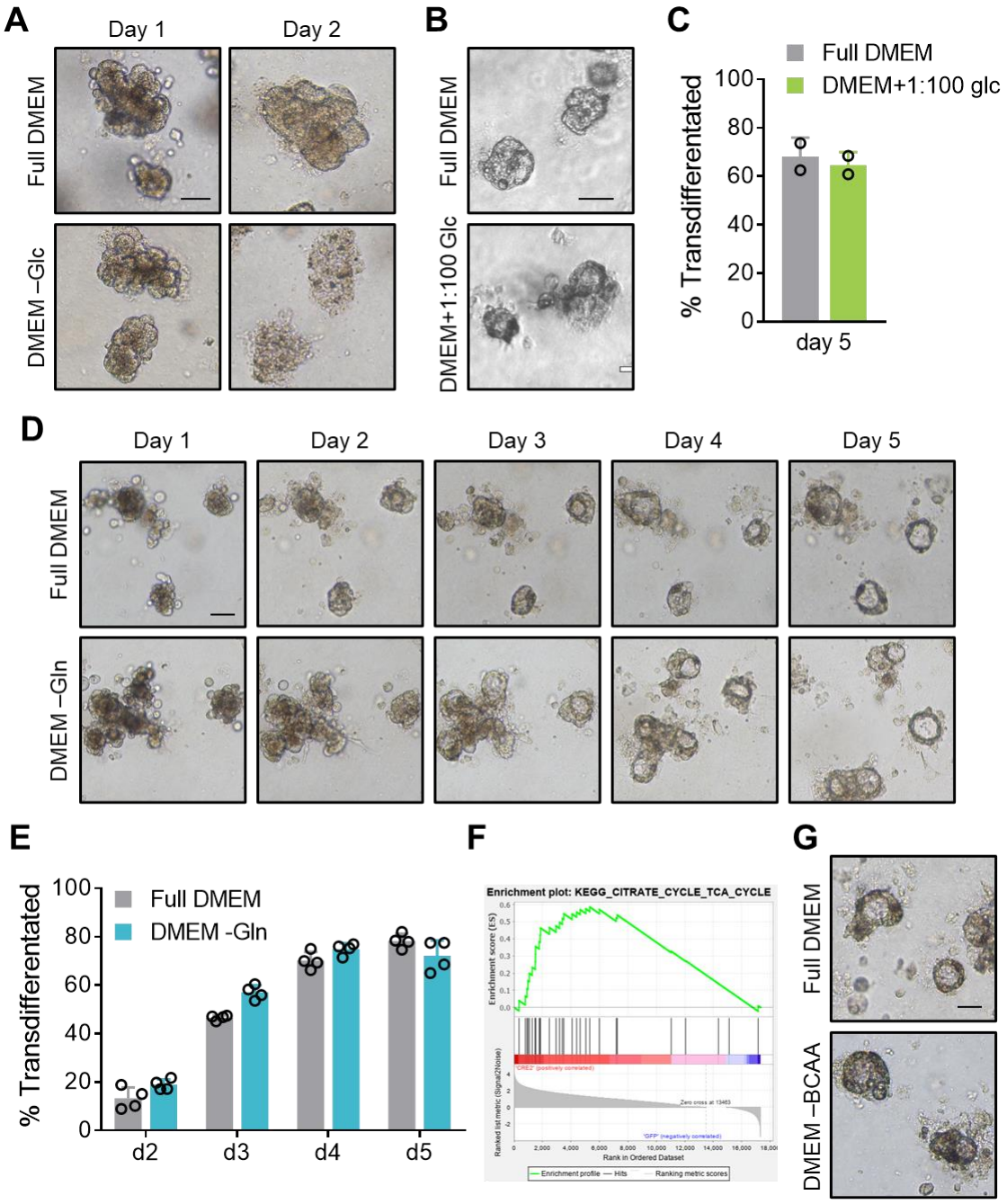

Figure 2.2 ADM requires exogenous glucose but not glutamine. (A) Representative images of wild-type acinar cells treated with TGFα and cultured with or without glucose (Glc). Acinar cells completely devoid of glucose supplementation died by day 2. **(B)** Representative images of ductal formations from day 5 wild-type acinar cells treated with TGFα and cultured in full DMEM media or supplemented with 1:100 (250 μM) the amount of glucose. **(C)** Quantification of ductal structures formed in collagen. Each point represents a technical replicate from one mouse. **(D)** Representative images of KC acinar cells cultured with or without glutamine (Gln). Acinar explants undergo ADM over the course of 5 days. **(E)** Quantification of ductal structures formed in collagen. Each point represents a technical replicate from one mouse. **(F)** GSEA enrichment plot of TCA cycle signature in *Kras*^{G12D}-expressing acinar cells. **(G)** Representative images of ductal formations from day 5 wild-type acinar cells treated with TGFα and cultured with or without branched-chain amino acids (BCAA). Scale bar = 50 μm.

acinar cells to transdifferentiate (**Fig. 2.2b,c**). We postulate minimal glucose concentrations are required to maintain anabolic pathways, such as the PPP and TCA cycle, that generate biosynthetic precursors for fatty acids, nucleotides, and amino acids.

Anaplerotic substrates are not required for ADM

Glutamine, like glucose, is a major fuel source for PDA cell proliferation and survival[14]. Given that so little glucose was needed, and together with the PDA data, we hypothesized acinar cells also utilized glutamine during ADM. Isolated acinar cells from *Kras*$^{LSL\text{-}G12D/+}$*; Ptf1a*$^{Cre/+}$ (KC) mice cultured without glutamine survived and transdifferentiated at the same rate as acinar cells in full media (**Fig. 2.2d,e**). This was unexpected because 1) proliferating cells increase demand for glutamine to replenish the TCA cycle, 2) *ex vivo* KC ductal structures stain positive for Ki67, a common proliferative marker, and 3) PDA cell lines are dependent on glutamine to grow and proliferate in culture[30,31]. Although previous studies have shown dependencies that are present in PDA tumors are also required to drive ADM *in vitro*[25,26], our data illustrates that exogenous glutamine is dispensable for acinar cell transdifferentiation *in vitro*.

Since glutamine may not be used as an anaplerotic substrate to replenish the TCA cycle and the TCA cycle is enriched in *Kras*^{G12D}-expressing acinar cells (**Fig. 2.2f**), we tested if dropping out other anaplerotic substrates effected ADM. Branched-chained amino acids (BCAA) were recently reported to be major anaplerotic substrates in the normal mouse pancreas and used more than other tissues[32]. Further, leucine is catabolized during ADM[25]. However, wild-type acinar explants treated with TGFα form ductal structures in the absence of BCAAs (**Fig. 2.2g**)[4]. Together, this data suggests glucose may be the main source that feeds into the TCA cycle and metabolic reprogramming to promote aerobic glycolysis may not occur as acinar cells transdifferentiate.

Acinar cells are profoundly sensitive to oxidative phosphorylation inhibition

The TCA cycle generates biosynthetic precursors for anabolic pathways and the reducing equivalents NADH and FADH2 that are used as electron sources for the electron transport chain (collectively, oxidative phosphorylation) to generate ATP[33]. The TCA cycle and oxidative phosphorylation metabolically regulate each other. Since ADM can occur with very low concentrations of glucose and no glutamine or BCAA supplementation, we

wanted to determine how reliant acinar cells are on oxidative phosphorylation. KC acinar cells were embedded in collagen and treated with low nanomolar (nM) concentrations of oligomycin, an ATP synthase/complex V inhibitor that prevents ATP generation and backs up the electron transport chain. Whereas PDA cells can survive in low micromolar concentrations[34], acinar cells were exquisitely sensitive to oligomycin and died within 24 hours of treatment with low nM doses (**Fig. 2.3a**). We next asked whether stronger ADM activation could overcome oligomycin sensitivity. KC acinar cells embedded in Matrigel undergo ADM at an accelerated rate and form larger ductal cysts than when plated in collagen. However, acinar cells were equally as sensitive to oligomycin even when stimulated with growth factors found in Matrigel (**Fig. 2.3b**). This data suggests acinar cells require oxidative phosphorylation for survival, consistent with the seemingly limited utilization of ATP generated in glycolysis, based on the glucose-dependence data.

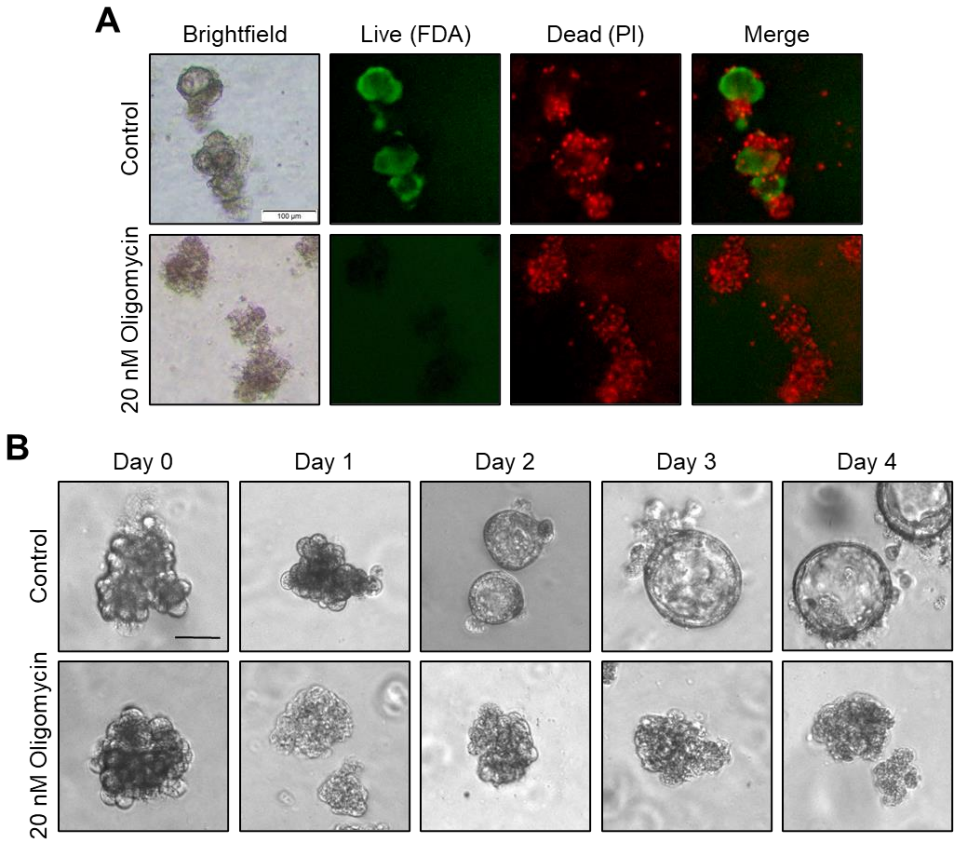

Figure 2.3 Acinar cells are sensitive to oligomycin treatment. (A) Representative images of Live/Dead staining on day 3 KC acinar cells treated with 20nM oligomycin. Fluorescein diacetate (FDA) was used to mark live cells and propidium iodine (PI) stains dead cells. Control acinar explants transdifferentiated by day 3. **(B)** Representative images of KC acinar cells embedded in Matrigel and treated with 20nM oligomycin. Control acinar explants undergo ADM over the course of 5 days. Scale bar = 100 µm (**a**) or 50 µm (**b**).

Kras^{G12D} increases expression of NADPH-producing enzymes

Not only is mitochondrial metabolism and oxidative phosphorylation a major source of ATP, it is also the largest generator of ROS[35]. ROS levels must be tightly regulated as to not damage cellular components and induce senescence or cell death. However, cancer cells, including PDA, enhance basal levels of ROS to promote proliferation and survival[36]. During tumorigenesis, Kras^{G12D} induces mitochondrial ROS (mROS) production in acinar cells, and this has been reported to drive ADM[26]. To prevent exceedingly high levels of ROS, antioxidant programs are activated during tumorigenesis and maintained in malignant cells[26,27]. Indeed, treatment with antioxidant N-acetylcysteine (NAC) slows the rate of acinar cell transdifferentiation (**Fig. 2.4a**).

A major cofactor that maintains cellular redox homeostasis is NADPH, which is used in the generation of the antioxidants glutathione (GSH) and thioredoxin[37]. Cytosolic NADPH is mainly generated by four enzymes: glucose-6-phosphate dehydrogenase (G6PD), 6-phosphogluconate dehydrogenase (PGD), malic enzyme 1 (ME1), and isocitrate dehydrogenase 1 (IDH1)[37,38]. Recent evidence demonstrates serine and folate metabolism can contribute to NADPH pools via methylenetetrahydrofolate dehydrogenase 1 (MTHFD1)[39,40]. Analysis our transcriptomics data revealed significantly increased expression of *G6pd* and *Me1* 48 and 72 hours after *Kras*^{G12D} expression (ad-CRE d2 and d3, respectively) and, to a lesser extent, increased expression of *Idh1* and *Mthfd1* (**Fig. 2.4b**).

G6PD mutation decreases oxidative PPP flux in *Kras*^{G12D}-expressing acinar cells

The PPP shunts off glycolysis and consists of two branches: oxidative and nonoxidative. In normal cells, both branches produce nucleotide precursors and the oxidative branch is a major source of NADPH via G6PD and PGD. We sought to determine the effects of oxidative PPP metabolism on ADM because 1) expression of *Kras*^{G12D} mediated a significant expression increase of *G6pd* (**Fig. 2.4b**), the first and rate limiting step of the oxidative PPP and a NADPH-producing enzyme, 2) primary acinar explants depend on glucose for survival (**Fig 2.2a**), 3) the PPP is in the top 10 Kyoto Encyclopedia of Genes and Genomes (KEGG) signatures from our GSEA analysis (**Fig. 2.4c, Table 2.2**), and 4) PDA cells downregulate oxidative PPP and compensate for NADPH production through

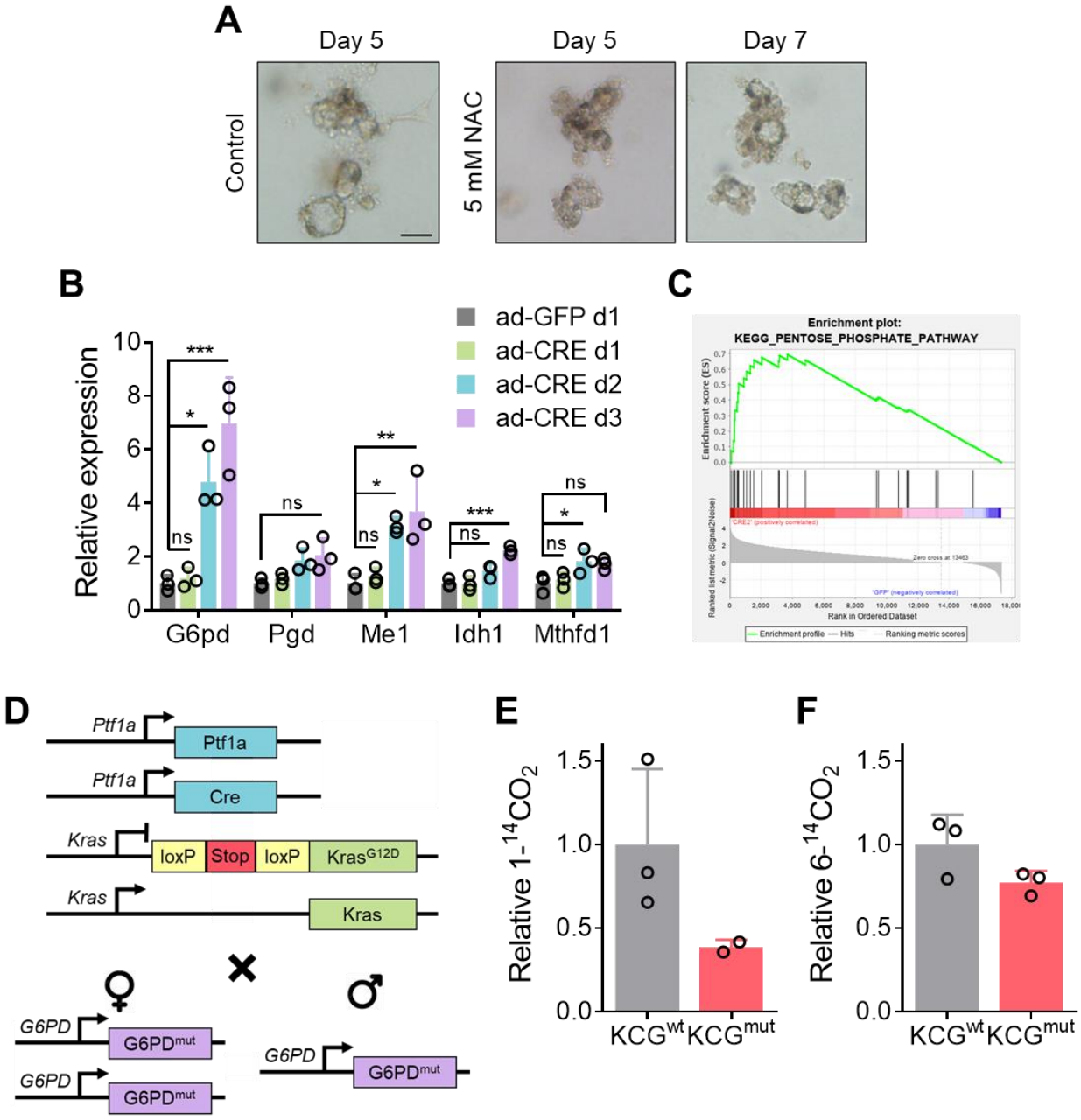

Figure 2.4 Kras^{G12D} induces expression of NADPH-producing enzymes and enhances the PPP. **(A)** Representative images of wild-type acinar cells treated with TGFα and 5 mM NAC. Control acinar cells transdifferentiate by day 5. NAC-treated acinar explants transdifferentiate by day 7. **(B)** Relative expression of NADPH-producing enzymes in control (ad-GFP) or *Kras^{G12D}*-expressing (ad-CRE) acinar cells collected days 1-3. n=3. **(C)** GSEA enrichment plot of PPP signature in *Kras^{G12D}*-expressing acinar cells. **(D)** Schematic of KCG^{mut} mice. **(E)** Relative amount of ^{14}C-labeld CO_2 derived from 1-^{14}C glucose. 1-$^{14}CO_2$ is generated from either oxidative PPP or the TCA cycle. **(F)** Relative amount of ^{14}C-labeld CO_2 derived from 6-^{14}C glucose. 6-$^{14}CO_2$ is only generated from the TCA cycle. Each point in E and F represents technical replicates from one mouse. G6PD, glucose-6-phosphate dehydrogenase; IDH1, isocitrate dehydrogenase 1; ME1, malic enzyme 1; MTHFD1, methylenetetrahydrofolate dehydrogenase 1, PGD, 6-phosphogluconate dehydrogenase. *, $P < 0.05$; **, $P < 0.01$; ***, $P < 0.001$; ns, not significant. One-way ANOVA (**B**).

rewired glutamine metabolism[13]. We generated a KC mouse model with G6PD-deficiency[41]: *Kras$^{LSL\text{-}G12D/+}$; Ptf1a$^{Cre/+}$; G6PD^{mut}* (KCG^{mut}) (**Fig. 2.4d**). G6PD-deficiency is an X-linked disorder and the most common gene mutation in the world[42]. Since oxidative PPP is the only source for NADPH in red blood cells, oxidative stressors can cause hemolytic anemia in patients. G6PD-deficient mouse models demonstrate enzyme activity with hemizygous, heterozygous, and homozygous mutations as 15-20%, 50-60%, and 15-20%, respectively[41,43].

To determine if oxidative PPP activity was decreased in our KCG^{mut} mice, we traced radioactive carbon incorporation into carbon dioxide (CO_2) that is produced from oxidative PPP and decarboxylation of pyruvate into the TCA cycle[13]. 1-^{14}C glucose labels CO_2 derived from oxidative PPP and the TCA cycle; 6-^{14}C glucose labels CO_2 derived from the TCA cycle and used as a control to determine oxidative PPP activity. As expected, G6PD-deficiency in KCG^{mut} acinar cells have decreased oxidative PPP flux, as measured by 1-$^{14}CO_2$, compared to mice with wild-type G6PD (KCG^{wt}), (**Fig. 2.4e**). TCA cycle flux was not affected, as measured by 6-$^{14}CO_2$, by G6PD status (**Fig. 2.4f**).

Decreasing oxidative PPP flux accelerates ADM and tumorigenesis

Since basal levels of ROS are increased during pancreatic tumorigenesis, glycolytic flux is reduced to shuttle intermediates into the oxidative PPP for NADPH generation, which is used to produce GSH and reduce ROS[26,44-47]. We hypothesized that decreasing oxidative PPP activity via mutant G6PD would promote Kras^{G12D}-driven ADM and tumorigenesis through increased ROS levels. Using primary acinar cells from KCG^{mut} and KCG^{wt} mice, we determined the rate of ADM is accelerated when oxidative PPP flux is decreased (**Fig. 2.5a,b**). We next determined whether the phenotype we saw *in vitro* recapitulates *in vivo*, as seen in other studies[8,9,26]. Mice from both cohorts were aged to 26 weeks—when low-grade PanINs (typically PanIN1a/b and occasionally PanIN2) are abundant in KC models[48]—and PanIN lesions were graded to determine the extent of tissue transformation. Like the accelerated rate of ADM in acinar explants, transformation of KCG^{mut} pancreata was significantly increased, although there is variability, consistent with previous reports using the KC model[48] (**Fig. 2.5c,d**). KCG^{mut} pancreata, unlike

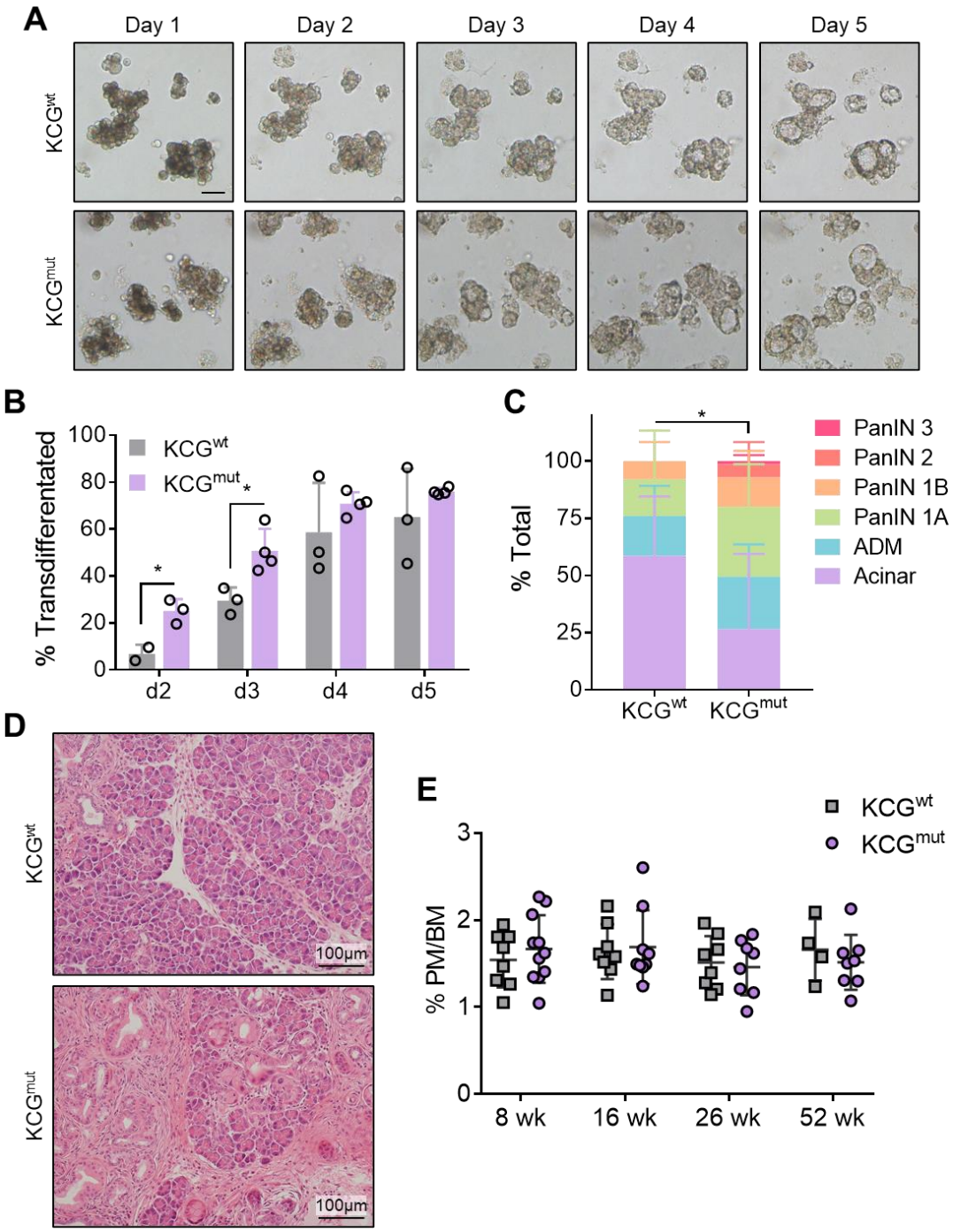

Figure 2.5 G6PD-deficiency accelerates Kras^{G12D}-driven ADM and tumorigenesis. **(A)** Representative images of KCG^{wt} and KCG^{mut} acinar cells. Acinar explants undergo ADM over the course of 5 days. **(B)** Quantification of ductal structures formed in collagen. Each point represents average of 3 technical replicates from independent mice. **(C)** Lesion grading of pancreata from 26-week-old KCG^{wt} and KCG^{mut} mice. KCG^{wt} n=5; KCG^{mut} n=7. **(D)** Representative hematoxylin and eosin (H&E) staining of pancreas tissue from 26-week-old KCG^{wt} and KCG^{mut} mice. **(E)** Percent ratio of pancreas mass to body mass (% PM/BM) from KCG^{wt} and KCG^{mut} mice collected at 8, 16, 26, and 52 weeks (wk). Scale bar = 50 μm unless otherwise noted. *, $P < 0.05$. Student's t-test (unpaired, two-tailed) (**B,E**); Two-way ANOVA (**C**).

KCG^{wt}, contain PanIN2 and high-grade PanIN3 lesions (**Fig. 2.5c**). Additional cohorts were aged to 8, 16, and 52 weeks. While there is no difference in the ratio of pancreas mass to body mass (PM/BM)—an indirect measure of tissue transformation—between KCG^{mut} and KCG^{wt} mice (**Fig. 2.5e**), detailed histological analysis needs to be completed to determine if accelerated tumorigenesis due to G6PD-deficiency is consistent at other time points during tumor development. Taken together, this data suggests decreasing oxidative PPP through G6PD mutation accelerates ADM *in vitro* and tumorigenesis *in vivo*.

G6PD-deficiency does not affect PDA survival

Most KC mice do not develop invasive carcinoma[48]. Pancreas-specific expression of *Kras^{G12D}* and an additional loss of tumor suppressor *Tp53—Kras$^{LSL\text{-}G12D/+}$; Tp53$^{LSL\text{-}R172H/+}$; Ptf1a$^{Cre/+}$* (KPC)—increases tumorigenesis, promotes invasive carcinoma and metastasis, and decreases survival[49]. We generated KPC mice with G6PD-deficiency (**Fig. 2.6a**) to determine if accelerated tumorigenesis enhances invasive PDA and decreases survival. At 90 days old, there is no difference in the PM/BM ratio between KPCG^{mut} and KPCG^{wt} mice (**Fig. 2.6b**) and there is no statistically significant difference in survival (**Fig. 2.6c**). Longitudinal studies are still on-going and histological analysis of 90-day-old mice will reveal if there are differences in tumor development. While G6PD-deficiency accelerates tumorigenesis KC mice, our current data indicate overall survival is not affected in the accelerated KPC background.

Discussion

In this study, we determined metabolic requirements for ADM. We used an *in vitro* ADM model to show that primary acinar cells require glucose to survive and undergo ADM. Surprisingly, acinar cells only need subphysiological concentrations of glucose to transdifferentiate. We also found that glutamine or BCAA supplementation is dispensable ADM, indicating these anaplerotic substrates may not be fueling the TCA cycle at this early point in tumorigenesis, that intracellular fuel sources (e.g. generated by autophagy) predominate, or that considerable redundancy in metabolic fuel selection exists. Since ADM needed very low concentrations of glucose, and did not require glutamine or BCAA, we questioned how reliant acinar cells were on mitochondrial metabolism, specifically

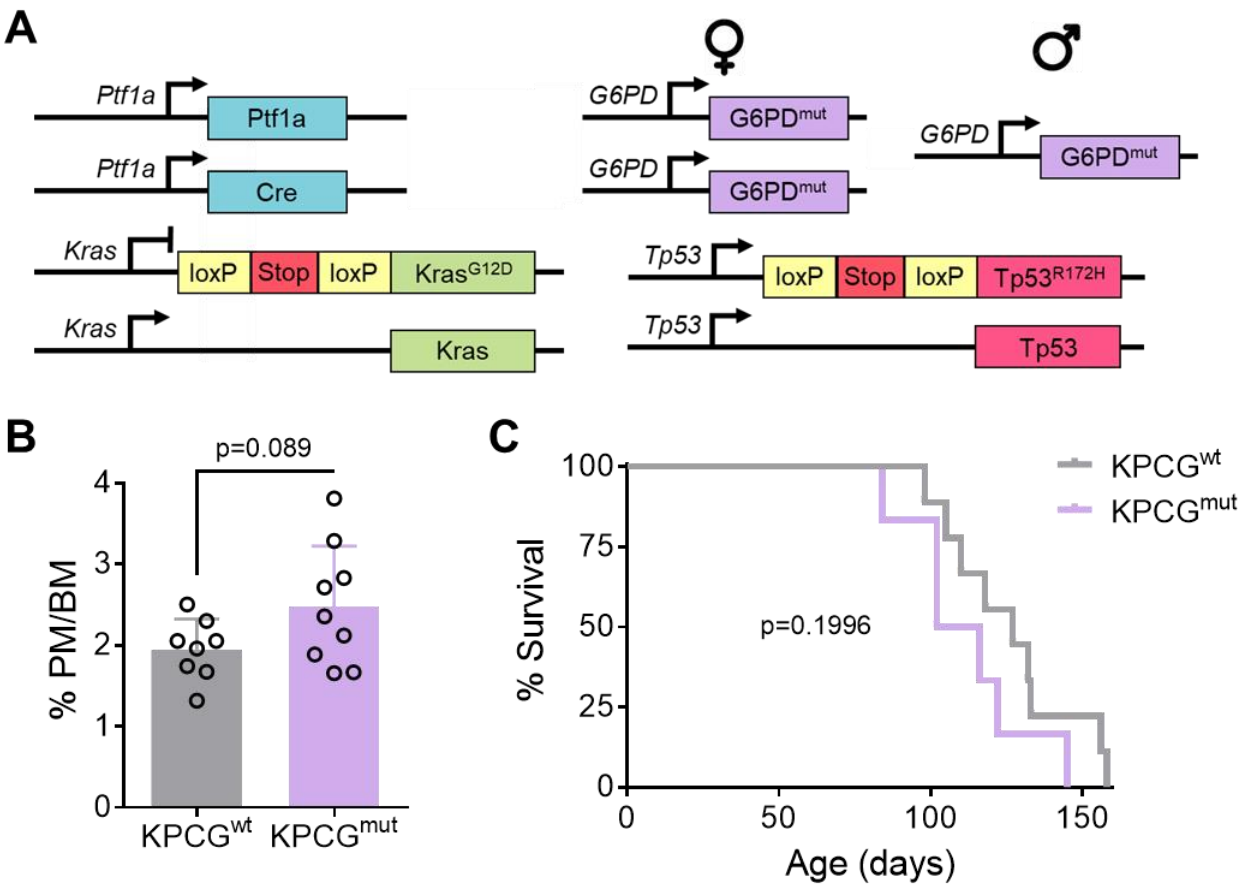

Figure 2.6 G6PD-deficiency does not decrease overall survival. (A) Schematic of KPCG^{mut} mice. **(B)** Percent ratio of pancreas mass to body mass (% PM/BM) from 90-day-old KPCG^{wt} and KPCG^{mut} mice. KPCG^{wt} n=8; KPCG^{mut} n=9. **(C)** Kaplan–Meier survival curve of KPCG^{wt} and KPCG^{mut} mice. KPCG^{wt} n=9; KPCG^{mut} n=6.

oxidative phosphorylation. When we blocked oxidative phosphorylation with oligomycin, primary acinar cells died within 24 hours, even when embedded in Matrigel which elicits a strong ADM response. Our data indicates glucose may be feeding into the TCA cycle and acinar cells are profoundly sensitive to disruptions of oxidative phosphorylation. Since acinar cells require glucose and recent evidence has shown the oxidative PPP plays an important role during ADM[44], we impeded oxidative PPP flux by introducing G6PD-deficiency into KC mice. KCG^{mut} acinar cells transdifferentiate at an accelerated rate *in vitro*, which was reproduced *in vivo* with KCG^{mut} mice showing augmented tumorigenesis. Although G6PD-deficiency accelerates tumorigenesis, we cannot yet conclude whether this impacts overall survival.

Metabolic reprograming in PDA cells, mediated by mutant KRAS, increases glucose uptake to fuel anabolic pathways that shuttle off glycolysis and rewire glutamine metabolism to fuel the TCA cycle[13,14]. We sought to understand how metabolism supports ADM. Compared to the metabolic reprogramming needed for PDA tumor maintenance[12], much less is known about metabolic requirements of tumorigenesis. Like PDA cells, primary acinar cells require glucose to survive. Surprisingly, 1:100 the concentration of glucose used in culture media was sufficient for acinar cell survival and transdifferentiation. This concentration is also well below physiological levels of glucose[28,29]. Mutant KRAS has been shown to rewire acetyl-CoA metabolism to support ADM by utilizing glucose to generate acetyl-CoA for cholesterol synthesis and histone acetylation. Lack of glucose likely negatively affects these processes that are required for ADM[25].

Cultured PDA cells are dependent on glutamine and rewire glutamine metabolism to fuel mitochondrial metabolism and maintain redox homeostasis[14]. In contrast, we found primary acinar cells not only survive without glutamine supplementation, they also do not require it for transdifferentiating. Glutamine, along with glucose, is a major fuel source for cells and contributes to biosynthetic precursors used in protein, lipid, and nucleotide synthesis and energy production. Although not required for ADM, glutamine likely becomes an important substrate during tumorigenesis to support tumor maintenance.

BCAAs are another anaplerotic source that can fuel the TCA cycle in normal cells. BCAAs are also used to generate precursors for fatty acid synthesis and can be directly incorporated into proteins[50]. Similar to glutamine, we found exogenous BCAAs are dispensable for ADM of acinar explants. This was somewhat surprising because *Kras*^{G12D}-expressing acinar cells utilize leucine as a major source for generating acetyl-CoA to support ADM[25]. Recent evidence shows differentiating adipocytes catabolize BCAA to fuel the TCA cycle and generate acetyl-CoA for lipogenesis, while pre-adipocytes utilize glucose and glutamine[51]. In the absence of BCAAs, dedifferentiating acinar cells may be able to catabolize glucose and/or glutamine to generate acetyl-CoA. Similar to the differentiated state of adipocytes, normal pancreatic tissue shows high rates of BCAA metabolism and incorporation of BCAAs into the TCA cycle[32,52].

Normal cells utilize glucose to fuel mitochondrial metabolism for ATP generation. Since ADM occurred with very low concentrations of glucose and did not require glutamine or BCAA supplementation, we wanted to determine how reliant acinar cells are on oxidative phosphorylation. We found acinar cells are extremely sensitive to ATP synthase inhibition with low nanomolar concentrations of oligomycin, in stark contrast to the low micromolar concentrations PDA cells can tolerate[34]. Interestingly, a subpopulation of tumor-initiating cells (TICs) that survive KRAS ablation in PDA tumors are more dependent on mitochondrial metabolism and are unable to compensate for ATP generation through glycolysis upon oxidative phosphorylation inhibition[53]. This subpopulation is as sensitive to nanomolar concentrations of oligomycin as acinar explants—dramatically reducing cell viability within 24 hours. This may suggest metabolic pathways that govern mutant Kras-driven ADM are relevant in TICs that give rise to tumor recurrence. Oligomycin is generally well tolerated in *in vivo* mouse models[53,54] so the sensitivity seen in treated *Kras*^{G12D}-expressing acinar cells could be from heightened demand of energy or increased induction of ROS resulting in death.

While basal ROS levels are elevated in malignant cells for increased mitogenic signaling and from increased metabolism, antioxidant programs must be initiated to maintain pro-tumorigenic levels of ROS. Kras^{G12D} elevates both ROS production and antioxidant pathways during ADM and pancreatic tumorigenesis[26,27]. We and others show antioxidant treatment impedes ADM *in vitro* and tumorigenesis *in vivo* by lowering ROS levels[26,55]. In contrast, abrogating antioxidant response through genetic deletion of NRF2, a primary antioxidant regulator, causes exceedingly high levels of ROS that induce cellular senescence[27]. An important effector of the antioxidant response during pancreatic tumorigenesis is *TP53*-induced glycolysis and apoptosis regulator (TIGAR), which maintains ROS levels by promoting glycolytic flux into the oxidative PPP for NADPH generation[44]. We inhibited oxidative PPP flux through mutation of *G6pd*, the first and rate limiting step of oxidative PPP. G6PD-deficiency increased the rate of ADM in acinar explants and tumorigenesis in KC mice. We believe this acceleration is due to increased oxidative stress from decreased production of NADPH-derived glutathione, though further analysis is required. Mutant G6PD accelerates tumorigenesis in KC mice and has a modest, but non-statistically significant, impact on overall survival in KPC mice. PDA cells

display less dependence on the oxidative PPP by rewiring glutamine metabolism to generate NADPH and uncoupling the nonoxidative PPP branch to generate nucleotide precursors[13,14]. In more advanced stages of tumor development, G6PD-deficiency may no longer provide an advantage once glutamine metabolism is reprogrammed to produce NADPH.

Pancreatic cancer is among the most lethal cancers[2]. There is a need for early disease detection methods and more effective therapies to improve the dismal prognosis patients face. Historically, KRAS has proven notoriously difficult to target pharmacologically[56]. However, a recently developed inhibitor against $Kras^{G12C}$ has shown promise in preclinical models and clinical trials[57,58]. Unfortunately, G12C mutations are found in only 2% of PDA patients[59]. Since oncogenic KRAS is the driving mutation for PDA development and maintenance, KRAS-dependent pathways, including metabolic, remain promising targets for the development of new therapeutics[60,61]. Understanding the metabolic pathways that initiate PDA could reveal vulnerabilities in established tumors that can be exploited for treatment or reveal biomarkers for diagnosis of early disease[25,62].

Materials and Methods

Mouse Strains

All animal studies were performed in accordance with the guidelines of Institutional Animal Care and Use Committee (IACUC) and approved protocols. *$Kras^{LSL\text{-}G12D/+}$*, *$Ptf1a^{Cre/+}$*, *$Tp53^{LSL\text{-}R172H/+}$*, and *$G6PD^{mut}$* mice have been previously described[41,43,48,63,64]. *$Kras^{LSL\text{-}G12D/+}$; $Ptf1a^{Cre/+}$* (KC) mice were maintained on a C57BL/6 background. *$Kras^{LSL\text{-}G12D/+}$; $Ptf1a^{Cre/+}$; G6PD* (KCG) and *$Kras^{LSL\text{-}G12D/+}$; $Tp53^{LSL\text{-}R172H/+}$; $Ptf1a^{Cre/+}$; G6PD* (KPCG) mice were maintained on a mixed background.

RNA isolation and purification from primary acinar cell cultures

Primary acinar cell cultures were harvested by pelleting the cells by centrifugation for 2 minutes at 300 g. The pellet was washed once with ice cold DPBS. Then the pellet was lysed in RLT+ buffer containing 1% β-mercaptoethanol (Sigma, M6250), which was then passed through a Qiashredder column (Qiagen, 79654). RNA was then purified using an RNeasy Plus Mini Kit (Qiagen, 74136) using gDNA eliminator columns to remove genomic DNA. RNA was then analyzed on a Nanodrop 2000c (Thermo Scientific)

spectrophotometer for quantification, and purity was assessed based on the A^{260}/A^{280} ratio. RNA quality was further assessed using a total RNA kit on a 2100 Bioanalyzer (Agilent Technologies) and using the generated RIN number to determine quality, and all samples sequenced had a RIN greater than 7.5. 1ug of each sample was submitted to the Mayo Clinic Genome Analysis Core, and transcriptomics libraries and data were generated and processed through their core pipelines. Raw gene counts were normalized to RPKM (Reads Per Kilobase of transcript, per Million mapped reads) for GSEA and expression analysis.

Gene Set Enrichment Analysis (GSEA)

Transcriptomic data was analyzed with GSEA 4.0.3 software using Hallmark Pathways h.all.v7.1, KEGG Signaling Pathways c2.cp.kegg.v7.1, and Mouse Gene Symbol Remapping to Human Orthologs MSigDB.v7.1 chip.

Three-dimensional Acinar Cell Explant Culture

Pancreas was harvested and rinsed twice in 5 mL cold HBSS (Gibco, 14170112). Tissue was minced with sterile scissors into 1-5 mm sized pieces then centrifuged for 2 minutes at 300 g and 4ºC. Media was aspirated and minced tissue was digested with ~5 mg of Collagenase P (Roche) in 5 mL cold HBSS for 15-18 minutes, shaking at 100 rpm at 37ºC. Collagenase P was inhibited by addition of 5 mL cold 5% FBS in HBSS. Cells were centrifuged for 2 minutes at 300 g and 4ºC then washed with 5 mL cold 5% FBS in HBSS. This was repeated twice more. Cells were passed through 500 µm polypropylene mesh (Pluriselect, Fisher, NC0822591). Mesh was washed with 5 mL cold 5% FBS in HBSS. Cells were passed through 100 µm polypropylene mesh (Fisherbrand, 22363549) then pelleted through 10 mL of 30% fetal bovine serum gradient. Cells were resuspended in media and incubated at 37ºC for 2-4 hours prior to embedding. All media was supplemented with 0.4 mg/mL soybean trypsin inhibitor (Gibco, 17075-029), 1 ug/mL dexamethasone (Sigma, D4902), and 0.5% gentamicin (Lonza, 17-519L). All media was adjusted to final pH 7.2-7.4 at 37ºC and sterilized through a 0.22 µm PVDF membrane (Millipore, Stericup Filter Unit, SCGVU01RE; Steriflip Filter Unit, SE1M179M6). Unless indicated, cells were cultured in 1x Waymouth's media (Sigma, W1625) supplemented with 2.2 g/L sodium bicarbonate (Sigma, S5761). Glucose and glutamine dropout media

were prepared from DMEM powder without glucose or glutamine (Sigma, D5030) supplemented with 3.7 g/L sodium bicarbonate and 25 mM D-glucose (Sigma, G7021) or 4 mM L-glutamine (Gibco, A2916801). Branch-chained amino acid (BCAA) dropout media was prepared using DMEM base powder (US Biological Life Sciences, D9800-26) supplemented with 25 mM D-glucose, 4 mM L-glutamine, 30 mg/L glycine (Sigma, G8790), 84 mg/L L-arginine (Sigma, A8094), 63 mg/L L-cystine (Sigma, C6727), 42 mg/L L-histidine (Sigma, H5659), 146 mg/L L-lysine (Sigma, L8662), 30 mg/L L-methionine (Sigma, M5308), 66 mg/L L-phenylalanine (Sigma, P5482), 42 mg/L L-serine (Sigma, S4311), 95 mg/L L-threonine (Sigma, T8441), 16 mg/L L-tryptophan (Sigma, T8941), and 104 mg/L L-tyrosine (Sigma, T1145). Control media contained 105 mg/L L-isoleucine (Sigma, I7403), 105 mg/L L-leucine (Sigma, L8912), and 94 mg/L L-valine (Sigma, V0513). Acinar cells were embedded in bovine collagen (Culturex, 344205001) according to the manufacturer's protocol or in Matrigel (Corning, 354234). Culture media was added on top of solidified matrix and changed on days 1, 3, and 5 after plating. Oligomycin A (Sigma, 75351) and N-acetyl cysteine (Sigma, A9165) were used at indicated concentrations.

Live/Dead Staining of Acinar Explants

Media was removed from wells containing collagen-embedded acinar explants. Embedded explants were washed twice with 500 µL PBS (Gibco, 10010023). Cells were incubated with 0.015 mg/mL fluorescein diacetate (FDA) (Sigma, F7378-5G) and 0.0046 mg/mL propidium iodide solution (PI) (Sigma, P4864) in PBS for 10 minutes at 37ºC. Wells were washed twice with 500 µL PBS. 500 µL PBS was added to the well prior to imaging. This procedure was performed on two wells at a time.

^{14}C glucose incorporation into CO_2

Cells were treated with 1 µCi 1-^{14}C (Perkin Elmer, NEC043X050UC) or 6-^{14}C glucose (Perkin Elmer, NEC045X050UC) and incubated at 37ºC for 4 hours. To release $^{14}CO_2$, 150 mL of 3 M perchloric acid (Sigma, 244252) was added to each well and immediately covered with phenylethylamine (Sigma, P6513) saturated Whatman paper and incubated at room temperature overnight. The Whatman paper was then analyzed by scintillation counting (Beckman, LS6500) and normalized to surrogate protein quantification.

Histology

Mice were sacrificed by CO_2 asphyxiation then tissue was quickly harvested and fixed overnight at room temperature with zinc formalin fixative (Z-Fix, Anatech LTD, 174). Tissues were processed using a Leica ASP300S Tissue Processor (Leica Microsystems Inc), paraffin embedded, and cut into 5 μm sections. Hematoxylin and eosin (H&E) staining was performed using Mayer's hematoxylin solution and Eosin Y (Thermo Fisher Scientific, HT110116). Slides were scanned with a Pannoramic SCAN scanner (Perkin Elmer). For tissue grading, 3 images were taken per slide at 20x magnification in a blinded manner and graded by a pathologist in a blinded manner.

Statistical Analysis

Statistics were calculated using GraphPad Prism 7. Groups of 2 were analyzed with two-tailed students t-test, groups greater than 2 with a single variable were compared using one-way ANOVA analysis with Tukey post hoc test, and groups greater than two multiple variables were compared with two-way ANOVA with Tukey post hoc test. A Student’s t-test (unpaired, two-tailed) was performed when comparing two groups to each other. Survival analysis was performed using log-rank (Mantel–Cox) test. All data are presented as mean ± s.d. (standard deviation).

Table 2.1 GSEA Hallmark Signatures Enriched in *Kras^{G12D}*-driven ADM

Rank	Gene Set	NES	FDR
1	ANGIOGENESIS	1.51	0.37
2	EPITHELIAL_MESENCHYMAL_TRANSITION	1.50	0.23
3	FATTY_ACID_METABOLISM	1.41	0.34
4	APICAL_SURFACE	1.41	0.27
5	COAGULATION	1.40	0.24
6	HYPOXIA	1.40	0.20
7	MYOGENESIS	1.40	0.18
8	GLYCOLYSIS	1.40	0.17
9	REACTIVE_OXYGEN_SPECIES_PATHWAY	1.37	0.18
10	OXIDATIVE_PHOSPHORYLATION	1.37	0.17
12	MTORC1_SIGNALING	1.36	0.16
14	PEROXISOME	1.34	0.17
20	P53_PATHWAY	1.27	0.25
21	CHOLESTEROL_HOMEOSTASIS	1.27	0.24
24	INFLAMMATORY_RESPONSE	1.24	0.24
25	KRAS_SIGNALING_UP	1.24	0.23

Table 2.2 GSEA KEGG Pathway Signatures Enriched in *Kras^{G12D}*-driven ADM

Rank	Gene Set	NES	FDR
1	O_GLYCAN_BIOSYNTHESIS	1.90	0.06
2	GLYCOSPHINGOLIPID_BIOSYNTHESIS_GANGLIO_SERIES	1.83	0.06
3	BIOSYNTHESIS_OF_UNSATURATED_FATTY_ACIDS	1.72	0.09
4	OTHER_GLYCAN_DEGRADATION	1.70	0.08
5	ECM_RECEPTOR_INTERACTION	1.70	0.08
6	GLYCOSAMINOGLYCAN_DEGRADATION	1.66	0.08
7	GALACTOSE_METABOLISM	1.63	0.09
8	TYPE_I_DIABETES_MELLITUS	1.62	0.08
9	NITROGEN_METABOLISM	1.58	0.09
10	PENTOSE_PHOSPHATE_PATHWAY	1.57	0.09
15	GLYCEROPHOSPHOLIPID_METABOLISM	1.50	0.14
17	PYRUVATE_METABOLISM	1.47	0.15
20	LYSOSOME	1.46	0.14
22	FATTY_ACID_METABOLISM	1.45	0.15
28	OXIDATIVE_PHOSPHORYLATION	1.43	0.14
32	GLYCEROLIPID_METABOLISM	1.41	0.16
35	LYSINE_DEGRADATION	1.39	0.17
39	ARGININE_AND_PROLINE_METABOLISM	1.38	0.18
44	GLYCOLYSIS_GLUCONEOGENESIS	1.36	0.18
52	CALCIUM_SIGNALING_PATHWAY	1.33	0.20
53	CITRATE_CYCLE_TCA_CYCLE	1.32	0.21
56	GLYCINE_SERINE_AND_THREONINE_METABOLISM	1.31	0.20
59	AMINO_SUGAR_AND_NUCLEOTIDE_SUGAR_METABOLISM	1.31	0.20
60	GLUTATHIONE_METABOLISM	1.30	0.21
65	PEROXISOME	1.29	0.23
74	CYSTEINE_AND_METHIONINE_METABOLISM	1.25	0.25

Top 10 plus selected GSEA Hallmark (**Table 2.1**) and KEGG Pathway (**Table 2.2**) signatures enriched in *Kras^{G12D}*-expressing acinar cells undergoing ADM. GSEA analysis of transcriptomics from day 1 ad-GFP and day 2 ad-CRE acinar explants. Gene sets ranked according to their normalized gene enrichment score (NES), signifying the degree a gene set is overrepresented at the top or bottom of a ranked list of genes. The false discovery rate (FDR) is the estimated probability a gene set with a given NES represents a false positive finding.

References

1 Kleeff, J. *et al.* Pancreatic cancer. *Nature reviews. Disease primers* **2**, 16022, doi:10.1038/nrdp.2016.22 (2016).

2 Siegel, R. L., Miller, K. D. & Jemal, A. Cancer statistics, 2020. *CA: a cancer journal for clinicians* **70**, 7-30, doi:10.3322/caac.21590 (2020).

3 Shi, C. *et al.* KRAS2 mutations in human pancreatic acinar-ductal metaplastic lesions are limited to those with PanIN: implications for the human pancreatic cancer cell of origin. *Molecular cancer research : MCR* **7**, 230-236, doi:10.1158/1541-7786.mcr-08-0206 (2009).

4 Means, A. L. & Leach, S. D. Lineage commitment and cellular differentiation in exocrine pancreas. *Pancreatology : official journal of the International Association of Pancreatology (IAP) ... [et al.]* **1**, 587-596, doi:10.1159/000055868 (2001).

5 Kopp, J. L. *et al.* Identification of Sox9-dependent acinar-to-ductal reprogramming as the principal mechanism for initiation of pancreatic ductal adenocarcinoma. *Cancer cell* **22**, 737-750, doi:10.1016/j.ccr.2012.10.025 (2012).

6 Storz, P. Acinar cell plasticity and development of pancreatic ductal adenocarcinoma. *Nature reviews. Gastroenterology & hepatology* **14**, 296-304, doi:10.1038/nrgastro.2017.12 (2017).

7 Collins, M. A. *et al.* Oncogenic Kras is required for both the initiation and maintenance of pancreatic cancer in mice. *J Clin Invest* **122**, 639-653, doi:10.1172/jci59227 (2012).

8 Ardito, C. M. *et al.* EGF receptor is required for KRAS-induced pancreatic tumorigenesis. *Cancer cell* **22**, 304-317, doi:10.1016/j.ccr.2012.07.024 (2012).

9 Collins, M. A., Yan, W., Sebolt-Leopold, J. S. & Pasca di Magliano, M. MAPK signaling is required for dedifferentiation of acinar cells and development of pancreatic intraepithelial neoplasia in mice. *Gastroenterology* **146**, 822-834.e827, doi:10.1053/j.gastro.2013.11.052 (2014).

10 Halbrook, C. J. *et al.* Mitogen-activated Protein Kinase Kinase Activity Maintains Acinar-to-Ductal Metaplasia and Is Required for Organ Regeneration in Pancreatitis. *Cellular and molecular gastroenterology and hepatology* **3**, 99-118, doi:10.1016/j.jcmgh.2016.09.009 (2017).

11 Vander Heiden, M. G., Cantley, L. C. & Thompson, C. B. Understanding the Warburg effect: the metabolic requirements of cell proliferation. *Science (New York, N.Y.)* **324**, 1029-1033, doi:10.1126/science.1160809 (2009).

12 Halbrook, C. J. & Lyssiotis, C. A. Employing Metabolism to Improve the Diagnosis and Treatment of Pancreatic Cancer. *Cancer cell* **31**, 5-19, doi:10.1016/j.ccell.2016.12.006 (2017).

13 Ying, H. *et al.* Oncogenic Kras maintains pancreatic tumors through regulation of anabolic glucose metabolism. *Cell* **149**, 656-670, doi:10.1016/j.cell.2012.01.058 (2012).

14 Son, J. *et al.* Glutamine supports pancreatic cancer growth through a KRAS-regulated metabolic pathway. *Nature* **496**, 101-105, doi:10.1038/nature12040 (2013).

15 Nelson, B. S. *et al.* Tissue of origin dictates GOT1 dependence and confers synthetic lethality to radiotherapy. *Cancer & metabolism* **8**, 1, doi:10.1186/s40170-019-0202-2 (2020).
16 Storz, P. & Crawford, H. C. Carcinogenesis of Pancreatic Ductal Adenocarcinoma. *Gastroenterology* **158**, 2072-2081, doi:10.1053/j.gastro.2020.02.059 (2020).
17 Subramanian, A. *et al.* Gene set enrichment analysis: a knowledge-based approach for interpreting genome-wide expression profiles. *Proc Natl Acad Sci U S A* **102**, 15545-15550, doi:10.1073/pnas.0506580102 (2005).
18 Mootha, V. K. *et al.* PGC-1alpha-responsive genes involved in oxidative phosphorylation are coordinately downregulated in human diabetes. *Nat Genet* **34**, 267-273, doi:10.1038/ng1180 (2003).
19 Rhim, A. D. *et al.* EMT and dissemination precede pancreatic tumor formation. *Cell* **148**, 349-361, doi:10.1016/j.cell.2011.11.025 (2012).
20 Lee, K. E. *et al.* Hif1a Deletion Reveals Pro-Neoplastic Function of B Cells in Pancreatic Neoplasia. *Cancer discovery* **6**, 256-269, doi:10.1158/2159-8290.cd-15-0822 (2016).
21 Criscimanna, A. *et al.* PanIN-specific regulation of Wnt signaling by HIF2α during early pancreatic tumorigenesis. *Cancer research* **73**, 4781-4790, doi:10.1158/0008-5472.can-13-0566 (2013).
22 Rosenfeldt, M. T. *et al.* p53 status determines the role of autophagy in pancreatic tumour development. *Nature* **504**, 296-300, doi:10.1038/nature12865 (2013).
23 Diakopoulos, K. N. *et al.* Impaired autophagy induces chronic atrophic pancreatitis in mice via sex- and nutrition-dependent processes. *Gastroenterology* **148**, 626-638.e617, doi:10.1053/j.gastro.2014.12.003 (2015).
24 Guerra, C. *et al.* Chronic pancreatitis is essential for induction of pancreatic ductal adenocarcinoma by K-Ras oncogenes in adult mice. *Cancer cell* **11**, 291-302, doi:10.1016/j.ccr.2007.01.012 (2007).
25 Carrer, A. *et al.* Acetyl-CoA Metabolism Supports Multistep Pancreatic Tumorigenesis. *Cancer discovery* **9**, 416-435, doi:10.1158/2159-8290.cd-18-0567 (2019).
26 Liou, G. Y. *et al.* Mutant KRas-Induced Mitochondrial Oxidative Stress in Acinar Cells Upregulates EGFR Signaling to Drive Formation of Pancreatic Precancerous Lesions. *Cell reports* **14**, 2325-2336, doi:10.1016/j.celrep.2016.02.029 (2016).
27 DeNicola, G. M. *et al.* Oncogene-induced Nrf2 transcription promotes ROS detoxification and tumorigenesis. *Nature* **475**, 106-109, doi:10.1038/nature10189 (2011).
28 Sullivan, M. R. *et al.* Quantification of microenvironmental metabolites in murine cancers reveals determinants of tumor nutrient availability. *eLife* **8**, doi:10.7554/eLife.44235 (2019).
29 Röder, P. V., Wu, B., Liu, Y. & Han, W. Pancreatic regulation of glucose homeostasis. *Experimental & molecular medicine* **48**, e219, doi:10.1038/emm.2016.6 (2016).
30 Vander Heiden, M. G. Targeting cancer metabolism: a therapeutic window opens. *Nature reviews. Drug discovery* **10**, 671-684, doi:10.1038/nrd3504 (2011).

31 Shi, G. *et al.* Maintenance of acinar cell organization is critical to preventing Kras-induced acinar-ductal metaplasia. *Oncogene* **32**, 1950-1958, doi:10.1038/onc.2012.210 (2013).
32 Neinast, M. D. *et al.* Quantitative Analysis of the Whole-Body Metabolic Fate of Branched-Chain Amino Acids. *Cell Metab* **29**, 417-429.e414, doi:10.1016/j.cmet.2018.10.013 (2019).
33 Martínez-Reyes, I. & Chandel, N. S. Mitochondrial TCA cycle metabolites control physiology and disease. *Nature communications* **11**, 102, doi:10.1038/s41467-019-13668-3 (2020).
34 Shukla, S. K. *et al.* MUC1 and HIF-1alpha Signaling Crosstalk Induces Anabolic Glucose Metabolism to Impart Gemcitabine Resistance to Pancreatic Cancer. *Cancer cell* **32**, 71-87.e77, doi:10.1016/j.ccell.2017.06.004 (2017).
35 Sullivan, L. B. & Chandel, N. S. Mitochondrial reactive oxygen species and cancer. *Cancer & metabolism* **2**, 17, doi:10.1186/2049-3002-2-17 (2014).
36 Schieber, M. & Chandel, N. S. ROS function in redox signaling and oxidative stress. *Curr Biol* **24**, R453-462, doi:10.1016/j.cub.2014.03.034 (2014).
37 Stanton, R. C. Glucose-6-phosphate dehydrogenase, NADPH, and cell survival. *IUBMB life* **64**, 362-369, doi:10.1002/iub.1017 (2012).
38 Chen, L. *et al.* NADPH production by the oxidative pentose-phosphate pathway supports folate metabolism. *Nature metabolism* **1**, 404-415 (2019).
39 Fan, J. *et al.* Quantitative flux analysis reveals folate-dependent NADPH production. *Nature* **510**, 298-302, doi:10.1038/nature13236 (2014).
40 Lewis, C. A. *et al.* Tracing compartmentalized NADPH metabolism in the cytosol and mitochondria of mammalian cells. *Mol Cell* **55**, 253-263, doi:10.1016/j.molcel.2014.05.008 (2014).
41 Pretsch, W., Charles, D. J. & Merkle, S. X-linked glucose-6-phosphate dehydrogenase deficiency in Mus musculus. *Biochemical genetics* **26**, 89-103, doi:10.1007/bf00555491 (1988).
42 Stincone, A. *et al.* The return of metabolism: biochemistry and physiology of the pentose phosphate pathway. *Biological reviews of the Cambridge Philosophical Society* **90**, 927-963, doi:10.1111/brv.12140 (2015).
43 Nicol, C. J., Zielenski, J., Tsui, L. C. & Wells, P. G. An embryoprotective role for glucose-6-phosphate dehydrogenase in developmental oxidative stress and chemical teratogenesis. *FASEB journal : official publication of the Federation of American Societies for Experimental Biology* **14**, 111-127, doi:10.1096/fasebj.14.1.111 (2000).
44 Cheung, E. C. *et al.* Dynamic ROS Control by TIGAR Regulates the Initiation and Progression of Pancreatic Cancer. *Cancer cell* **37**, 168-182.e164, doi:10.1016/j.ccell.2019.12.012 (2020).
45 Bensaad, K. *et al.* TIGAR, a p53-inducible regulator of glycolysis and apoptosis. *Cell* **126**, 107-120, doi:10.1016/j.cell.2006.05.036 (2006).
46 Yin, L., Kosugi, M. & Kufe, D. Inhibition of the MUC1-C oncoprotein induces multiple myeloma cell death by down-regulating TIGAR expression and depleting NADPH. *Blood* **119**, 810-816, doi:10.1182/blood-2011-07-369686 (2012).

47 Bensaad, K., Cheung, E. C. & Vousden, K. H. Modulation of intracellular ROS levels by TIGAR controls autophagy. *The EMBO journal* **28**, 3015-3026, doi:10.1038/emboj.2009.242 (2009).
48 Hingorani, S. R. *et al.* Preinvasive and invasive ductal pancreatic cancer and its early detection in the mouse. *Cancer cell* **4**, 437-450, doi:10.1016/s1535-6108(03)00309-x (2003).
49 Hingorani, S. R. *et al.* Trp53R172H and KrasG12D cooperate to promote chromosomal instability and widely metastatic pancreatic ductal adenocarcinoma in mice. *Cancer cell* **7**, 469-483, doi:10.1016/j.ccr.2005.04.023 (2005).
50 Neinast, M., Murashige, D. & Arany, Z. Branched Chain Amino Acids. *Annual review of physiology* **81**, 139-164, doi:10.1146/annurev-physiol-020518-114455 (2019).
51 Green, C. R. *et al.* Branched-chain amino acid catabolism fuels adipocyte differentiation and lipogenesis. *Nat Chem Biol* **12**, 15-21, doi:10.1038/nchembio.1961 (2016).
52 Mayers, J. R. *et al.* Tissue of origin dictates branched-chain amino acid metabolism in mutant Kras-driven cancers. *Science (New York, N.Y.)* **353**, 1161-1165, doi:10.1126/science.aaf5171 (2016).
53 Viale, A. *et al.* Oncogene ablation-resistant pancreatic cancer cells depend on mitochondrial function. *Nature* **514**, 628-632, doi:10.1038/nature13611 (2014).
54 Franchi, L. *et al.* Inhibiting Oxidative Phosphorylation In Vivo Restrains Th17 Effector Responses and Ameliorates Murine Colitis. *Journal of immunology (Baltimore, Md. : 1950)* **198**, 2735-2746, doi:10.4049/jimmunol.1600810 (2017).
55 Al Saati, T. *et al.* Oxidative stress induced by inactivation of TP53INP1 cooperates with KrasG12D to initiate and promote pancreatic carcinogenesis in the murine pancreas. *Am J Pathol* **182**, 1996-2004, doi:10.1016/j.ajpath.2013.02.034 (2013).
56 Cox, A. D., Fesik, S. W., Kimmelman, A. C., Luo, J. & Der, C. J. Drugging the undruggable RAS: Mission possible? *Nature reviews. Drug discovery* **13**, 828-851, doi:10.1038/nrd4389 (2014).
57 Canon, J. *et al.* The clinical KRAS(G12C) inhibitor AMG 510 drives anti-tumour immunity. *Nature* **575**, 217-223, doi:10.1038/s41586-019-1694-1 (2019).
58 Misale, S. *et al.* KRAS G12C NSCLC Models Are Sensitive to Direct Targeting of KRAS in Combination with PI3K Inhibition. *Clin Cancer Res* **25**, 796-807, doi:10.1158/1078-0432.ccr-18-0368 (2019).
59 Bailey, P. *et al.* Genomic analyses identify molecular subtypes of pancreatic cancer. *Nature* **531**, 47-52, doi:10.1038/nature16965 (2016).
60 Kempf, E., Rousseau, B., Besse, B. & Paz-Ares, L. KRAS oncogene in lung cancer: focus on molecularly driven clinical trials. *European respiratory review : an official journal of the European Respiratory Society* **25**, 71-76, doi:10.1183/16000617.0071-2015 (2016).
61 Bryant, K. L. & Der, C. J. Blocking autophagy to starve pancreatic cancer. *Nature reviews. Molecular cell biology* **20**, 265, doi:10.1038/s41580-019-0120-8 (2019).
62 Mayers, J. R. *et al.* Elevation of circulating branched-chain amino acids is an early event in human pancreatic adenocarcinoma development. *Nature medicine* **20**, 1193-1198, doi:10.1038/nm.3686 (2014).

CHAPTER 3

Tissue of Origin Dictates GOT1 Dependence and Confers Synthetic Lethality to Radiotherapy[#]

Summary

Metabolic programs in cancer cells are influenced by genotype and the tissue of origin. We have previously shown that central carbon metabolism is rewired in pancreatic ductal adenocarcinoma (PDA) to support proliferation through a glutamate oxaloacetate transaminase 1 (GOT1)-dependent pathway. Here we tested if tissue type impacted GOT1 dependence by comparing PDA and colorectal cancer (CRC) cell lines and tumor models of similar genotype. We found CRC to be insensitive to GOT1 inhibition, contrasting markedly with PDA, which exhibit profound growth inhibition upon GOT1 knockdown. Utilizing a combination of metabolomics strategies and computational modeling, we found that GOT1 inhibition disrupted glycolysis, nucleotide metabolism, and redox homeostasis in PDA but not CRC. These insights were leveraged in PDA, where we demonstrate that radiotherapy potently enhanced the effect of GOT1 inhibition on tumor growth. Taken together, these results illustrate the role of tissue type in dictating metabolic dependencies and provide new insights for targeting metabolism to treat PDA.

Introduction

Metabolic processes are rewired in cancer to facilitate tumor survival and growth[1]. Accordingly, there is interest in defining the metabolic pathways utilized by cancer cells to design new drug targets and therapies. A wealth of studies in the past decade have detailed cell autonomous metabolic reprogramming and associated liabilities centering on those processes activated by oncogenes or upon loss of tumor suppressors[2]. More recent studies have built upon this work to describe how the cell of origin influences metabolic programs and liabilities in cancer[3,4]. In addition to these intrinsic programs,

[#] Nelson, B. S. *et al.* Tissue of origin dictates GOT1 dependence and confers synthetic lethality to radiotherapy. *Cancer & metabolism* 8, 1, doi:10.1186/s40170-019-0202-2 (2020).

properties of the tumor microenvironment can also influence metabolic programs and liabilities in cancer cells[5]. Collectively, these studies have revealed that a common set of genetic alterations can lead to different metabolic dependencies contingent on the tissue type, tumor location, and/or properties of the tumor microenvironment[6-10].

Previously we found that expression of mutant KRAS, the signature transforming oncogene in pancreatic ductal adenocarcinoma (PDA), rewires central carbon metabolism to support tumor maintenance[11-13]. This includes the diversion of glucose-derived carbon into anabolic pathways that branch from glycolysis and enhanced utilization of glutamine-derived carbon to support anaplerosis in the mitochondria. Of note, these studies demonstrated that oncogenic KRAS enhances activity of the non-oxidative pentose phosphate pathway (PPP), which results in diminished activity of the NADPH-generating oxidative PPP[11]. NADPH is required for the biosynthesis of lipids and deoxynucleotides while simultaneously also serving as an important co-factor to support redox homeostasis. To account for the decreased flux through the oxidative PPP, we reported on a rewired form of the malate-aspartate shuttle that PDA cells utilize to maintain NADPH levels (**Fig. 3.1a**). This pathway is mediated by the mutant KRAS-driven activation of glutamate oxaloacetate transaminase 1 (GOT1) expression.

Importantly, our previous work demonstrated that PDA cells use the NADPH from the GOT1 pathway to manage reactive oxygen species (ROS) through the maintenance of reduced glutathione (GSH) pools[12]. Further, we illustrated that PDA cells were dependent on GOT1 activity for growth in culture, whereas non-transformed fibroblasts and epithelial cells tolerated GOT1 knockdown without consequence. In an effort to leverage these findings about metabolic dependencies in PDA to design new therapies, we recently developed novel small molecule inhibitors that target GOT1[14,15]. Furthermore, GOT1-metabolic pathways have also been shown to play a role in other cancers[16-19], indicating that GOT1 inhibitors may have utility beyond PDA. However, a rigorous comparison of GOT1 sensitivity in different cancer types has not been performed.

In the current study, we set forth to determine whether the tissue of origin impacts GOT1 dependence to understand which cancers are most likely to benefit from this emerging therapeutic strategy. We found that colorectal cancer (CRC) cell lines harboring *KRAS*

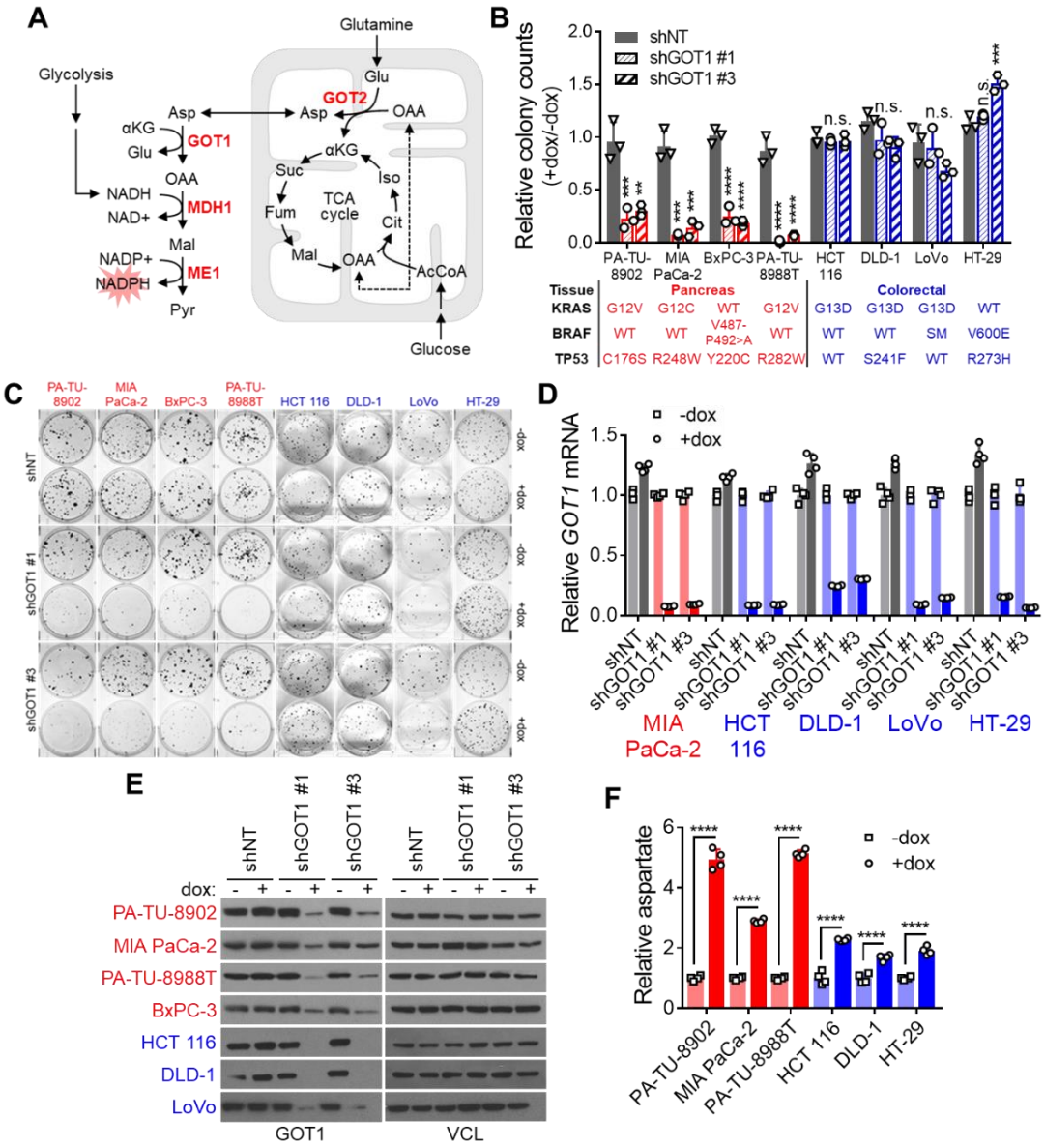

Figure 3.1 GOT1 dependence exhibits tissue specificity *in vitro*. (**A**) Schematic of the GOT1 pathway in PDA. (**B**) Colony number after dox treatment in PDA (red) and CRC (blue) cell lines expressing dox-inducible (iDox) shRNAs against GOT1 (two independent hairpins; shGOT1 #1, shGOT1 #3) relative to a non-targeting hairpin (shNT). Error bars represent s.d. from biological replicates (n=3). Mutations in *KRAS*, *BRAF*, and *TP53* are presented in the table below. WT, wildtype; SM, silent mutation. (**C**) Representative wells from colony forming assays of cells expressing the iDox-shNT, iDox-shGOT1 #1, and iDox-shGOT1 #3 hairpins +/-dox. (**D**) *GOT1* mRNA expression, as determined by qPCR. Error bars represent s.d. from biological replicates (n=3). (**E**) Western blots for GOT1 and vinculin (VCL) loading control from iDox-shNT, iDox-shGOT1 #1, and iDox-shGOT1 #3 PDA and CRC cell lines +/- dox treatment. (**F**) Relative aspartate levels in iDox-shGOT1 PDA and CRC cell lines, as determined by LC/MS. Error bars represent s.d. from biological replicates (n=4). AcCoA, acetyl-CoA; αKG, alpha-ketoglutarate; Asp, aspartate; Cit, citrate; Fum, fumarate; Glu, glutamate; GOT1, glutamate oxaloacetate transaminase 1; GOT2, glutamate oxaloacetate transaminase 2; Iso, isocitrate; Mal, malate; MDH1, malate dehydrogenase 1; ME1, malic enzyme 1; NADP+, oxidized nicotinamide adenine dinucleotide phosphate; NADPH, reduced nicotinamide adenine dinucleotide phosphate; OAA, oxaloacetate; Pyr, pyruvate; Suc, succinate. **, $P < 0.01$; ***, $P < 0.001$; ****, $P < 0.0001$; Student's t-test (unpaired, two-tailed).

and *TP53* mutations, two of the most common mutations in PDA patients[20], were insensitive to GOT1 inhibition *in vitro* and *in vivo*. This was in dramatic contrast to the PDA models. We then utilized liquid chromatography-coupled mass spectrometry (LC/MS)-based metabolomics strategies, including isotope tracing flux analysis and computational modeling of metabolomics data, to dissect the metabolic consequences of GOT1 knockdown and to contrast how these differed between CRC and PDA cells and tumors. This analysis revealed that GOT1 inhibition uniquely disrupted glycolysis, nucleotide metabolism, and redox homeostasis pathways in PDA. Based on these results, we then designed a combination treatment approach consisting of GOT1 inhibition and radiotherapy. This provided a considerable increase in the efficacy of either single arm treatment uniquely in PDA. Together, these results suggest that the clinical investigation of therapies targeting GOT1, either as monotherapy or in combination with radiation, should begin in PDA. Finally, our data also highlight the importance of tissue of origin in PDA and CRC when studying metabolic wiring and associated dependencies.

Results

GOT1 dependence exhibits tissue specificity

To determine whether the tissue of origin impacts GOT1 dependence, we compared GOT1 knockdown in a panel of PDA and CRC cell lines that similarly exhibit mutant KRAS (or BRAF) and mutant TP53 expression (**Fig. 3.1b,c**). We standardized GOT1 inhibition across experiments by developing doxycycline (dox)-inducible (iDox)-shRNA reagents that target the coding region of GOT1 (shGOT1 #1), the 3' untranslated region of GOT1 (shGOT1 #3), or a non-targeting shRNA (shNT). shRNA activity was validated after dox administration by assessing GOT1 mRNA and protein expression and intracellular aspartate (Asp), a product of the GOT1 reaction (**Fig. 3.1d-f**). Additionally, shRNA specificity was validated by rescue with a GOT1 cDNA construct (**Fig. 3.2**). These constructs were then used to assess GOT1 sensitivity in the panel of PDA and CRC cell lines (**Fig. 3.1b,c**). As we observed previously with constitutive shRNA targeting GOT1, the colony forming potential of PDA lines was significantly blunted upon inducible GOT1 inhibition. In stark contrast, the CRC cell lines were entirely resistant to growth inhibition in this assay. Importantly, this occurred despite efficient protein knockdown and Asp accumulation in both the PDA and CRC cell lines (**Fig. 3.1e,f**).

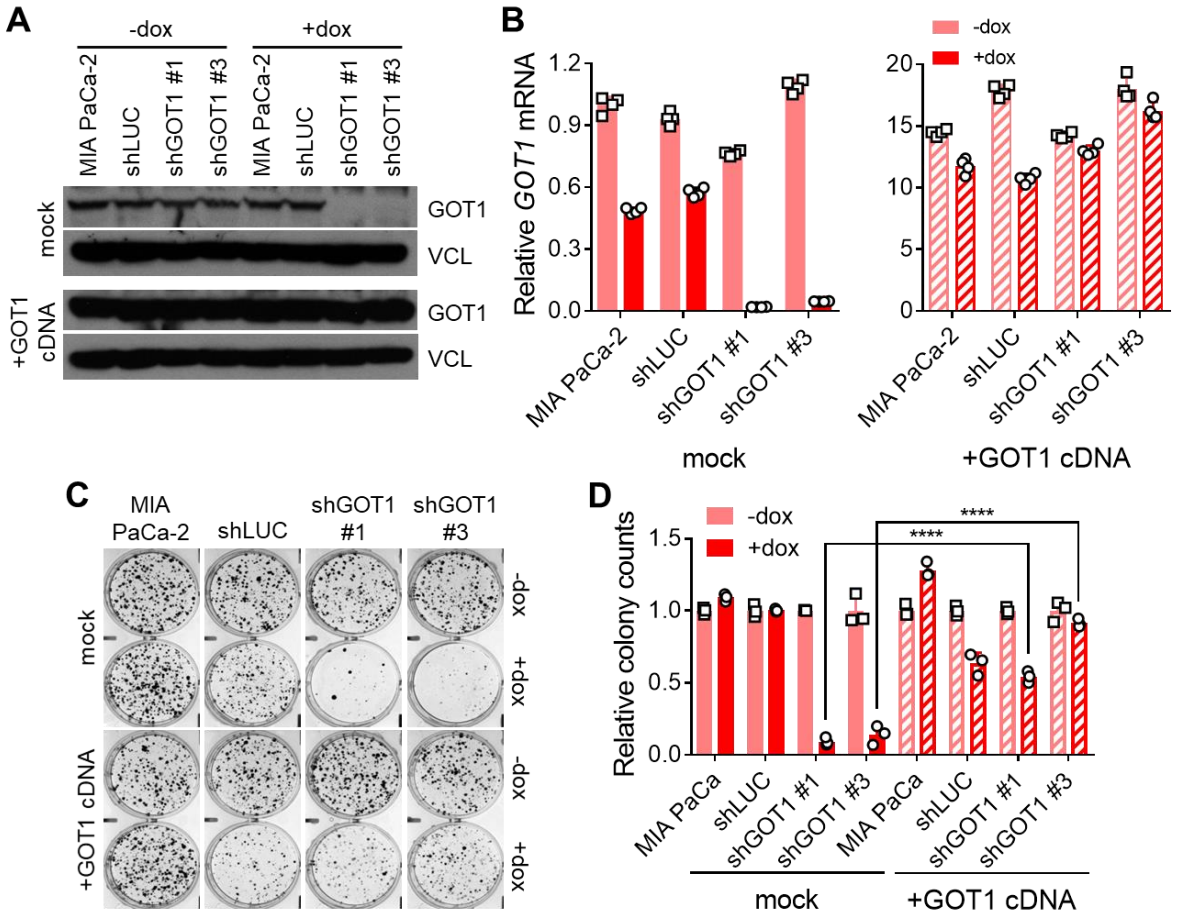

Figure 3.2 Validation of GOT1 knockdown system. (**A**) Western blots for GOT1 and VCL from iDox-shGOT1 #1 and iDox-shGOT1 #3 MIA PaCa-2 PDA cells +/- dox treatment, +/- rescue with an ectopic shRNA-resistant GOT1 cDNA. (**B**) *GOT1* mRNA expression in MIA PaCa-2 PDA cells +/- dox treatment, +/- rescue with an ectopic shRNA-resistant GOT1 cDNA. Error bars represent s.d. from biological replicates (n=4). (**C**) Representative wells from colony forming assays and (**D**) associated quantitation in MIA PaCa-2 PDA cells +/- dox treatment, +/- GOT1 cDNA rescue. Error bars represent s.d. from biological replicates (n=3). ****, $P < 0.0001$; Student's t-test (unpaired, two-tailed).

Next, we examined how GOT1 inhibition affected established PDA and CRC tumors. To this end, cells were implanted in the flanks of mice and tumors were allowed to establish for 1 week. Dox was then administered in the chow to initiate GOT1 knockdown (**Fig. 3.3a**). PDA tumors exhibited a profound retardation of tumor growth (**Fig. 3.3b-d**). Consistent with our *in vitro* observations, CRC lines were insensitive to GOT1 knockdown *in vivo* (**Fig. 3.3e-g**). Xenografts expressing shNT, to control for hairpin and dox effects, showed no difference in growth in either PDA or CRC (**Fig. 3.3h-k**). The results from these data indicated that, unlike PDA, CRC cell lines and tumors are not dependent on GOT1 for growth.

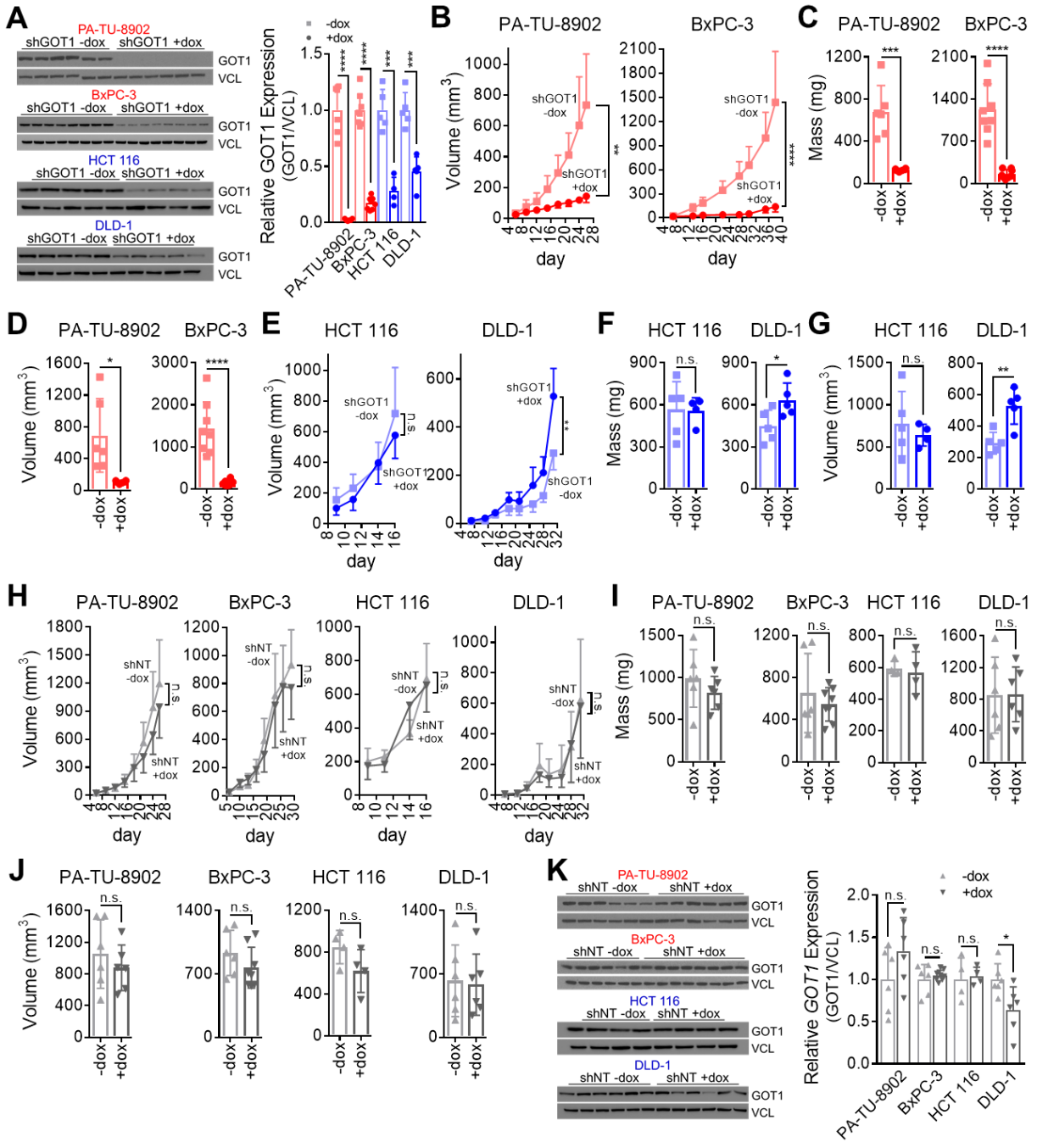

Figure 3.3 GOT1 dependence exhibits tissue specificity *in vivo*. (**A**) Western blots (left) and quantification (right) for GOT1 and vinculin (VCL) loading control from iDox-shGOT1 #1 PDA and CRC tumors. (**B**) Tumor growth curves, (**C**) final tumor mass, and (**D**) final tumor volume from subcutaneous PDA xenografts (n=8, BxPC-3 +/- dox tumors; n=6, PA-TU-8902 +/- dox tumors). Error bars represent s.d. (**E**) Tumor growth curves, (**F**) final tumor mass, and (**G**) final tumor volume from subcutaneous CRC xenografts (n=5, DLD-1 +/-dox, HCT 116 +dox tumors; n=4, HCT 116 -dox tumors). Error bars represent s.d. (**H**) Subcutaneous xenograft tumor growth, (**I**) final tumor mass, and (**J**) final tumor volume of PDA and CRC cells expressing iDox-shNT in mice administered chow with or without dox (n=8, BxPC-3 +dox tumors; n=6, BxPC-3 -dox, PA-TU-8902 +/- dox, DLD-1 +/-dox tumors; n=4 HCT 116 +/- dox tumors). (**K**) Western blots for GOT1 and VCL from iDox-shNT PDA and CRC tumors. *, $P < 0.05$; **, $P < 0.01$; ***, $P < 0.001$; ****, $P < 0.0001$; Student's t-test (unpaired, two-tailed).

Expression of GOT1 pathway components does not distinguish PDA from CRC

Next, we tested if GOT1 dependence was due to lack of, or major differences in, the expression of GOT1-pathway components. Aside from ME1, which showed a modest but statistically significant higher expression in CRC, the GOT1-pathway components examined were expressed at similar levels in the PDA and CRC cells (**Fig. 3.4**). Importantly, GOT1 is biochemically active in both PDA and CRC cells, as knockdown led to Asp accumulation (**Fig. 3.1f**). Notably, the Asp build up occurred to a lesser extent in CRC cells compared to PDA cells, suggesting CRC cells may be utilizing compensatory pathways upon GOT1 knockdown. Collectively, these results indicated that while the pathway machinery in PDA and CRC are intact and functional, the differential dependence on GOT1 may result from distinct metabolic pathway activity, rather than enzyme expression, between these two tumor types.

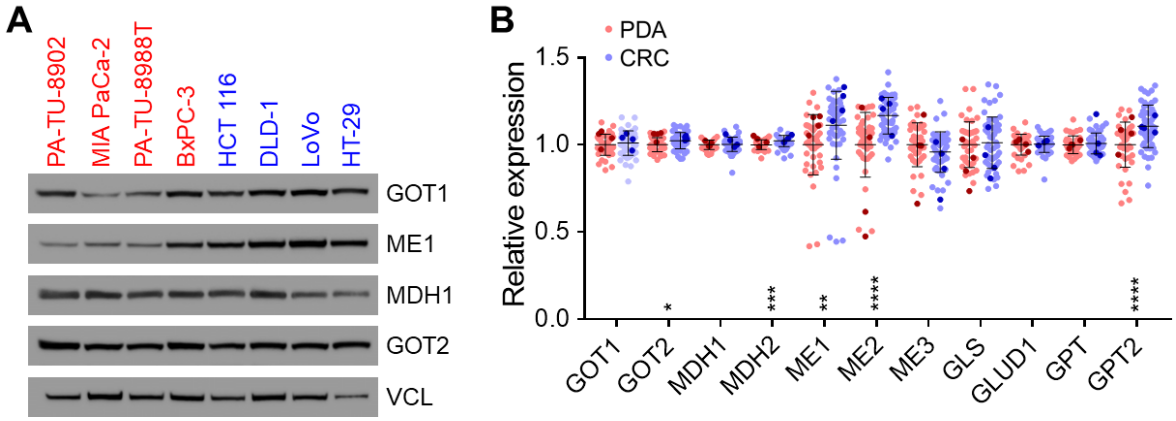

Figure 3.4 GOT1 pathway expression. (**A**) Western blot (left) and quantification (right) for GOT1 pathway components from **Fig. 3.1a** in wild type PDA and CRC cell lines. (**B**) Relative mRNA expression level of the GOT1-pathway members, homologues, and adjacent components in PDA and CRC cells. Data obtained from the Cancer Cell Line Encyclopedia (CCLE). Data for the PDA and CRC cell lines used herein are highlighted in darker shades of red and blue, respectively. GLS, glutaminase; GLUD1, glutamate dehydrogenase 1; GOT1, glutamate oxaloacetate transaminase 1; GOT2, glutamate oxaloacetate transaminase 2; GPT, glutamate pyruvate transaminase; GPT2, glutamate pyruvate transaminase 2; MDH1, malate dehydrogenase 1; MDH2, malate dehydrogenase 2; ME1, malic enzyme 1; ME2, malic enzyme 2; ME3, malic enzyme 3. n.s., not significant; *, $P < 0.05$; **, $P < 0.01$; ***, $P < 0.001$; ****, $P < 0.0001$; Student's t-test (unpaired, two-tailed).

Differential metabolic pathway activity between PDA and CRC

In order to determine differences in the basal metabolic state between PDA and CRC cells, we used LC/MS-based metabolomics[21-24] to profile a panel of 3 PDA and 3 CRC parental cell lines in exponential growth phase. Analysis of statistically significant

differences in the relative abundance of the steady state metabolite pools indicated that the PDA lines had more glucono-delta lactone-6 phosphate (GdL6P) and 6-phospho gluconate (6PG), metabolites in the oxidative arm of the PPP, and smaller metabolite pools of alanine and lactate (**Fig. 3.5**). Many additional differences were observed that did not reach statistical significance, and collectively these revealed an inflection point in glycolysis at the level of aldolase (ALDO).

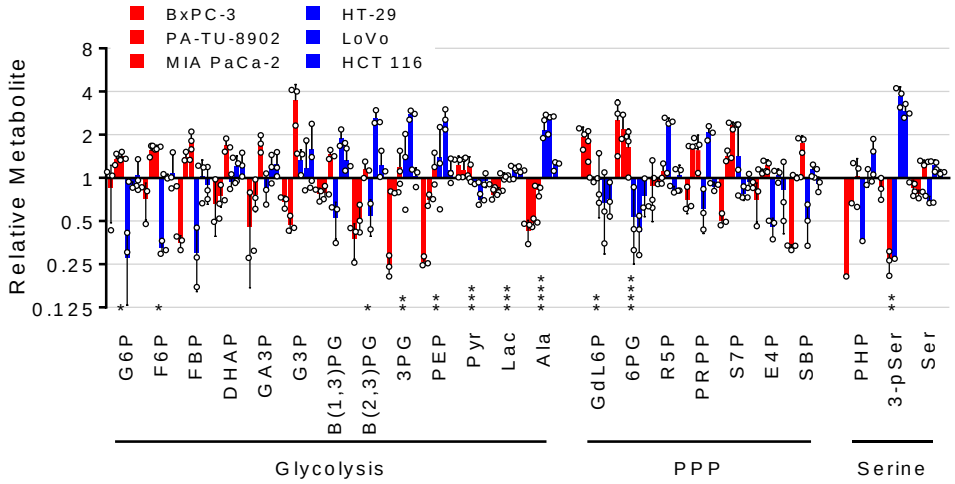

Figure 3.5 Steady-state metabolic profile of PDA and CRC. Relative metabolite levels as determined by LC/MS for glycolysis, pentose phosphate pathway (PPP), and serine metabolism in parental PDA (red) and CRC (blue) cell lines. Error bars represent s.d. from biological replicates (n=3). 3-pSer, 3-phosphoserine; 3PG, 3-phosphogycerate; 6PG, 6-phosphogluconate; Ala, alanine; B(1,3)PG, 1,3-bisphosphoglycerate; B(2,3)PG, 2,3-bisphosphoglycerate; DHAP, dihydroxyacetone phosphate; E4P, erythrose 4-phosphate; F6P, fructose 6-phosphate; FBP, fructose-1,6-bisphosphate; G3P, glycerol-3-phosphate; G6P, glucose 6-phosphate; GA3P, glyceraldehyde 3-phosphate; GdL6P, glucono-delta-lactone 6-phosphate; Lac, lactate; PEP, phosphoenolpyruvate; PHP, phosphohydroxypyruvate; PRPP, phosphoribosyl pyrophosphate; Pyr, pyruvate; R5P, ribose 5-phosphate; S7P, sedoheptulose-7 phosphate; SBP, sedoheptulose-1,7-bisphosphate; Ser, serine. *, $P < 0.05$; **, $P < 0.01$; ***, $P < 0.001$; ****, $P < 0.0001$; Student t-test (unpaired, two-tailed).

Thus, we set out to further interrogate the metabolic differences between GOT1 dependent and independent cells, and to determine differential central carbon utilization. To this end we performed isotope tracing metabolomics using either uniformly-labeled 13C (U-^{13}C) glucose (Glc) or glutamine (Gln)[22-24] in the parental PDA and CRC lines. Metabolites were collected from log phase cell lines grown overnight in labeled media, and fractional labeling patterns (**Figs. 3.6, 3.7**) and metabolite pool sizes (**Figs. 3.8, 3.9**) were analyzed.

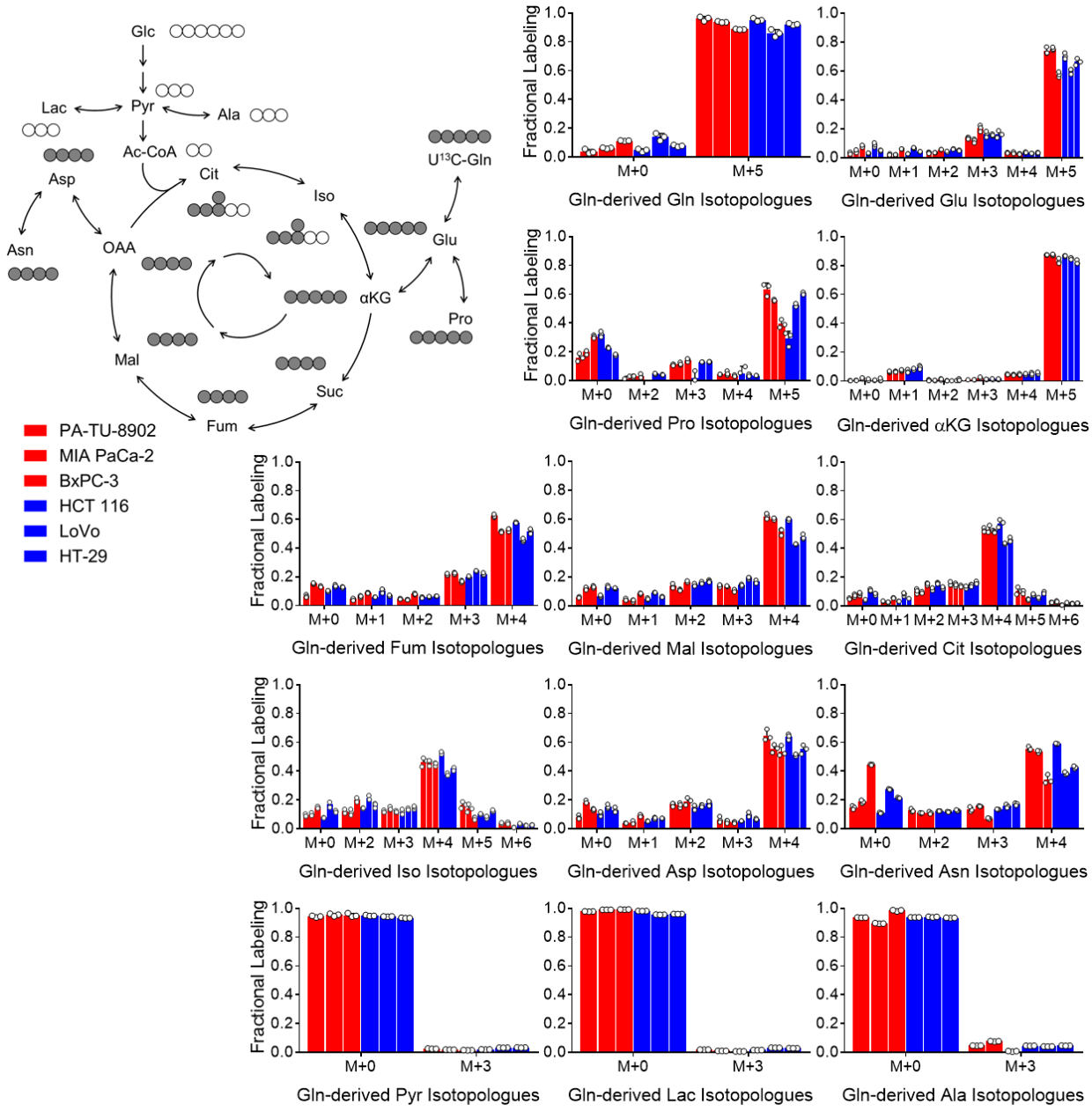

Figure 3.6 Steady state fractional labeling patterns of TCA cycle and branching metabolites from glutamine carbon tracing in PDA and CRC cell lines. Fractional labeling patterns reflect the percentage of a given metabolite pool labeled by an input metabolic substrate (in this case, glutamine carbon). Isotopologue distributions presented as fractional enrichment from overnight labeling with ^{13}C-glutamine (Gln) in PDA (red) and CRC (blue) cell lines, as determined by LC/MS, except for pyruvate, lactate, alanine, asparagine, and proline, which were generated by gas chromatography (GC)/MS. In the schemes at top left, filled circles represent ^{13}C-labeled carbon, and open circles represent unlabeled carbon. The labeling pattern for one turn of the TCA cycle is presented. Citrate data previously published in a methods paper[22]. Error bars represent s.d. from biological replicates (n=3). Ac-CoA, acetyl-CoA; αKG, alpha-ketoglutarate; Ala, alanine; Asn, asparagine; Asp, aspartate; Cit, citrate; Fum, fumarate; Glu, glutamate; Iso, isocitrate; Lac, lactate; Mal, malate; OAA, oxaloacetate; Pro, proline; Pyr, pyruvate; U^{13}C, uniformly labeled carbon.

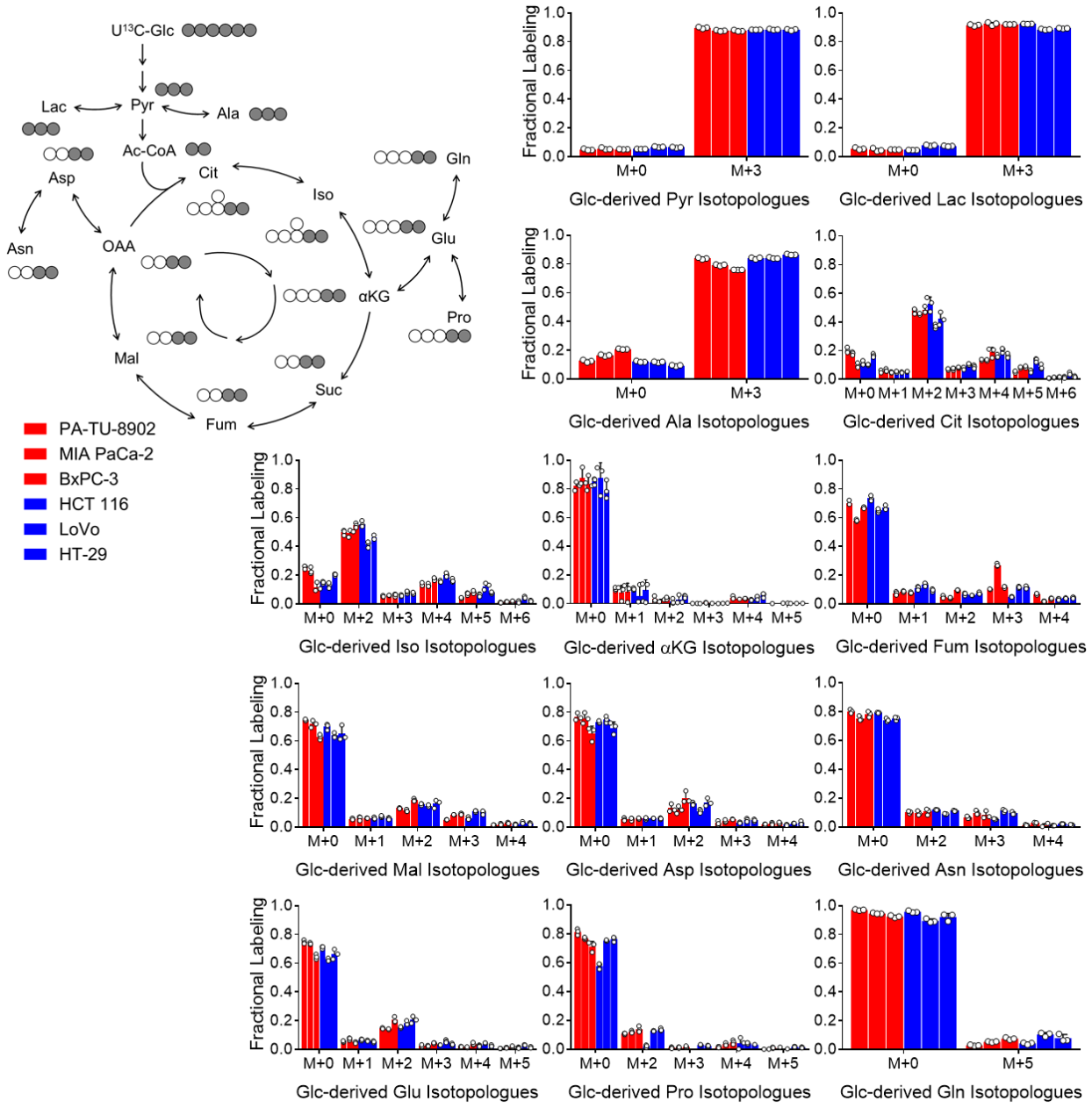

Figure 3.7 Steady state fractional labeling patterns of TCA cycle and branching metabolites from glucose carbon tracing in PDA and CRC cell lines. Fractional labeling patterns reflect the percentage of a given metabolite pool labeled by an input metabolic substrate (in this case, glucose carbon). Isotopologue distributions presented as fractional enrichment from overnight labeling with ^{13}C-glucose (Glc) in PDA (red) and CRC (blue) cell lines, as determined by LC/MS, except for pyruvate, lactate, alanine, asparagine, and proline, which were generated by gas chromatography (GC)/MS. In the schemes at top left, filled circles represent ^{13}C-labeled carbon, and open circles represent unlabeled carbon. The labeling pattern for one turn of the TCA cycle is presented. Citrate data previously published in a methods paper[22]. Error bars represent s.d. from biological replicates (n=3). Ac-CoA, acetyl-CoA; αKG, alpha-ketoglutarate; Ala, alanine; Asn, asparagine; Asp, aspartate; Cit, citrate; Fum, fumarate; Glu, glutamate; Iso, isocitrate; Lac, lactate; Mal, malate; OAA, oxaloacetate; Pro, proline; Pyr, pyruvate; U^{13}C, uniformly labeled carbon.

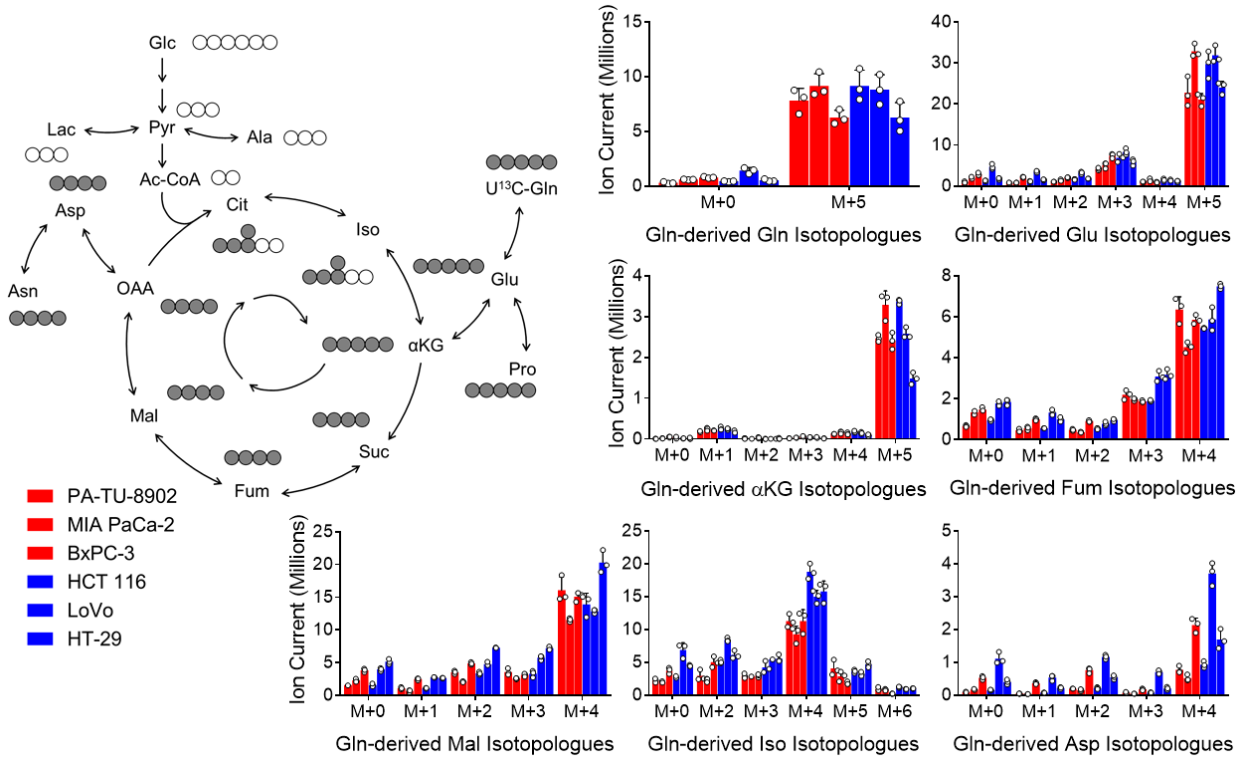

Figure 3.8 Steady state pools of TCA cycle and branching metabolites from glutamine carbon tracing in PDA and CRC cell lines. Pool sizes reflect the relative abundance of a given metabolite. Herein, these are presented as the total of labeled and unlabeled metabolite. Isotopologue distributions presented as total metabolite pools from overnight labeling with ^{13}C-glutamine (Gln) in PDA (red) and CRC (blue) cell lines, as determined by LC/MS. In the schemes at top left, filled circles represent ^{13}C-labeled carbon, and open circles represent unlabeled carbon. Labeling pattern for one turn of the TCA cycle is presented. Citrate data previously published in a methods paper[22]. Error bars represent s.d. from biological replicates (n=3). Ac-CoA, acetyl-CoA; αKG, alpha-ketoglutarate; Ala, alanine; Asn, asparagine; Asp, aspartate; Cit, citrate; Fum, fumarate; Glu, glutamate; Iso, isocitrate; Lac, lactate; Mal, malate; OAA, oxaloacetate; Pro, proline; Pyr, pyruvate; U^{13}C, uniformly labeled carbon.

The fractional labeling patterns between the PDA and CRC cell lines displayed remarkable similarity (**Figs. 3.6, 3.7**). In contrast, several notable changes were observed among the relative pool sizes. Similar to our steady state metabolomics (**Fig. 3.5**), we observed less lactate (**Fig. 3.10a**) and alanine (**Fig. 3.10b**) in the PDA lines, with the majority of this being derived from glucose. Further consistent with the steady state profiling in **Fig. 3.5**, the CRC lines have more active serine biosynthetic pathway activity, as illustrated by glucose-derived labeling of serine and glycine (**Fig. 3.10c,d**). In contrast to these differences, obvious differences in the abundance of Asp, glutamate and alpha-ketoglutarate, the substrates and products of the GOT1 reaction, were not evident between GOT1 dependent and independent lines (**Figs. 3.8, 3.9**). This was consistently

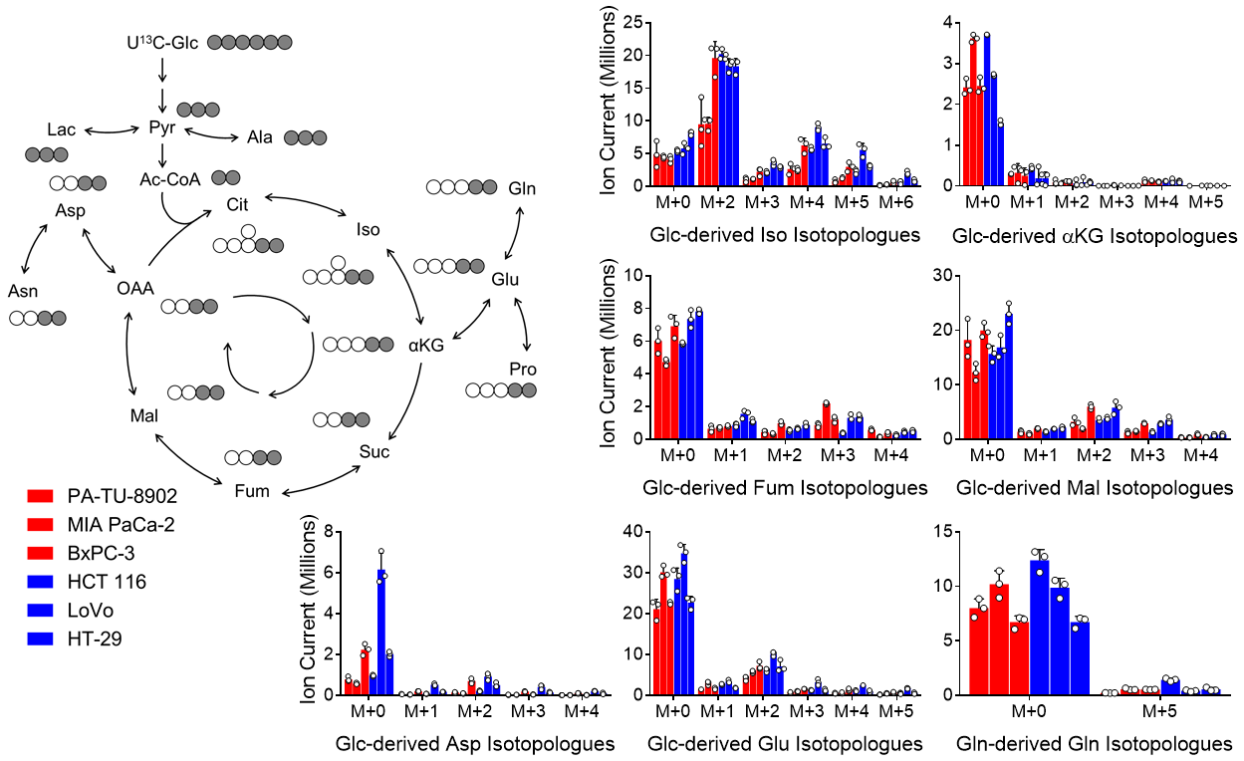

Figure 3.9 Steady state pools of TCA cycle and branching metabolites from glucose carbon tracing in PDA and CRC cell lines. Pool sizes reflect the relative abundance of a given metabolite. Herein, these are presented as the total of labeled and unlabeled metabolite. Isotopologue distributions presented as total metabolite pools from overnight labeling with ^{13}C-glucose (Glc) in PDA (red) and CRC (blue) cell lines, as determined by LC/MS. In the schemes at top left, filled circles represent ^{13}C-labeled carbon, and open circles represent unlabeled carbon. Labeling pattern for one turn of the TCA cycle is presented. Citrate data previously published in a methods paper[22]. Error bars represent s.d. from biological replicates (n=3). Ac-CoA, acetyl-CoA; αKG, alpha-ketoglutarate; Ala, alanine; Asn, asparagine; Asp, aspartate; Cit, citrate; Fum, fumarate; Glu, glutamate; Iso, isocitrate; Lac, lactate; Mal, malate; OAA, oxaloacetate; Pro, proline; Pyr, pyruvate; U^{13}C, uniformly labeled carbon

observed in the glucose and glutamine tracing studies. Similarly, the relative abundance of other TCA cycle intermediates did not exhibit notable differences between the PDA and CRC lines, with the exception of citrate, which is lower in the PDA lines (**Fig. 3.10e**). These data are summarized together with the unlabeled metabolomic profiling in **Fig. 3.10f**.

GOT1 inhibition impairs glycolysis in PDA

It was our expectation that differential GOT1 dependence would be reflected by differences in the baseline wiring of intermediary metabolism between GOT1 dependent and independent parental cell lines. However, given that the steady state profiling data for the unperturbed cells were largely similar (**Figs. 3.6-3.9**), we then examined how the

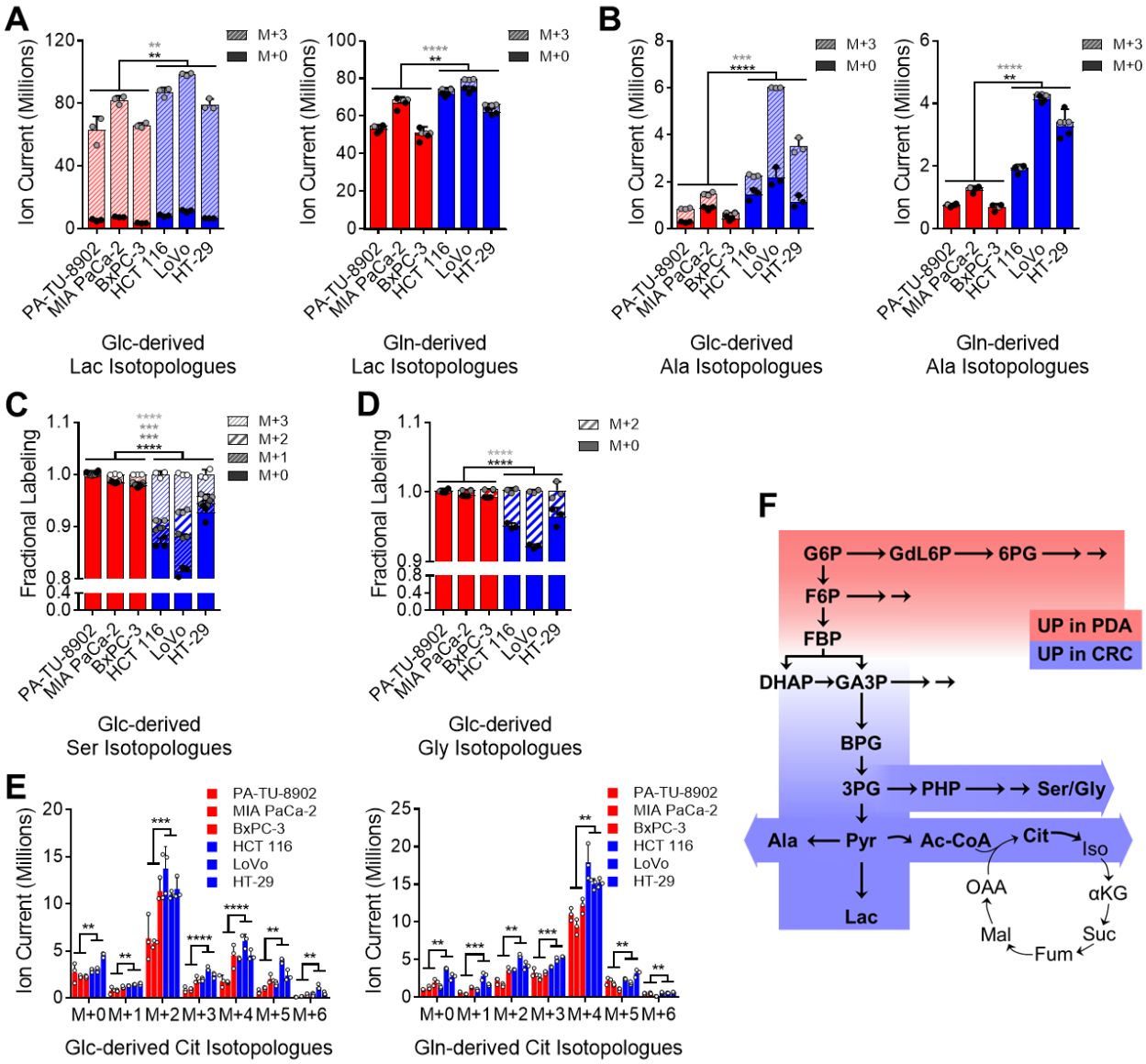

Figure 3.10 Isotope tracing metabolomic profile of PDA and CRC. Uniformly labeled (M+3, hashed bars) and unlabeled (M+0, solid bars) metabolite pools derived from U-13C-glucose (Glc, left) or U-13C-glutamine (Gln, right) for (A) lactate (Lac) and (B) alanine (Ala) as determined by LC/MS. (C) Relative U-13C-Glc-labeling of serine (Ser) and (D) glycine (Gly), as determined by gas chromatography (GC)/MS. (E) Ion currents for isotopologue distribution of citrate (Cit) derived from U-13C-Glc (left) or U-13C-Gln (right) in PDA and CRC cell lines. (F) Schematic summary of metabolic patterns observed in parental PDA and CRC cells. Red represents increased pool sizes in GOT1-sensitive PDA cells and blue represents increased metabolite pools in GOT1-insensitive CRC cells. 3PG, 3-phosphogycerate; 6PG, 6-phosphogluconate; Ac-CoA, acetyl-CoA; αKG, alpha-ketoglutarate; BPG, bisphosphoglycerate; DHAP, dihydroxyacetone phosphate; F6P, fructose 6-phosphate; FBP, fructose-1,6-bisphosphate; Fum, fumarate; G6P, glucose 6-phosphate; GA3P, glyceraldehyde 3-phosphate; GdL6P, glucono-delta-lactone 6-phosphate; Iso, isocitrate; Mal, malate; OAA, oxaloacetate; PHP, phosphohydroxypyruvate; Pyr, pyruvate; Suc, succinate. Error bars represent s.d. from biological replicates (n=3). Stacked P-values are presented for isotopologues in 3.10a-c correspond by color. *, P < 0.05; **, P < 0.01; ***, P < 0.001; ****, P < 0.0001; Student t-test (unpaired, two-tailed).

metabolome of GOT1 dependent and independent lines responded to knockdown using 3 PDA and 3 CRC iDox-shGOT1 cell lines. In this analysis, we found that Asp increased in all 6 lines and malate decreased in most (**Fig. 3.11a**), reflecting inhibition of the GOT1 pathway[12]. In addition, all 6 lines showed a consistent accumulation of glycolytic intermediates between the ALDO-catalyzed and pyruvate kinase (PK)-catalyzed steps of glycolysis (**Fig. 3.11b,c**). Despite these consistencies, extracellular acidification as measured by Seahorse Metabolic Flux Assay, a readout for glycolytic flux, was only impaired in GOT1 knockdown PDA (**Fig. 3.11d**).

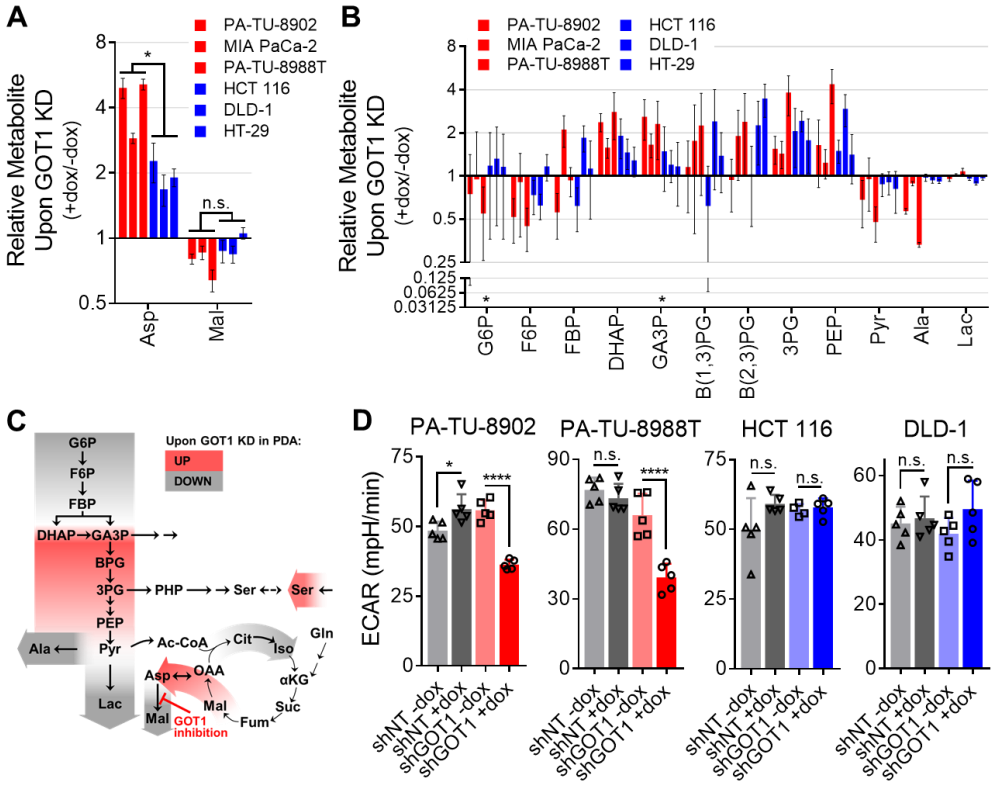

Figure 3.11 Steady state metabolic profile of PDA and CRC following GOT1 inhibition. (**A**) Relative aspartate (Asp) and malate (Mal) pools as determined by LC/MS in iDox-shGOT1 #1 PDA and CRC, presented as GOT1 knockdown over mock (+dox/-dox). (**B**) Relative glycolysis metabolite pools, as presented in **3.11a**. (**C**) Summary of changes to central carbon metabolism upon GOT1 knockdown PDA cells. Red represents increased pool sizes in PDA cells upon GOT1 knockdown and gray represents decreased metabolite pools. (**D**) Basal extracellular acidification rate (ECAR) levels in iDox-shGOT1 #1 and control shNT PDA and CRC cells, as determined by Seahorse Metabolic Flux Analysis. 3PG, 3-phosphogycerate; Ac-CoA, acetyl-CoA; αKG, alpha-ketoglutarate; Ala, alanine; B(1,3)PG, 1,3-bisphosphoglycerate; B(2,3)PG, 2,3-bisphosphoglycerate; Cit, citrate; DHAP, dihydroxyacetone phosphate; F6P, fructose 6-phosphate; FBP, fructose-1,6-bisphosphate; Fum, fumarate; G6P, glucose 6-phosphate; GA3P, glyceraldehyde 3-phosphate; Iso, isocitrate; Lac, lactate; OAA, oxaloacetate; PEP, phosphoenolpyruvate; Pyr, pyruvate; Suc, succinate. Error bars represent s.d. from biological replicates (n=3, **a, b**; n=5, **d**). *, $P < 0.05$; **, $P < 0.01$; ***, $P < 0.001$; ****, $P < 0.0001$; Student t-test (unpaired, two-tailed).

To further interrogate these metabolic differences, we also employed ^{13}C-Glc and Gln tracing analyses following GOT1 knockdown in the PA-TU-8902 PDA and DLD-1 CRC lines (**Figs. 3.12-3.15**). In cells of both tissue types, glycolytic intermediates were entirely Glc-derived, TCA cycle intermediates were predominantly Gln-derived, and GOT1 knockdown did not promote differential nutrient utilization to fuel these pathways (**Figs. 3.12-3.15**). As expected, pronounced accumulation of Asp was observed, and, as we have seen previously[12], this is predominantly derived from Gln in cultured cells (**Fig. 3.16**). Again, the fractional labeling data indicate largely consistent patterns of metabolite changes and nutrient utilization in glycolysis and the TCA cycle, and yet despite this, glycolytic activity and proliferation are only impaired in the PDA cells (**Fig. 3.1b, 3.11d**).

GOT1 inhibition disrupts nucleotide metabolism in PDA cells

The growth inhibitory activity of GOT1 knockdown in PDA has prompted ongoing efforts to develop small molecule GOT1 inhibitors[14,15]. To further harness the GOT1 selective dependence of PDA, we sought to identify metabolic pathways that could be targeted in combination with GOT1. Thus, to look more broadly at how GOT1 knockdown impacts metabolism between GOT1-dependent PDA and -independent CRC cell lines, we analyzed the unlabeled metabolomics data, as follows. The ~250 metabolites across central carbon metabolism were plotted as the average of the 3 PDA lines (dox/mock) over the average of the 3 CRC lines (dox/mock) (**Fig. 3.17a**). We identified pathways that are uniquely disrupted upon GOT1 knockdown in the PDA lines by analyzing metabolites with a greater than 2-fold change via MetaboAnalyst Pathway Analysis[25]. Among the differentially represented pathways, we observed that pyrimidine and purine metabolism were the most significantly enriched between PDA and CRC cell lines (**Fig. 3.17b**). Metabolites from PDA and CRC xenografts were analyzed in a similar manner with pyrimidine and purine metabolism also significantly enriched (**Fig. 3.17c**). We also found that several nodes in nucleotide metabolism were deregulated in PDA cells upon GOT1 inhibition by modeling our metabolomics data with the Recon1 genome-scale network model[26,27] with dynamic flux analysis (DFA)[28,29] (**Fig. 3.17d,e**). Given the importance of nucleic acid metabolism in proliferation and the response to damage, we hypothesized that GOT1 inhibition would modulate the cellular response to additional perturbations to these pathways.

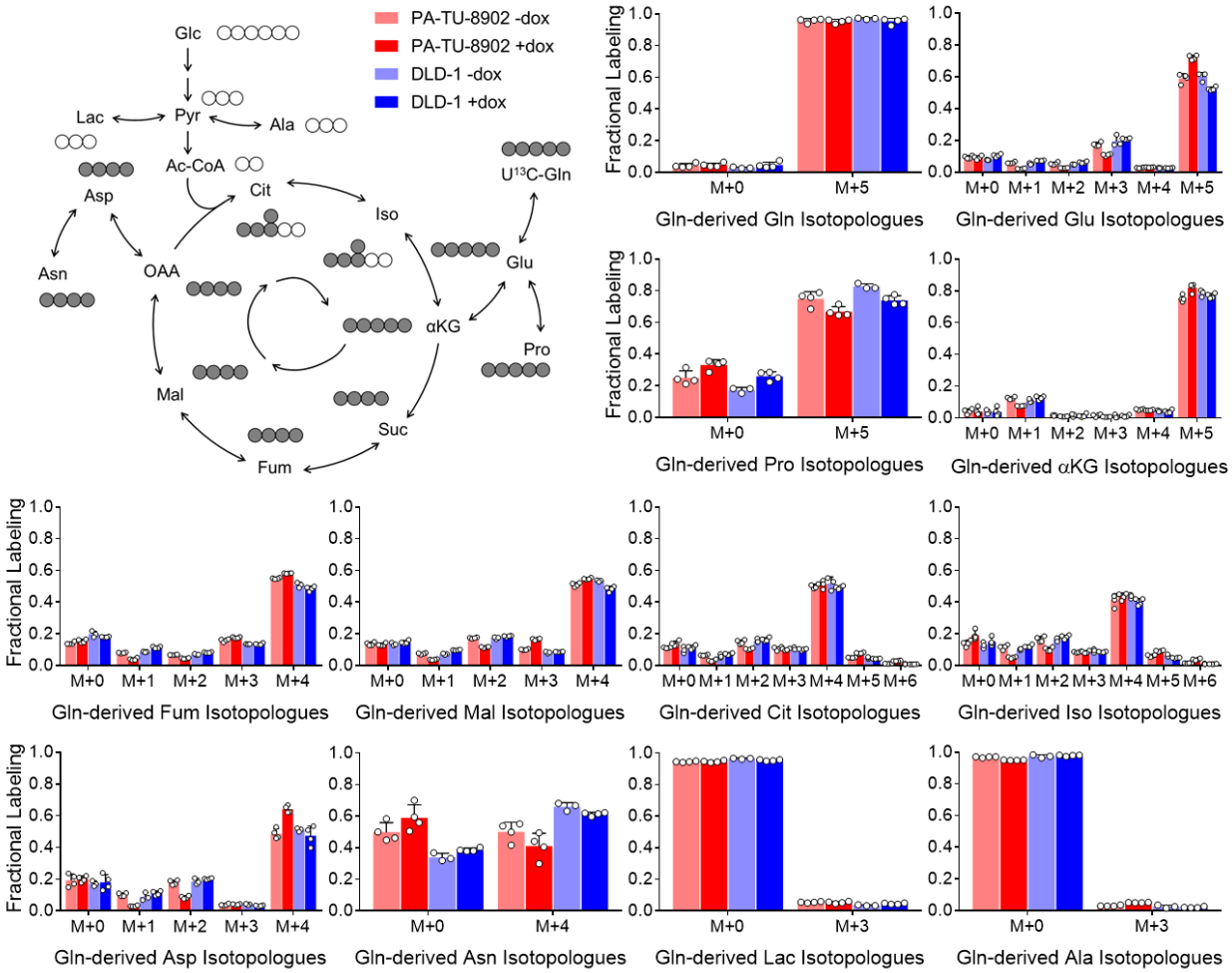

Figure 3.12 Steady state fractional labeling patterns of TCA cycle and branching metabolites from glutamine carbon tracing in PDA and CRC after GOT1 knockdown. Isotopologue distributions presented as fractional enrichment from overnight labeling with ^{13}C-glutamine (Gln) in iDox-shGOT1 #1 PA-TU-8902 PDA (red) and DLD-1 CRC (blue) cell lines. GOT1 was knocked down for 5 days via dox treatment; metabolites patterns determined by LC/MS. In the schemes at top left, filled circles represent ^{13}C-labeled carbon, and open circles represent unlabeled carbon. Labeling pattern for one turn of the TCA cycle is presented. Error bars represent s.d. from biological replicates (n=4, except n=3 for DLD-1 -dox Gln labeling). Ac-CoA, acetyl-CoA; αKG, alpha-ketoglutarate; Ala, alanine; Asn, asparagine; Asp, aspartate; Cit, citrate; Fum, fumarate; Glu, glutamate; Iso, isocitrate; Lac, lactate; Mal, malate; OAA, oxaloacetate; Pro, proline; Pyr, pyruvate; U^{13}C, uniformly labeled carbon.

GOT1 inhibition protects PDA cells from cytotoxic chemotherapy

Gemcitabine and 5-fluorouracil (5-FU) are pyrimidine analogs and front-line chemotherapies used to treat PDA patients[30-32]. Inspection of pyrimidine metabolism in our datasets revealed that it scored among the top differentially active pathways in both the MetaboAnalyst and DFA. Accordingly, we analyzed the unlabeled metabolomics data for nucleobase, nucleoside, and nucleotide pool levels after GOT1 knockdown and found

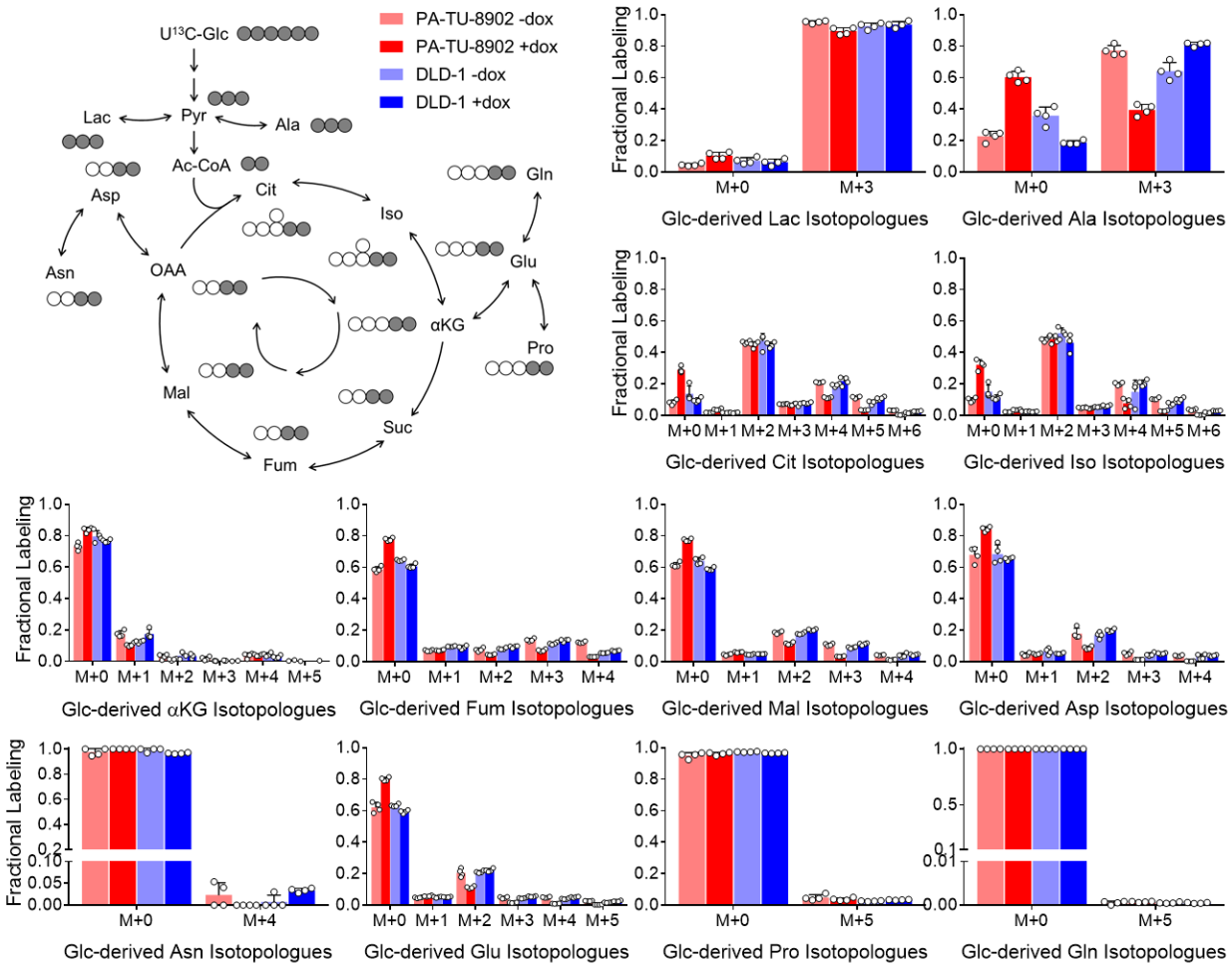

Figure 3.13 Steady state fractional labeling patterns of TCA cycle and branching metabolites from glucose carbon tracing in PDA and CRC after GOT1 knockdown. Isotopologue distributions presented as fractional enrichment from overnight labeling with ^{13}C-glucose (Glc) in iDox-shGOT1 #1 PA-TU-8902 PDA (red) and DLD-1 CRC (blue) cell lines. GOT1 was knocked down for 5 days via dox treatment; metabolites patterns determined by LC/MS. In the schemes at top left, filled circles represent ^{13}C-labeled carbon, and open circles represent unlabeled carbon. Labeling pattern for one turn of the TCA cycle is presented. Error bars represent s.d. from biological replicates (n=4, except n=3 for DLD-1 -dox Gln labeling). Ac-CoA, acetyl-CoA; αKG, alpha-ketoglutarate; Ala, alanine; Asn, asparagine; Asp, aspartate; Cit, citrate; Fum, fumarate; Glu, glutamate; Iso, isocitrate; Lac, lactate; Mal, malate; OAA, oxaloacetate; Pro, proline; Pyr, pyruvate; U^{13}C, uniformly labeled carbon.

that many are increased in PDA cells compared to CRC cells (**Fig. 3.18a**). We hypothesized that the increase in these metabolites upon GOT1 inhibition may serve to compete with anti-metabolite based therapies, as we have seen in other contexts[24,33,34]. To test this hypothesis, we treated PDA and CRC lines with a dose response of gemcitabine and 5-FU in the presence or absence of GOT1 inhibition. We also included oxaliplatin, a mechanistically distinct alkylating agent used in PDA front-line therapy. In line with our hypothesis, GOT1 knockdown in PDA cells promoted resistance to

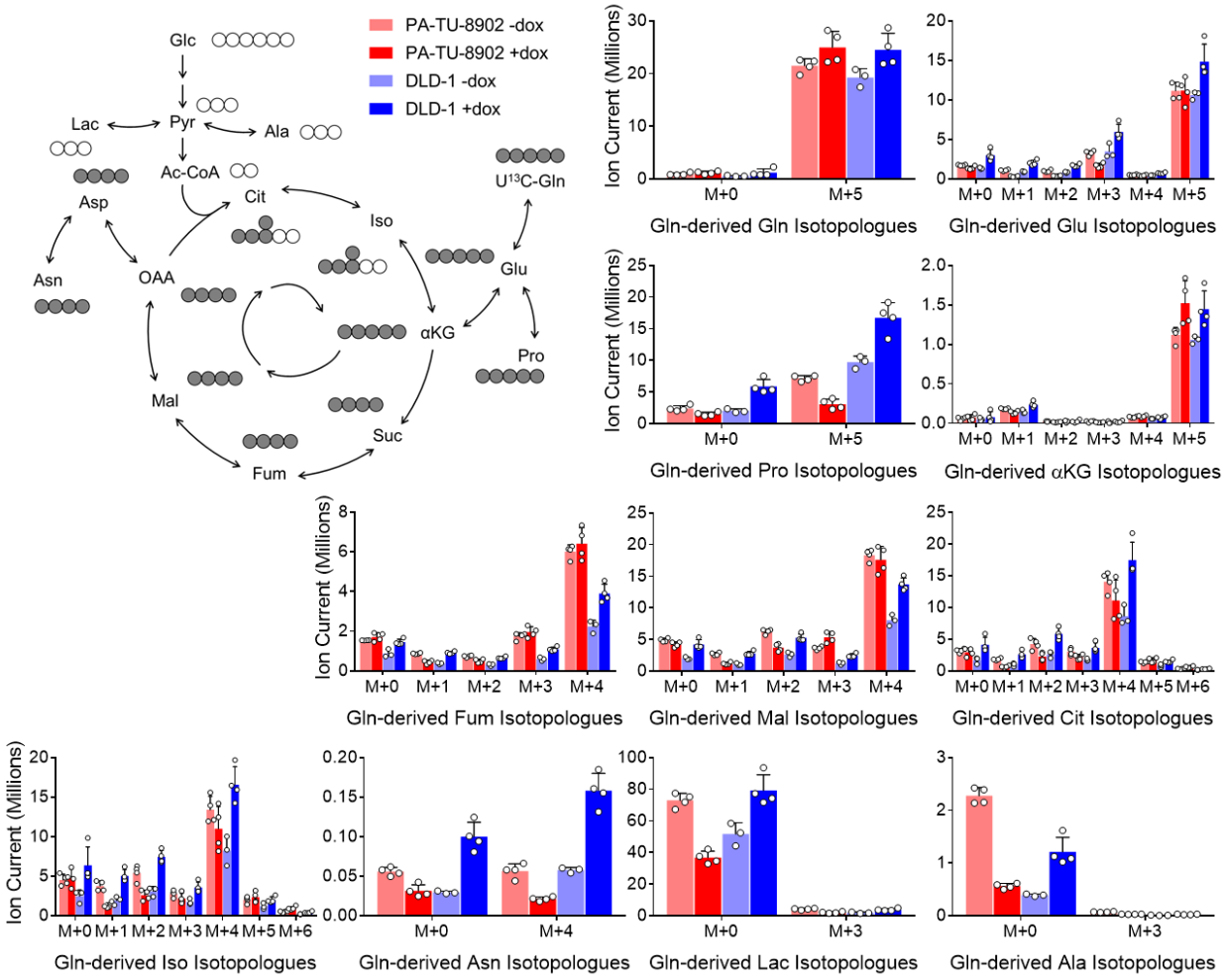

Figure 3.14 Steady state pools of TCA cycle and branching metabolites from glutamine carbon tracing in PDA and CRC after GOT1 knockdown. Isotopologue distributions presented as total metabolite pools from overnight labeling with ^{13}C-glutamine (Gln) in iDox-shGOT1 #1 PA-TU-8902 PDA (red) and DLD-1 CRC (blue) cell lines. GOT1 was knocked down for 5 days via dox treatment; metabolites patterns determined by LC/MS. In the schemes at top left, filled circles represent ^{13}C-labeled carbon, and open circles represent unlabeled carbon. Labeling pattern for one turn of the TCA cycle is presented. Error bars represent s.d. from biological replicates (n=4, except n=3 for DLD-1 -dox Gln labeling). Ac-CoA, acetyl-CoA; αKG, alpha-ketoglutarate; Ala, alanine; Asn, asparagine; Asp, aspartate; Cit, citrate; Fum, fumarate; Glu, glutamate; Iso, isocitrate; Lac, lactate; Mal, malate; OAA, oxaloacetate; Pro, proline; Pyr, pyruvate; U^{13}C, uniformly labeled carbon.

gemcitabine and 5-FU, whereas knockdown did not similarly impact resistance to chemotherapy in the CRC lines (**Fig. 3.18b,c**).

GOT1 inhibition decreases GSH and sensitizes PDA cells to radiation therapy

Cysteine and sulfur metabolism were the next most deregulated pathways between GOT1 inhibited PDA and CRC cells (**Fig. 3.17b**). In tumors, cysteine metabolism was the third most significantly enriched pathway (**Fig. 3.17c**) and DFA shows GSH metabolism

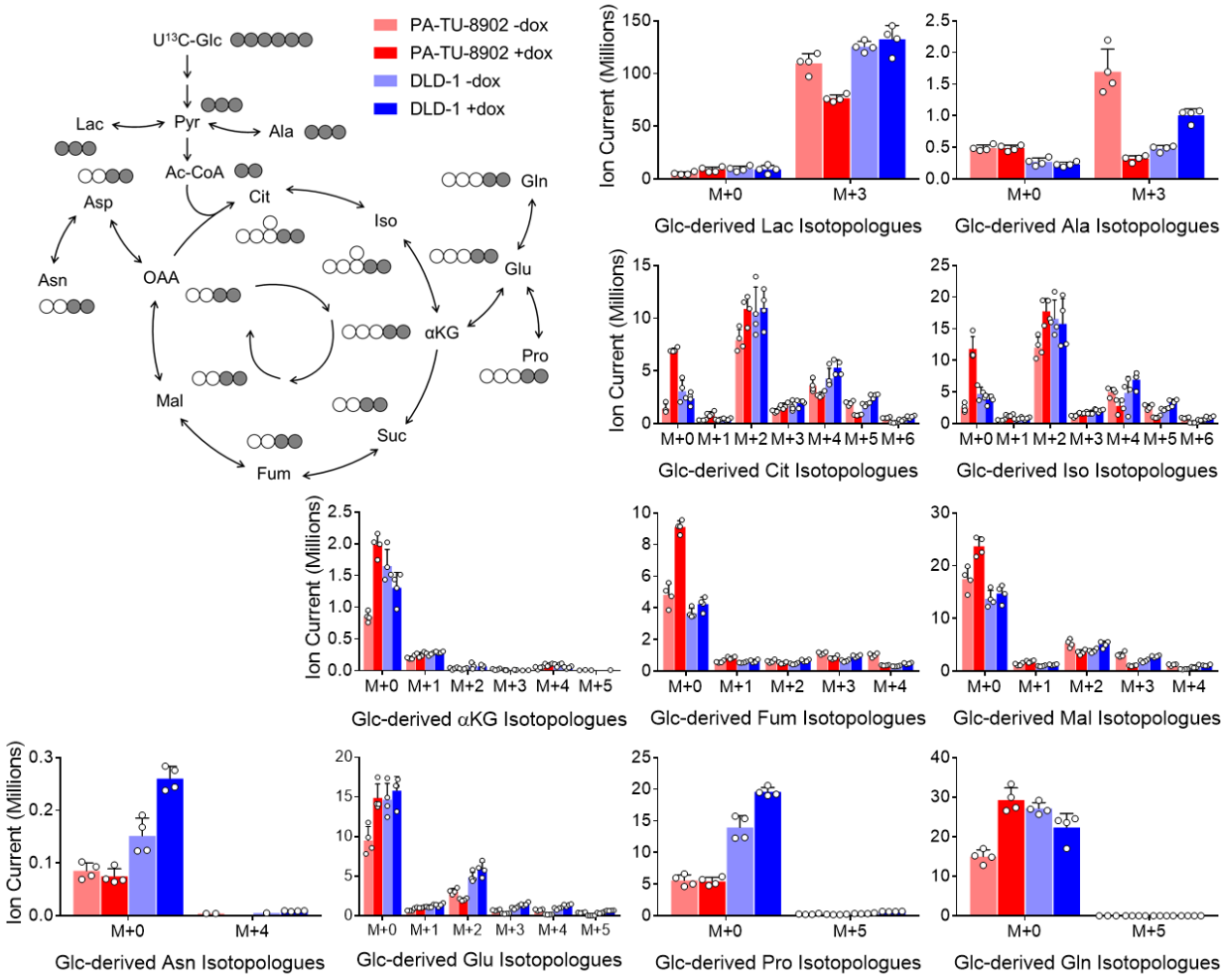

Figure 3.15 Steady state pools of TCA cycle and branching metabolites from glucose carbon tracing in PDA and CRC after GOT1 knockdown. Isotopologue distributions presented as total metabolite pools from overnight labeling with ^{13}C-glucose (Glc) in iDox-shGOT1 #1 PA-TU-8902 PDA (red) and DLD-1 CRC (blue) cell lines. GOT1 was knocked down for 5 days via dox treatment; metabolites patterns determined by LC/MS. In the schemes at top left, filled circles represent ^{13}C-labeled carbon, and open circles represent unlabeled carbon. Labeling pattern for one turn of the TCA cycle is presented. Error bars represent s.d. from biological replicates (n=4, except n=3 for DLD-1 -dox Gln labeling). Ac-CoA, acetyl-CoA; αKG, alpha-ketoglutarate; Ala, alanine; Asn, asparagine; Asp, aspartate; Cit, citrate; Fum, fumarate; Glu, glutamate; Iso, isocitrate; Lac, lactate; Mal, malate; OAA, oxaloacetate; Pro, proline; Pyr, pyruvate; U^{13}C, uniformly labeled carbon.

is a vulnerability in PDA (**Fig. 3.17d,e**). Cysteine is the rate limiting amino acid in GSH biosynthesis, and in our previous studies, we observed a drop in GSH pools following GOT1 knockdown[12]. Thus, we directed our attention to changes in GSH between PDA and CRC lines. Here, as determined by LC/MS, we found that both GSH and the reduced to oxidized glutathione (GSSG) ratio (GSH/GSSG), were uniquely decreased in PDA cells (**Fig. 3.19a**). The decrease in the GSH/GSSG ratio was similarly observed using a

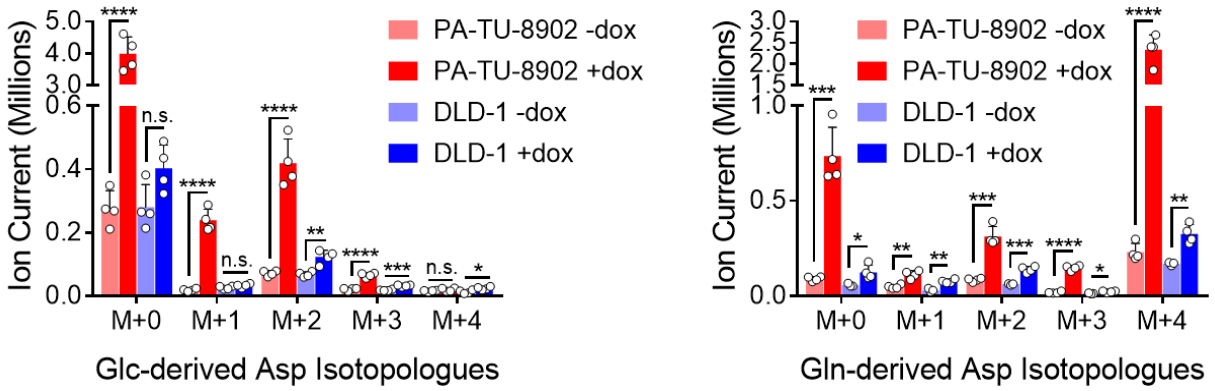

Figure 3.16 Metabolic profile of Asp in PDA and CRC following GOT1 inhibition. Ion currents for isotopologue distribution of aspartate (Asp) derived from U-^{13}C-Glc (left) or U-^{13}C-Gln (right) in iDox-shGOT1 #1 PA-TU-8902 PDA and DLD-1 CRC cell lines. Error bars represent s.d. from biological replicates (n=3). *, $P < 0.05$; **, $P < 0.01$; ***, $P < 0.001$; ****, $P < 0.0001$; Student t-test (unpaired, two-tailed).

biochemical assay in our panel of 3 PDA and 3 CRC cell lines (**Fig. 3.19b**). Furthermore, we also observed that the GSH/GSSG ratio decreased as a function of the duration of GOT1 knockdown, which similarly paralleled with increasing levels of Asp (**Fig. 3.19c-g**).

Radiotherapy is a pro-oxidant treatment modality frequently used to treat locally advanced PDA, but its efficacy can be limited by both the intrinsic treatment resistance of PDA and the risk of inducing toxicity in the nearby small bowel[35,36]. Given that radiation induces cell death through oxidative damage to DNA, and its effects can be mitigated by high levels of antioxidants such as GSH, we hypothesized that GOT1 inhibition would selectively radiosensitize PDA with minimal effects in other tissues that do not depend on GOT1 to maintain redox balance. To test this, we first examined the response of PDA to radiation using an *in vitro* clonogenic assay (**Fig. 3.20a**). This demonstrated that PDA cells were sensitized to radiation after dox-induced GOT1 knockdown, whereas no effect was observed in CRC cells (**Fig. 3.20b,c**). Importantly, this effect was not observed in controls (**Fig. 3.20d**). GOT1 knockdown provided a radiation enhancement ratio of 1.4, a similar score observed with classical radiosensitizers[37-39] (**Fig. 3.20c**).

Based on these results, we then explored the utility of GOT1 inhibition as a radiosensitizing strategy in PDA and CRC tumor models *in vivo*. PDA or CRC tumors were established as in **Fig. 3.3b,e**, with radiation treatment administered in 6 daily doses beginning on day 10. GOT1 knockdown significantly impaired tumor growth in PDA but

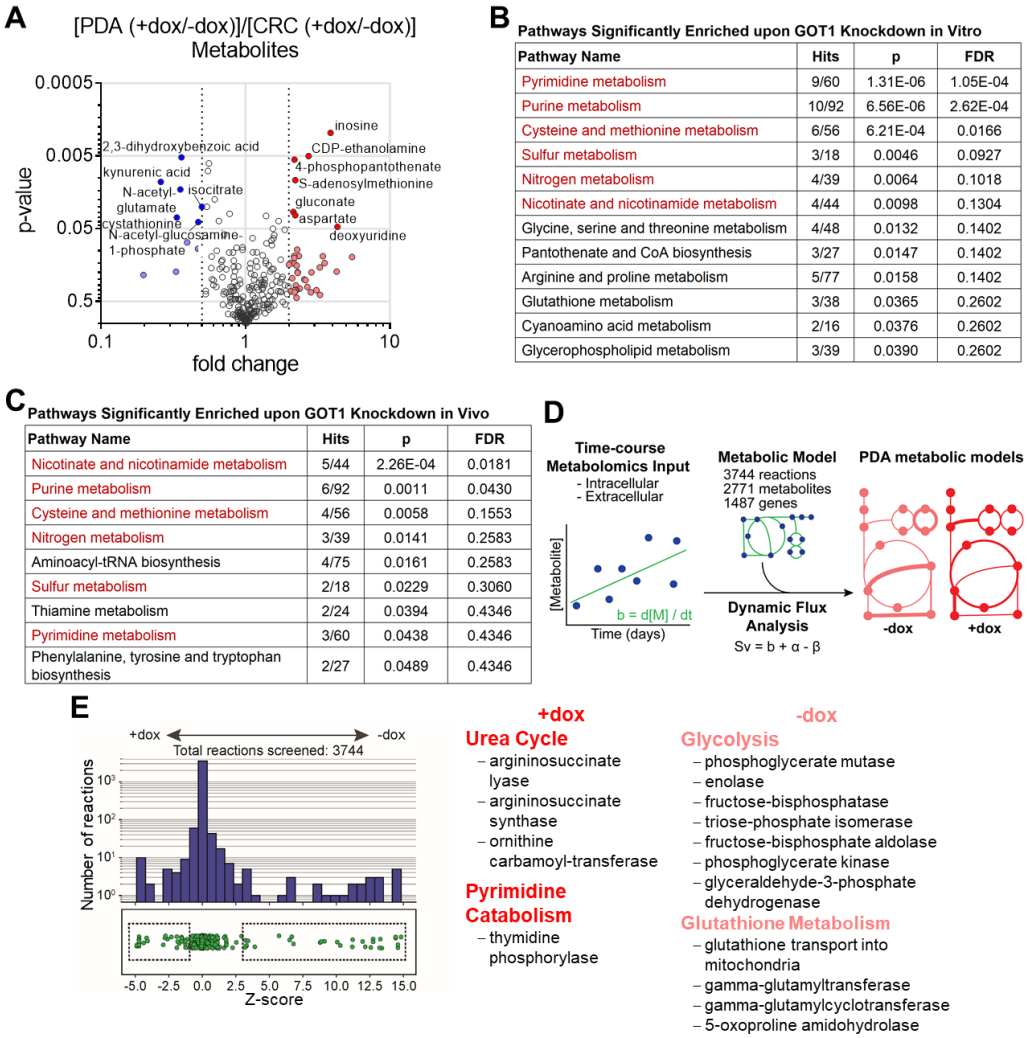

Pathway Name	Hits	p	FDR
Pyrimidine metabolism	9/60	1.31E-06	1.05E-04
Purine metabolism	10/92	6.56E-06	2.62E-04
Cysteine and methionine metabolism	6/56	6.21E-04	0.0166
Sulfur metabolism	3/18	0.0046	0.0927
Nitrogen metabolism	4/39	0.0064	0.1018
Nicotinate and nicotinamide metabolism	4/44	0.0098	0.1304
Glycine, serine and threonine metabolism	4/48	0.0132	0.1402
Pantothenate and CoA biosynthesis	3/27	0.0147	0.1402
Arginine and proline metabolism	5/77	0.0158	0.1402
Glutathione metabolism	3/38	0.0365	0.2602
Cyanoamino acid metabolism	2/16	0.0376	0.2602
Glycerophospholipid metabolism	3/39	0.0390	0.2602

Pathway Name	Hits	p	FDR
Nicotinate and nicotinamide metabolism	5/44	2.26E-04	0.0181
Purine metabolism	6/92	0.0011	0.0430
Cysteine and methionine metabolism	4/56	0.0058	0.1553
Nitrogen metabolism	3/39	0.0141	0.2583
Aminoacyl-tRNA biosynthesis	4/75	0.0161	0.2583
Sulfur metabolism	2/18	0.0229	0.3060
Thiamine metabolism	2/24	0.0394	0.4346
Pyrimidine metabolism	3/60	0.0438	0.4346
Phenylalanine, tyrosine and tryptophan biosynthesis	2/27	0.0489	0.4346

Figure 3.17 Metabolic pathways associated with GOT1 inhibition. (**A**) Fold-change versus p-value are plotted per metabolite as the average from 3 iDox-shGOT1 #1 PDA lines (+dox/-dox) over the average from 3 iDox-shGOT1 #1 CRC lines (+dox/-dox). Metabolites with filled circles were used for the pathway analysis in (**b**). Metabolites identity is indicated for those with $P < 0.05$ and fold change +/- 2. (**B**) Pathway Analysis of metabolites from (**a**) with greater than 2-fold change, as determined using the Metaboanalyst web tool (https://www.metaboanalyst.ca/). Hits reflects number of metabolites that were significant over total of metabolites considered for a given pathway. FDR, false discovery rate. (**C**) Pathway Analysis via Metaboanalyst of metabolites determined by LC/MS with greater than 2-fold change from PA-TU-8902 and HCT 116 tumors from **Fig. 3.3b,e**. Pathways highlighted in red were observed *in vitro* and *in vivo*. (**D**) Schematic overview of Dynamic Flux Analysis (DFA) approach for constructing genome-scale metabolic models of timecourse intracellular and extracellular metabolites from iDox-shGOT1 #1 PA-TU-8902 cells (+/- dox) as determined by LC/MS. In the schemes, circles represent metabolites connected in a metabolic pathway. DFA uses 3744 reactions, 2771 metabolites and 1487 genes. The network represented as the stoichiometric matrix (S) and is used to solve the reaction flux vector (v), determined by change of metabolite concentration over time (d[M] / dt or b). See Methods for further description. (**E**) Systematic reaction knockout analysis using DFA identifies differentially active metabolic reactions in PDA +/- GOT1 knockdown. “Knocked-out” reactions with negative Z-scores resulted in a computationally predicted decrease in PDA “growth” in cells under +dox conditions, while reactions with positive Z-scores decreased PDA “growth” in cells under -dox conditions. The y-axis shows the total number of reactions in each Z-score bin. Select KEGG pathways from +/- dox DFA with related enzymes that reached statistical significance are shown to the right and bottom. Reactions shown have $P < 0.05$ (two-sample t-test).

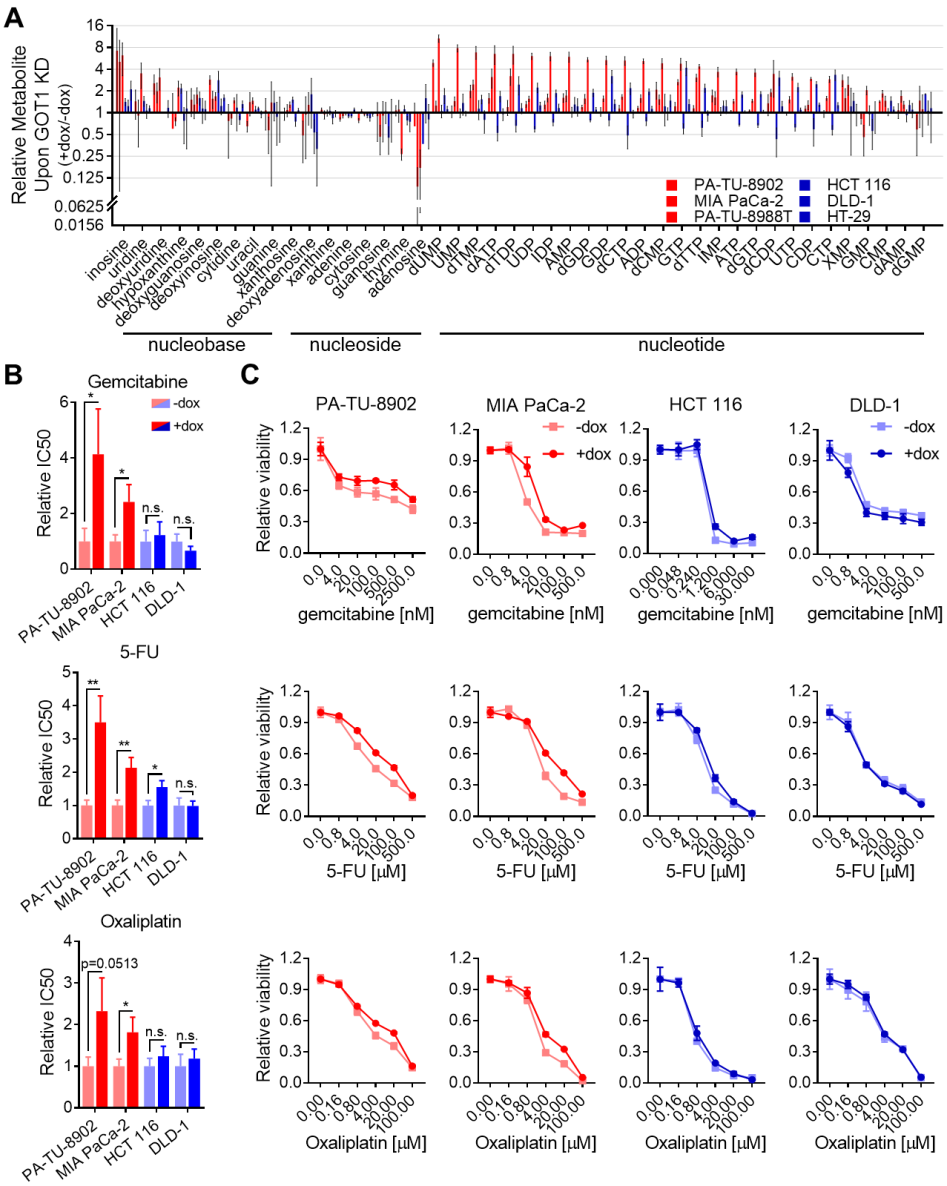

Figure 3.18 GOT1 inhibition disrupts nucleotide metabolism in PDA. (**A**) Relative nucleic acid pools as determined by LC/MS in iDox-shGOT1 #1 PDA and CRC, presented as GOT1 knockdown over mock (+dox/-dox). (**B**) Relative IC50 of gemcitabine, 5-fluorouracil (5-FU) and oxaliplatin in iDox-shGOT1 #1 PDA and CRC cells upon GOT1 knockdown. (**C**) Relative viability of iDox-shGOT1 #1 PDA and CRC cells treated with a dose response of gemcitabine (top), 5-FU (middle), and oxaliplatin (bottom). IC50s in (**b**) were derived from dose response curves. ADP, adenosine diphosphate; AMP, adenosine monophosphate; ATP, adenosine triphosphate; CDP, cytidine diphosphate; CMP, cytidine monophosphate; CTP, cytidine triphosphate; dAMP, deoxyadenosine monophosphate; dATP, deoxyadenosine triphosphate; dCDP, deoxycytidine diphosphate; dCMP, deoxycytidine monophosphate; dCTP, deoxycytidine triphosphate; dGDP, deoxyguanosine diphosphate; dGMP, deoxyguanosine monophosphate; dGTP, deoxyguanosine triphosphate; dTDP, deoxythymidine diphosphate; dTMP, deoxythymidine monophosphate; dTTP, deoxythymidine triphosphate; dUMP, deoxyuridine monophosphate; GDP, guanosine diphosphate; GMP, guanosine monophosphate; GTP, guanosine triphosphate; IDP, inosine diphosphate; IMP, inosine monophosphate; UDP, uridine diphosphate; UMP, uridine monophosphate; UTP, uridine triphosphate; XMP, xanthosine monophosphate. Error bars in represent s.d. from biological replicates (n=3). n.s., not significant; *, $P < 0.05$; **, $P < 0.01$; Student t-test (unpaired, two-tailed).

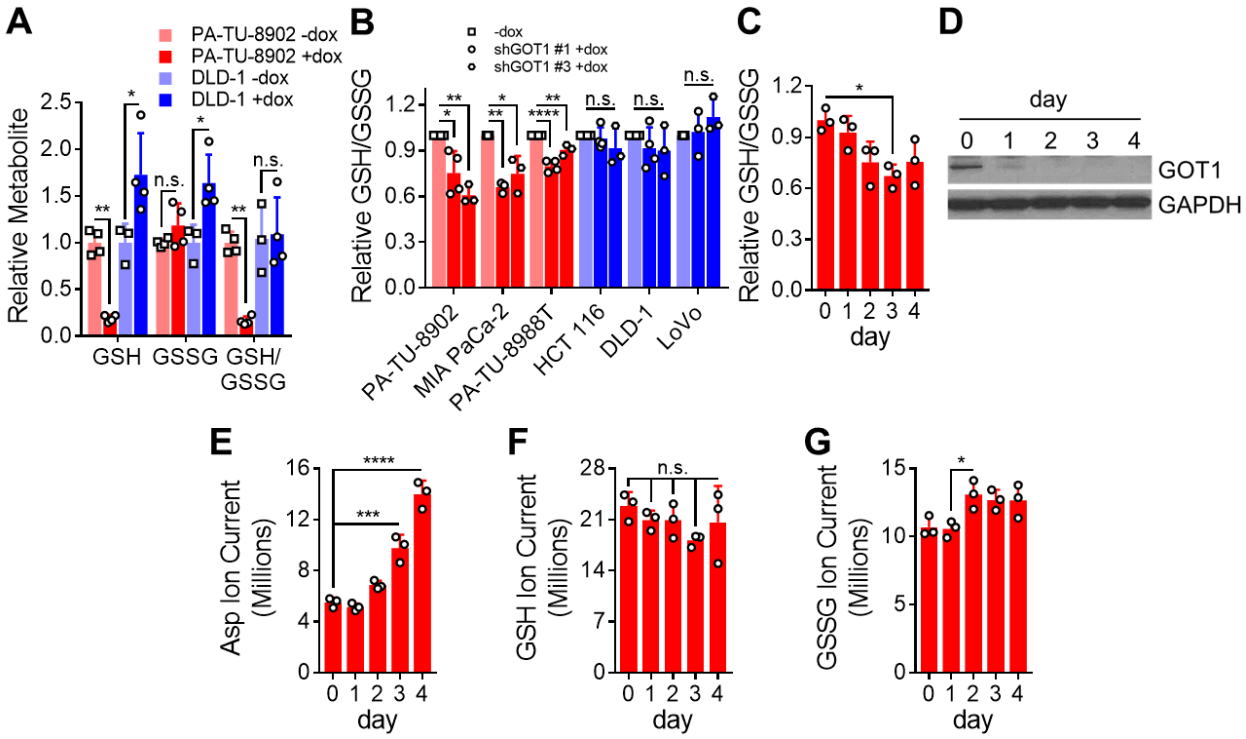

Figure 3.19 GOT1 inhibition induces redox imbalance. (**A**) Relative reduced glutathione (GSH), oxidized glutathione (GSSG), and the ratio (GSH/GSSG) pools upon GOT1 knockdown in iDox-shGOT1 #1 PDA and CRC cells. Data were obtained by LC/MS and are normalized as GOT1 knockdown over mock (+dox/-dox). (**B**) Relative GSH/GSSG upon GOT1 knockdown as determined by enzymatic assay in PDA and CRC and normalized as GOT1 knockdown over mock (+dox/-dox). (**C**) Timecourse of relative GSH/GSSG pools upon GOT1 knockdown in iDox-shGOT1 #1 PA-TU-8902 PDA cells. Data were obtained by LC/MS and are normalized as GOT1 knockdown over mock (+dox/-dox). (**D**) GOT1 protein expression during dox-mediated knockdown timecourse in iDox-shGOT1 #1 PA-TU-8902 cells. GAPDH serves as the protein loading control. (**E**) Total aspartate (Asp) pools in PA-TU-8902 cells, as determined by LC/MS and plotted as GOT1 knockdown over mock (+dox/-dox). Timecourse of total (**F**) reduced glutathione (GSH) and (**G**) oxidized glutathione (GSSG) pools in iDox-shGOT1 #1 PA-TU-8902 cells, as determined by LC/MS. Error bars represent s.d. from biological replicates in **a,c,e-g** (n=3) and in **b** (n=4, iDox-shGOT1 #1 PA-TU-8902, PA-TU-8988T, HCT 116, DLD-1; n=3, iDox-shGOT1 #1 MIA PaCa-2, LoVo and iDox-shGOT1 #3). n.s., not significant; *, $P < 0.05$; **, $P < 0.01$; ***, $P < 0.001$; ****, $P < 0.0001$; Student t-test (unpaired, two-tailed) (**a**); one-way ANOVA (**b,c,e-g**).

not CRC (**Fig. 3.21a-d**). Radiotherapy was efficacious as a single agent in both models and delayed tumor growth. However, GOT1 inhibition uniquely increased the time to tumor tripling in PDA (**Fig. 3.21e,f**). Together with our mechanistic studies above, these results demonstrate that GOT1 inhibition promotes redox imbalance uniquely in PDA, which results in a drop in GSH levels and the GSH/GSSG ratio, leading to radiosensitization of PDA cells *in vitro* and PDA tumors *in vivo*.

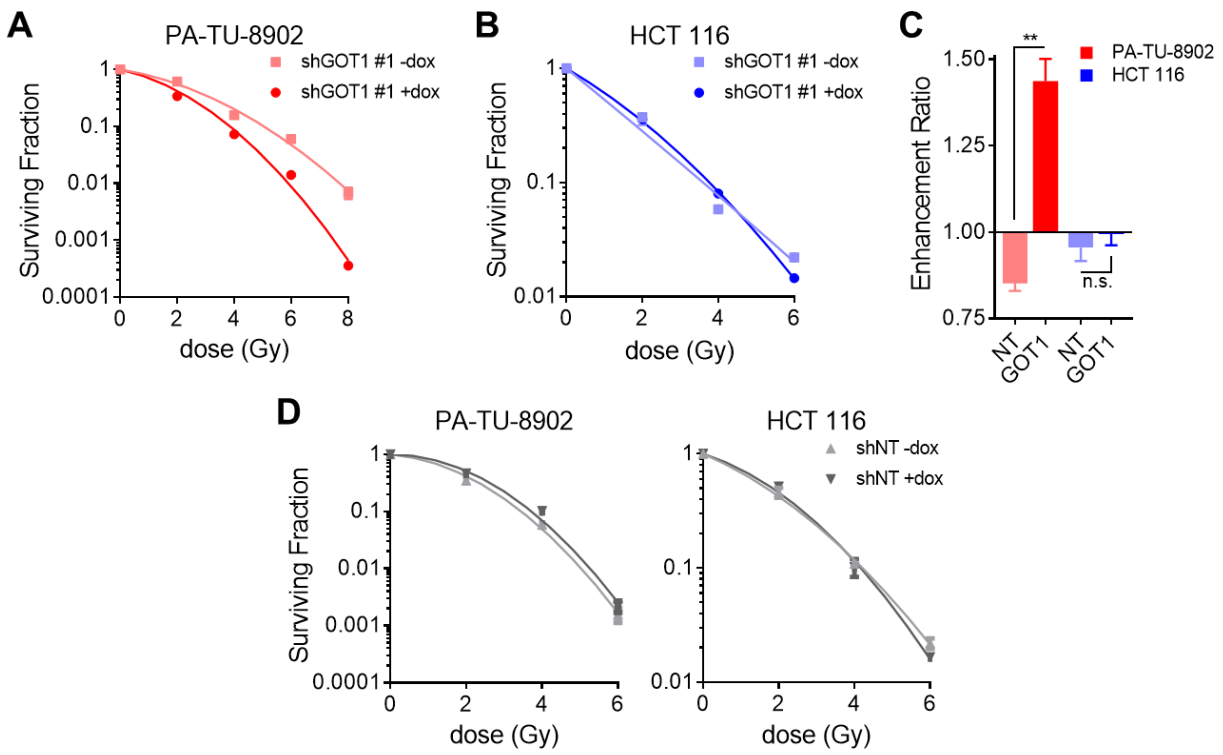

Figure 3.20 GOT1 inhibition sensitizes PDA to radiation therapy *in vitro*. (**A**) Surviving fraction from clonogenic cell survival assays of radiation-treated iDox-shGOT1 #1 PA-TU-8902 and (**B**) HCT 116. Gy, Gray. (**C**) Enhancement ratio of radiation treated iDox-shGOT1 #1 PDA and CRC cells. (**D**) Surviving fraction from clonogenic assay of radiation-treated iDox-shNT PA-TU-8902 (left) and HCT116 (right), +/- dox. Error bars represent s.d. from biological replicates (n=3). Gy, Gray. n.s., not significant; **, $P < 0.01$. Student t-test (unpaired, two-tailed).

Discussion

Precision oncology aims to assign new medicines based on the genotype of a patient[40]. In PDA and CRC, activating mutations of the MAPK pathway (e.g. in *KRAS* and *BRAF*) and loss of tumor suppressor *TP53* are common[41,42], and these mutations play important roles in the reprogramming of cancer metabolism[11,18,43]. Yet, despite this, metabolic gene expression programs in tumors more closely resemble their cell of origin rather than their oncogenotype[44]. Our results similarly add to the growing body of literature that metabolic dependencies exhibit tissue specificity[3,4]. Herein, we report that among typically mutant KRAS-expressing PDA and CRC lines, PDA cells are uniquely responsive to GOT1 knockdown. This is manifest as profound growth inhibition *in vitro* and in tumor xenografts *in vivo*. Through an integrated analysis utilizing multiple metabolomics profiling approaches together with computational modeling, we demonstrate that GOT1

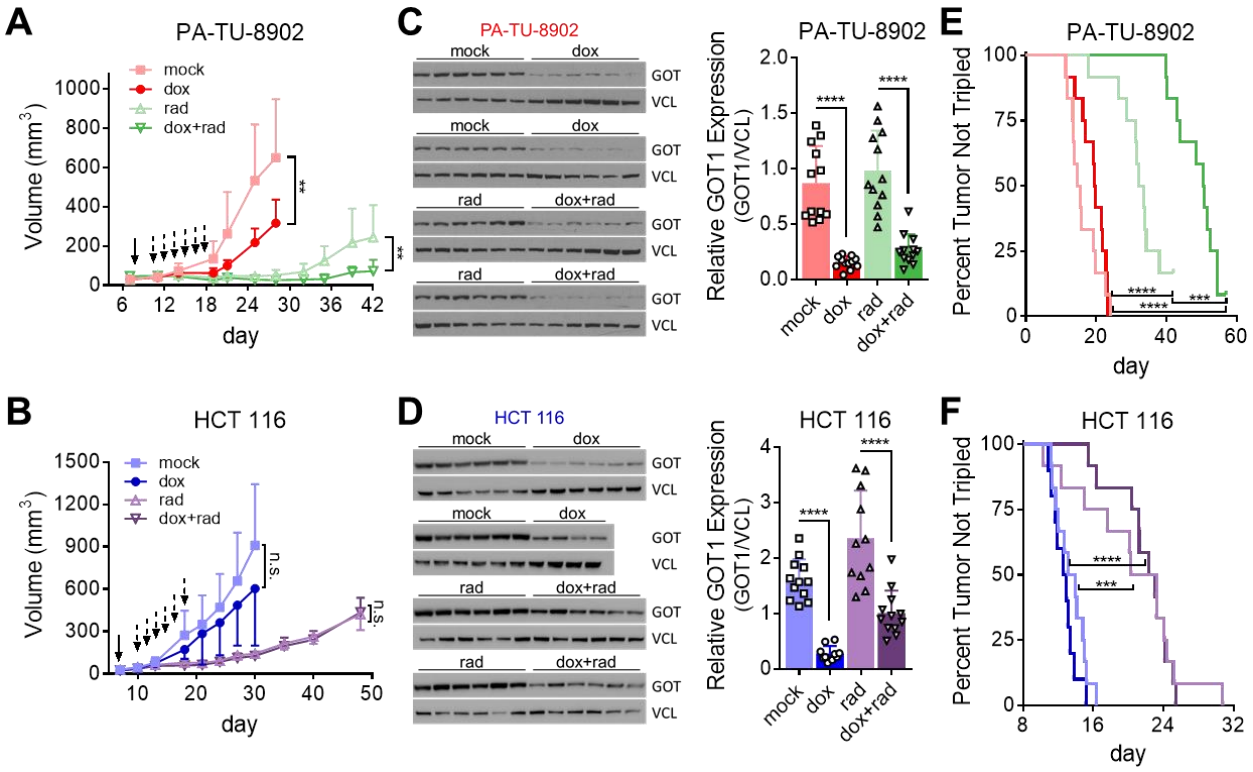

Figure 3.21 GOT1 inhibition sensitizes PDA to radiation therapy *in vivo*. (**A**) Tumor growth of iDox-shGOT1 #1 PA-TU-8902 or (**B**) iDox-shGOT1 #1 HCT116 xenografts treated with dox (solid arrow; maintained for the duration of the experiment) and/or radiation (rad; dashed arrows). Error bars represent s.d. n=12 tumors per arm, except for dox HCT 116 tumors where n=10. Western blot (left) and quantification (right) for GOT1 expression in iDox-shGOT1 #1 (**C**) PA-TU-8902 and (**D**) HCT116 xenograft tumors treated with dox and/or radiation (rad). Error bars represent s.d from n=12 tumors per arm except n=10 dox HCT 116 tumors. (**E**) Time to tumor tripling of iDox-shGOT1 #1 PA-TU-8902 or (**F**) iDox-shGOT1 #1 HCT116 xenografts. n.s., not significant; **, $P < 0.01$; ***, $P < 0.001$; ****, $P < 0.0001$; Student t-test (unpaired, two-tailed) (**a-d**); one-way ANOVA (**e,f**).

knockdown uniquely impacts glycolysis, nucleotide metabolism, and GSH-mediated redox regulation in PDA. Based on the disrupted GSH profile, we demonstrated that GOT1 knockdown can serve as a radiosensitizing strategy for PDA.

Despite observing a stark difference in the GOT1 dependence between our PDA and CRC cell lines, the baseline metabolic profiles and nutrient utilization in central carbon metabolism was surprisingly comparable (**Figs. 3.5-3.9**). This similarity may reflect adaptations that have occurred during prolonged exposure of these cell lines to culture, which serve to meet an optimal metabolic flux program to facilitate maximal proliferation. Regardless, metabolic dependences remain hard-wired. Upon GOT1 inhibition, unique shifts in metabolism are observed between the two tissue types, which account for the growth inhibition of PDA cells and tumors upon GOT1 knockdown.

A disruption of nucleotide metabolism was the most notable metabolic change across PDA lines upon GOT1 knockdown (**Fig. 3.17b, 3.18a**). Generally, this led to the accumulation of numerous phosphorylated nucleic acid species. We also observed that GOT1 knockdown reduced the sensitivity of PDA cells to the anti-metabolite chemotherapies gemcitabine and 5-FU. Our proposed explanation for these results is that the increase in the pool of deoxycytidine and uracil species, respectively, decreases the relative intracellular concentration of the anti-metabolite therapies and thereby their activity[24,33]. This explanation, however, does not apply to oxaliplatin, whose cytotoxic activity is similarly impaired upon GOT1 knockdown in PDA cells. Thus, a non-mutually exclusive explanation for the chemoprotective effect of GOT1 is that GOT1 knockdown is cytostatic in PDA cells and tumors (**Fig. 3.1b, 3.3b**). Chemotherapy is thought to work by selectively targeting dividing cells. Given that GOT1 knockdown impairs proliferation, the chemoprotective effect may simply result from impairing cycling, an effect not observed in GOT1 inhibition resistant CRC. It is also curious to note that GSH, which is diminished in GOT1 knockdown PDA cells, can protect cells from cytotoxic chemotherapy. Despite having lower GSH, the GOT1 knockdown PDA cells are less sensitive to the chemotherapies tested. Collectively, these results indicated that the use of chemotherapy in conjunction with GOT1 is not a practical therapeutic strategy and highlights the need to test combination treatment strategies in the preclinical setting.

PDA is an extremely aggressive disease and therapeutic options are largely ineffective[45]. The odds of surviving the first year are only 24%, and the five-year survival rate is a dismal 9%[46]. One of the main factors underscoring this low survival rate is the lack of effective clinical treatments[47]. *KRAS* mutations are observed in >90% of PDA, yet despite great efforts, current means to inhibit RAS are limited to the G12C mutation[48], which is only observed in 2% of patients[41]. Immunotherapy, while promising in other types of cancer, has proven ineffective to treat PDA[49,50]. Thus, improving current therapeutic modalities represents the best immediate hope for PDA patients. Radiotherapy is a standard of care for PDA in many institutions, although this remains controversial[51]. For patients that have undergone surgical resection for PDA, the receipt of adjuvant radiation (in combination with chemotherapy) is associated with a survival benefit in large institutional series, and this is currently being evaluated in a phase III randomized trial (RTOG 0848,

ClinicalTrials.gov NCT01013649)[52,53]. Despite these encouraging results, nearly 40% of patients receiving adjuvant radiation experience treatment failures within the irradiated field, indicating that PDA radiation resistance remains an important barrier to improving outcomes in the adjuvant setting[54]. Radiation also plays an important role for patients with locally advanced PDA that cannot be resected[55,56]. As in the adjuvant setting, nearly 40% of patients receiving radiation for locally advanced PDA will experience local tumor progression, again highlighting the clinical challenge of radiation resistance in PDA[57].

Our findings suggest that GOT1 inhibition could improve outcomes in PDA by overcoming this radiation resistance. Importantly, this strategy is unlikely to increase the normal tissue toxicity that often limits the intensification of radiotherapy-based treatment regimens. This potential therapeutic window is supported by our previous reports that GOT1 inhibition is well tolerated in non-transformed cells, as radiation dose is often limited so as not to harm nearby normal tissues. The GOT1 independence of CRC cell lines provide further support that a therapeutic window may exist for systemically targeting GOT1 in a subset of cancer types. To this end, we and others have engaged in developing GOT1 inhibitors[14,15]. Future work on optimized GOT1 drugs will be required to test the activity of these agents in combination with radiotherapy.

Metabolic programs in malignant cells are determined by the cell of origin and the oncogenotype. Here, we show that PDA and CRC lines respond differently to GOT1 inhibition, even though both groups harbor oncogenic KRAS and P53 mutations. Upon GOT1 knockdown, growth of PDA cells and xenografts is profoundly impaired, while CRC remains insensitive. Metabolic profiling of PDA and CRC cell lines following GOT1 inhibition revealed that glycolysis, nucleotide metabolism, and redox homeostasis were uniquely perturbed in PDA. Due to the disruption in redox balance in PDA, GOT1 inhibition enhanced sensitivity to radiotherapy, a standard of care for PDA patients. These results demonstrate a prominent role of cell of origin dictating metabolic dependencies and reveals new insights for targeting metabolic vulnerabilities to treat PDA.

Materials and Methods

Cell culture

Cell lines were obtained from the American Type Culture Collection or the German Collection of Microorganisms and Cell Cultures: PDA cell lines PA-TU-8902 (RRID:CVCL_1845), BxPC-3 (RRID:CVCL_0186), MIA PaCa-2 (RRID:CVCL_0428), and PA-TU-8988T (RRID:CVCL_1847); and CRC cell lines HCT 116 (RRID:CVCL_0291), DLD-1 (RRID:CVCL_0248), LoVo (RRID:CVCL_0399), and HT-29 (RRID:CVCL_0320). All cell lines were routinely tested for mycoplasma contamination (Lonza MycoAlert Plus, LT07-710). BxPC-3 cells were cultured in RPMI-1640 (Gibco, 11875-093) with 10% FBS (Corning, 35-010-CV). All other cell lines were cultured in DMEM (Gibco, 11965-092) with 10% FBS.

shRNA constructs and iDox-shRNA stable cell lines

The lentiviral vector containing tetracycline inducible system Tet-pLKO-puro (a gift from Dmitri Wiederschain) was engineered to contain the following shRNAs: GOT1 coding region (shGOT1 #1, TRCN0000034784) or GOT1 3'UTR (shGOT1 #3, 5'-CCGGTTGGAGGTCAAAGCAAATTAACTCGAGTTAATTTGCTTTGACCTCCAATTTTT-3'). Oligonucleotides were obtained (Integrated DNA Technologies Inc.), annealed and cloned at AgeI and EcoRI sites in tet-pLKO-puro (Addgene, 21915; http://www.addgene.org/21915, RRID:Addgene_21915)[58] following the Wiederschain Protocol (https://media.addgene.org/data/plasmids/21/21915/21915-attachment_Jws3xzJOO5Cu.pdf). A tet-pLKO non-targeting control vector (shNT, 5'-CCGGCAACAAGATGAAGAGCACCAACTCGAGTTGGTGCTCTTCATCTTGTTGTTTTT-3'; or shLUC, TRCN0000072259) was constructed similarly. Tet-pLKO-shGOT1 and tet-pLKO-shNT lentiviruses were produced by the University of Michigan Vector Core using the purified plasmids. Parental PDA and CRC cell lines were then transduced with optimized viral titers and stable cell lines were established post puromycin selection.

Colony forming and clonogenic cell survival assays

Colony forming assays (CFA) were performed as previously described with slight modifications[12]. Briefly, cells were plated in 6-well plates at 300-600 cells per well (dependent on the cell line) in 2 mL of media. 24 hours after seeding, dox was added at

1 ug/mL and culture medium was changed every 48 hours. After 8-13 days, colonies were fixed with 100% methanol and stained with 0.5% crystal violet solution. Colonies in triplicate wells were counted in ImageJ and graphed. Statistical analyses performed using GraphPad Prism7 software.

For radiotherapy studies, clonogenic assays were performed as described previously[59,60]. Briefly, 3 to 4 days after dox-induced shRNA expression, cells were irradiated with varying doses of radiation and then replated at clonal density. After 10 to 14 days of growth, colonies of 50 or more cells were enumerated and corrected for plating efficiency using unirradiated samples. Cell survival curves were fitted using the linear-quadratic equation. Enhancement ratios were calculated as the ratio of the mean inactivation dose under no dox conditions divided by the mean inactivation dose under +dox conditions.

cDNA rescues

Direct mutagenesis of shGOT1 #1 in pDONR223 resulted in GOT1 cDNA (sequence GCGGTGGTATAACGGCACCAA) resistant to shRNA targeting. GOT1 cDNA was Gateway cloned into DEST vector pLVX-GW-Hygro.

qPCR

RNA was extracted using RNeasy Mini Kit (Qiagen, 74104) according to manufacturer's instructions. cDNA was generated using SuperScript III CellsDirect™ cDNA Synthesis Kit (Invitrogen, 18080300). RT–PCR was done using SYBR Green PCR Master Mix (Applied Biosystems, 4309155) on a ViiA 7 Real-Time PCR System (Applied Biosystems). Relative mRNA levels were normalized to expression of human β-actin. RT–PCR was performed in quadruplicate.

Western blot analysis

Stable shNT and shGOT1 cells were cultured with or without dox media and protein lysates were collected after five days using RIPA buffer (Sigma, R0278) containing protease inhibitor cocktail (Sigma/Roche, 04 693 132 001). Samples were quantified with Pierce BCA Protein Assay Kit (ThermoFisher, 23225). 10 to 40 µg of protein per sample were resolved on NuPAGE Bis-Tris Gels (Invitrogen, NP0336) and blotted to PVDF membranes (Millipore, IPVH00010). Membranes were blocked in Tris-buffered saline (Bio-Rad, 170-6435) containing 0.5% of Tween 20 (Sigma, P2287) (TBS-T buffer) and

5% non-fat dry milk (LabScientific, M0841) then incubated with primary antibody overnight at 4ºC. The membranes were then washed with TBS-T buffer followed by exposure to the appropriate horseradish peroxidase-conjugated secondary antibody for 1h and visualized on either Kodak X-ray film (GeneMate, F-9023-8x10) or BioRad ChemiDoc Imaging System using either SuperSignal West Pico Chemiluminescent Substrate (Thermo Scientific, 34080) or ECL Prime Western Blotting Detection Reagent (Amersham, RPN2232). The following antibodies were used: anti-aspartate aminotransferase (anti-GOT1) at a 1:1,000 dilution (Abcam, ab171939), anti-GOT2 at a 1:1,000 dilution (Atlas Antibodies Sigma-Aldrich, HPA018139), anti-ME1 at a 1:1,000 dilution (Santa Cruz, sc-100569), anti-MDH1 at a 1:10,000 dilution (Abcam, ab180152), and loading control vinculin at a 1:10,000 dilution (Cell Signaling Technology, 13901) or GAPDH at a 1:1,000 dilution (Cell Signaling Technology, 2118). Anti-GOT1 at a dilution of 1:1,000 (Abnova, H00002805-B01P) was used in **Fig. 3.19d** and **Fig. 3.2a**. Anti-rabbit IgG, HRP-linked (Cell Signaling Technology, 7074) and anti-mouse IgG, HRP-linked (Cell Signaling Technology, 7076) secondary antibody was used at a 1:10,000 dilution. Protein expression was quantified with ImageJ.

Mass Spectrometry-Based Metabolomics

Unlabeled targeted metabolomics: Cells were plated at 500,000 cells per well in 6-well plates or ~1.5 million cells per 10 cm dish. At the end of indicated time points, 1 mL of medium was saved for metabolite extraction. Cells were lysed with dry-ice cold 80% methanol and extracts were then centrifuged at 10,000 g for 10 min at 4°C and the supernatant was stored at -80°C until further analyses. Protein concentration was determined by processing a parallel well/dish for each sample and used to normalize metabolite fractions across samples. Based on protein concentrations, aliquots of the supernatants were transferred to a fresh micro centrifuge tube and lyophilized using a SpeedVac concentrator. Dried metabolite pellets from cells or media were re-suspended in 35 µl 50:50 methanol:water mixture for LC–MS analysis. Data was collected using previously published parameters (ref:[22]).

Raw data were pre-processed with Agilent MassHunter Workstation Software Quantitative QqQ Analysis Software (B.07.00). Additional statistical analyses were

carried out in Excel (Microsoft) where each sample was normalized by the total intensity of all metabolites to reflect the protein content as a normalization factor. We then retained only those metabolites with at least 2 replicate measurements. The remaining missing value in each condition for each metabolite was filled with the median value of the other replicate measurements. Finally, each metabolite abundance level in each sample was divided by the median of all abundance levels across all samples to obtain relative metabolites. Significance testing was a two-tailed t-test with a significance threshold level of 0.05.

13C-tracing analysis: Cells were cultured in DMEM lacking Glc or Gln (ThermoScientific, A1443001) and supplemented with 10% dialyzed FBS (ThermoScientific, 26400036), the appropriate labeled substrate U-^{13}C-Gln (Cambridge Isotope Laboratories, CLM-1822-H) or U-^{13}C-Glc (Cambridge Isotope Laboratories, CLM-1396), and the appropriate complementary substrate (unlabeled glutamine or glucose). Cells were plated 24 hours prior to labeling at 500,000 cells per well in 6-well plates. Cells were labeled overnight to achieve steady-state labeling. Metabolites were extracted and data was collected according to previously described procedures (ref:[22]). Data were processed as described in the unlabeled targeted metabolomics section.

Gas chromatography: Cells were cultured as described above. Metabolite extraction was performed as described[61]. Briefly, cells were lysed with dry-ice cold 80% methanol and metabolite extracts were then centrifuged at 20,000 g for 7 min at 4°C. Chloroform (stabilized with amylene) was added to each clarified supernatant. Phase separation was reached by centrifugation at 20,000 g for 15 min at 4°C. The aqueous phase was lyophilized using a SpeedVac concentrator, snap frozen in liquid nitrogen, and stored at -80°C for further processing. Samples were dissolved in 30 µl of 2% methoxyamine hydrochloride in pyridine (MOX) (Pierce, TS-45950) at 37°C for 1.5 hrs. Samples were derivatized by adding 45µl of N-methyl-N-(tert-butyldimethylsilyl)trifluoroacetamide (MBTSTFA) + 1% tert-butyldimethylchlorosilane (TBDMCS) (Pierce, TS-48927) at 60°C for 1 hr.

GC-MS analysis was performed as described[62]. Briefly, analysis was performed on an Agilent 6890 GC instrument that contained a 30m DB-35MS capillary column, which was

interfaced to an Agilent 5975B MS. Electron impact (EI) ionization was set at 70 eV. Each analysis was operated in scanning mode, recording mass-to-charge-ratio spectra in the range of 100 – 605 m/z. For each sample 1µl was injected at 270°C, using helium as the carrier gas at a flow rate of 1 ml/min. To mobilize metabolites, the GC oven temperature was held at 100°C for 3 min and increased to 300°C at 3.5°C/min.

Xenograft tumors and treatments

All animal studies were performed in accordance with the guidelines of Institutional Animal Care and Use Committee (IACUC) and approved protocols. NOD scid gamma (NSG) mice (Jackson Laboratory, 005557), 6-8 or 8-10 weeks old of both sexes, were maintained in the facilities of the Unit for Laboratory Animal Medicine (ULAM) under specific pathogen-free conditions. Mice were subcutaneously (s.c.) injected in both flanks with $0.5x10^6$ total cells ($2.0x10^6$ for HCT 116) of iDox-shGOT1 #1 or shNT (n=8, iDox-shGOT1 BxPC-3 +/- dox, iDox-shNT BxPC-3 +dox tumors; n=6, iDox-shGOT1 PA-TU-8902 +/- dox, iDox-shNT PA-TU-8902 +/- dox, iDox-shNT BxPC-3 -dox, iDox-shNT DLD-1 +/- dox tumors; n=5, iDox-shGOT1 HCT 116 +dox, iDox-shGOT1 DLD-1 +/-dox tumors; n=4 iDox-shGOT1 HCT 116 -dox, iDox-shNT HCT 116 +/- dox tumors). Stable cells were trypsinized (Gibco, 25300-054) and suspended at 1:1 ratio of DMEM (Gibco, 11965-092) cell suspension:Matrigel (Corning, 354234) in 150-200 µL/injection. Dox chow (BioServ, F3949) was fed to the +dox groups on day 7 post tumor s.c. injection. Tumor size was assessed using a digital caliper twice/week after tumor cell implantation. Tumor volume (V, mm^3) was calculated as $V = 1/2(\text{length} \times \text{width}^2)$ or $V = \pi/6(\text{length} \times \text{width}^2)$ (ref:[63]). At endpoint, mice were sacrificed, and final volume and mass of tumors were measured prior to tissue processing. Tissue was either snap-frozen in liquid nitrogen and stored at -80°C until processed for protein or metabolite analysis, or fixed in zinc formalin fixative (Z-Fix, Anatech LTD, 174) solution for >24 hours then replaced with 70% ethanol for future histological and/or histochemical staining

For radiotherapy studies, mice were randomized to receive no treatment (mock), dox alone (dox), radiation alone (rad), or combined treatment (dox+rad) (n=12 tumors per arm except n=10 dox HCT 116 tumors). Radiation (2 Gy/fraction) was administered over 6 daily fractions, beginning day 10 after implantation) using a Philips RT250 (Kimtron

Medical) unit at a dose rate of approximately 2 Gy/minute. Dosimetry was performed using an ionization chamber directly traceable to a National Institute of Standards and Technology calibration. Animals were anesthetized with isoflurane and positioned such that the apex of each flank tumor was at the center of a 2.4 cm aperture in the secondary collimator, with the rest of the mouse shielded from radiation[60].

CCLE Dataset Analysis

The cancer cell line encyclopedia (CCLE) dataset with accession number GSE36133 (ref:[64]) was downloaded from the NCBI Gene Expression Omnibus[65]. The mRNA expression value of genes encoding GOT1-related enzymes, i.e. malic enzymes (ME1/2), malate dehydrogenases (MDH1/2), transaminases (GOT1/2, GPT1/2), and glutaminolysis enzymes (GLS, GLUD1) in PDA cell lines were compared to those of CRC.

Seahorse Analysis

Extracellular acidification rates (ECAR) were performed using the XF-96 Extracellular Flux Analyzer (Agilent Technologies). Cells were treated with dox for four days then plated on Seahorse Microplates in DMEM media (+/-dox) at: PA-TU-8902 30,000 cells/well, PA-TU-8988T 60,000 cells/well, HCT 116 60,000 cells/well, DLD-1 60,000 cells/well. The next day, media was replaced with Seahorse XF Base DMEM (Agilent, 103335-100) containing 25 mM glucose and 2 mM glutamine adjusted to pH ~7.4, and the plate was allowed to incubate for 1 hour in a non-CO_2, 37°C incubator. For the mitostress test, ECAR was measured under basal conditions and in response to mitochondrial inhibitors: oligomycin (0.5 μM), FCCP (0.25 μM), rotenone (0.5 μM), and antimycin A (0.5 μM).

Genome-Scale Metabolic Network Modeling Using Dynamic Flux Analysis

PA-TU-8902 cells were plated in 6-well plates in triplicate for each timepoint (4, 2, or 0 days of dox treatment). Media and cells were collected separately for unlabeled targeted metabolomics. The metabolomics data were used as constraints in the human metabolic reconstruction[26] to create a metabolic model using the dynamic flux analysis (DFA) approach[28,29]. DFA determines the optimal metabolic state that satisfies the biomass objective function and metabolomic constraints. DFA uses measured rate of change from time-course metabolomics data to constrain fluxes. Because subcellular compartment

information is lost during metabolomics measurement, we assumed that the measured metabolites represent the sum total in the cytoplasm, nucleus, and mitochondrial compartments. We used both intracellular and extracellular metabolite measurements to construct the metabolic models. Single gene and reaction knockouts were conducted on the metabolic models to estimate their impact on cellular growth rate. These models were used to identify genes and metabolic reactions that were differentially active between +/- dox cells.

Cell Viability Assay

PDA and CRC cells were plated at densities for log growth in the presence of dox (or mock treatment) for 4 days. On day 4, cells were trypsinized (Gibco, 25300-054) and replated in triplicate in 100 µL at 1,000 cells/well for -dox groups (PDA and CRC) and at 1,000 cells/well (CRC) or 3,000 cells/well (PDA) for +dox groups in white-walled 96 well plates (Corning/Costar, 3917). Cells were treated the following day with serial dilution of gemcitabine (Cayman Chemical, 9003096), 5-FU (Cayman Chemical, 14416), or oxaliplatin (Cayman Chemical, 13106). Cell viability was measured after 3 days using the CellTiter-Glo 2.0 Cell Viability Assay (Promega, G9243). Luminescence was measured for 500ms using a SpectraMax M3 Microplate Reader (Molecular Devices). IC50 values were calculated using GraphPad Prism 7 using three-parameter nonlinear regression analysis (except gemcitabine treated PA-TU-8902 used normalized response nonlinear regression analysis).

Glutathione Enzymatic Assay

Cells were grown in +/- dox media for 3 days then plated in 96-well plates in +/-dox media. The following day, GSH/GSSG ratio was measured according to the manufacturer instructions (Promega, V6611).

Statistical Analysis

Statistics were calculated using GraphPad Prism 7. One-way ANOVA was performed for experiments comparing multiple groups with one changing variable. ANOVA analyses were followed by Tukey's post hoc tests to allow multiple group comparisons. A Student's t-test (unpaired, two-tailed) was performed when comparing two groups to each other. Metabolomics data comparing 3 PDA and 3 CRC cell lines was analyzed by performing

a Student's t-test (unpaired, two-tailed) between all PDA metabolites and CRC metabolites. Time to tumor tripling analysis was performed using log-rank (Mantel–Cox) test. Outliers were removed with GraphPad using Grubbs' test, alpha=0.05. Groups were considered significantly different when $P< 0.05$. All data are presented as mean ± s.d. (standard deviation).

References

1 Hanahan, D. & Weinberg, R. A. Hallmarks of cancer: the next generation. *Cell* **144**, 646-674, doi:10.1016/j.cell.2011.02.013 (2011).

2 Vander Heiden, M. G. & DeBerardinis, R. J. Understanding the Intersections between Metabolism and Cancer Biology. *Cell* **168**, 657-669, doi:10.1016/j.cell.2016.12.039 (2017).

3 Mayers, J. R. *et al.* Tissue of origin dictates branched-chain amino acid metabolism in mutant Kras-driven cancers. *Science* **353**, 1161-1165, doi:10.1126/science.aaf5171 (2016).

4 Yuneva, M. O. *et al.* The metabolic profile of tumors depends on both the responsible genetic lesion and tissue type. *Cell Metab* **15**, 157-170, doi:10.1016/j.cmet.2011.12.015 (2012).

5 Lyssiotis, C. A. & Kimmelman, A. C. Metabolic Interactions in the Tumor Microenvironment. *Trends Cell Biol* **27**, 863-875, doi:10.1016/j.tcb.2017.06.003 (2017).

6 Davidson, S. M. *et al.* Environment Impacts the Metabolic Dependencies of Ras-Driven Non-Small Cell Lung Cancer. *Cell Metab* **23**, 517-528, doi:10.1016/j.cmet.2016.01.007 (2016).

7 Carmona-Fontaine, C. *et al.* Metabolic origins of spatial organization in the tumor microenvironment. *Proc Natl Acad Sci U S A* **114**, 2934-2939, doi:10.1073/pnas.1700600114 (2017).

8 Christen, S. *et al.* Breast Cancer-Derived Lung Metastases Show Increased Pyruvate Carboxylase-Dependent Anaplerosis. *Cell Rep* **17**, 837-848, doi:10.1016/j.celrep.2016.09.042 (2016).

9 Hensley, C. T. *et al.* Metabolic Heterogeneity in Human Lung Tumors. *Cell* **164**, 681-694, doi:10.1016/j.cell.2015.12.034 (2016).

10 Sellers, K. *et al.* Pyruvate carboxylase is critical for non-small-cell lung cancer proliferation. *J Clin Invest* **125**, 687-698, doi:10.1172/JCI72873 (2015).

11 Ying, H. *et al.* Oncogenic Kras maintains pancreatic tumors through regulation of anabolic glucose metabolism. *Cell* **149**, 656-670, doi:10.1016/j.cell.2012.01.058 (2012).

12 Son, J. *et al.* Glutamine supports pancreatic cancer growth through a KRAS-regulated metabolic pathway. *Nature* **496**, 101-105, doi:10.1038/nature12040 (2013).

13 Viale, A. *et al.* Oncogene ablation-resistant pancreatic cancer cells depend on mitochondrial function. *Nature* **514**, 628-632, doi:10.1038/nature13611 (2014).

14 Holt, M. C. *et al.* Biochemical Characterization and Structure-Based Mutational Analysis Provide Insight into the Binding and Mechanism of Action of Novel Aspartate Aminotransferase Inhibitors. *Biochemistry* **57**, 6604-6614, doi:10.1021/acs.biochem.8b00914 (2018).

15 Anglin, J. *et al.* Discovery and optimization of aspartate aminotransferase 1 inhibitors to target redox balance in pancreatic ductal adenocarcinoma. *Bioorganic & medicinal chemistry letters* **28**, 2675-2678, doi:10.1016/j.bmcl.2018.04.061 (2018).

16 Feld, F. M. *et al.* GOT1/AST1 expression status as a prognostic biomarker in pancreatic ductal adenocarcinoma. *Oncotarget* **6**, 4516-4526, doi:10.18632/oncotarget.2799 (2015).
17 Yang, C. S. *et al.* Glutamine-utilizing transaminases are a metabolic vulnerability of TAZ/YAP-activated cancer cells. *EMBO reports* **19**, doi:10.15252/embr.201643577 (2018).
18 Gaglio, D. *et al.* Oncogenic K-Ras decouples glucose and glutamine metabolism to support cancer cell growth. *Molecular systems biology* **7**, 523, doi:10.1038/msb.2011.56 (2011).
19 Thornburg, J. M. *et al.* Targeting aspartate aminotransferase in breast cancer. *Breast cancer research : BCR* **10**, R84, doi:10.1186/bcr2154 (2008).
20 Hingorani, S. R. *et al.* Trp53R172H and KrasG12D cooperate to promote chromosomal instability and widely metastatic pancreatic ductal adenocarcinoma in mice. *Cancer Cell* **7**, 469-483, doi:10.1016/j.ccr.2005.04.023 (2005).
21 Yuan, M., Breitkopf, S. B., Yang, X. & Asara, J. M. A positive/negative ion-switching, targeted mass spectrometry-based metabolomics platform for bodily fluids, cells, and fresh and fixed tissue. *Nature protocols* **7**, 872-881, doi:10.1038/nprot.2012.024 (2012).
22 Yuan, M. *et al.* Ex vivo and in vivo stable isotope labelling of central carbon metabolism and related pathways with analysis by LC-MS/MS. *Nature protocols* **14**, 313-330, doi:10.1038/s41596-018-0102-x (2019).
23 Sousa, C. M. *et al.* Pancreatic stellate cells support tumour metabolism through autophagic alanine secretion. *Nature* **536**, 479-483, doi:10.1038/nature19084 (2016).
24 Halbrook, C. J. *et al.* Macrophage-Released Pyrimidines Inhibit Gemcitabine Therapy in Pancreatic Cancer. *Cell Metab*, doi:10.1016/j.cmet.2019.02.001 (2019).
25 Treutler, H. *et al.* Discovering Regulated Metabolite Families in Untargeted Metabolomics Studies. *Analytical chemistry* **88**, 8082-8090, doi:10.1021/acs.analchem.6b01569 (2016).
26 Duarte, N. C. *et al.* Global reconstruction of the human metabolic network based on genomic and bibliomic data. *Proc Natl Acad Sci U S A* **104**, 1777-1782, doi:10.1073/pnas.0610772104 (2007).
27 Yizhak, K., Chaneton, B., Gottlieb, E. & Ruppin, E. Modeling cancer metabolism on a genome scale. *Molecular systems biology* **11**, 817, doi:10.15252/msb.20145307 (2015).
28 Chandrasekaran, S. *et al.* Comprehensive Mapping of Pluripotent Stem Cell Metabolism Using Dynamic Genome-Scale Network Modeling. *Cell reports* **21**, 2965-2977, doi:10.1016/j.celrep.2017.07.048 (2017).
29 Shen, F., Cheek, C. & Chandrasekaran, S. Dynamic Network Modeling of Stem Cell Metabolism. *Methods in molecular biology (Clifton, N.J.)* **1975**, 305-320, doi:10.1007/978-1-4939-9224-9_14 (2019).
30 Conroy, T. *et al.* Randomized phase III trial comparing FOLFIRINOX (F: 5FU/leucovorin [LV], irinotecan [I], and oxaliplatin [O]) versus gemcitabine (G) as first-line treatment for metastatic pancreatic adenocarcinoma (MPA): Preplanned

interim analysis results of the PRODIGE 4/ACCORD 11 trial. *Journal of Clinical Oncology* **28**, 4010-4010, doi:10.1200/jco.2010.28.15_suppl.4010 (2010).
31 Von Hoff, D. D. *et al.* Increased Survival in Pancreatic Cancer with nab-Paclitaxel plus Gemcitabine. *New England Journal of Medicine* **369**, 1691-1703, doi:10.1056/NEJMoa1304369 (2013).
32 Springfeld, C. *et al.* Chemotherapy for pancreatic cancer. *Presse medicale (Paris, France : 1983)* **48**, e159-e174, doi:10.1016/j.lpm.2019.02.025 (2019).
33 Shukla, S. K. *et al.* MUC1 and HIF-1alpha Signaling Crosstalk Induces Anabolic Glucose Metabolism to Impart Gemcitabine Resistance to Pancreatic Cancer. *Cancer Cell* **32**, 71-87 e77, doi:10.1016/j.ccell.2017.06.004 (2017).
34 Santana-Codina, N. *et al.* Oncogenic KRAS supports pancreatic cancer through regulation of nucleotide synthesis. *Nat Commun* **9**, 4945, doi:10.1038/s41467-018-07472-8 (2018).
35 Raufi, A. G., Manji, G. A., Chabot, J. A. & Bates, S. E. Neoadjuvant Treatment for Pancreatic Cancer. *Seminars in oncology* **46**, 19-27, doi:10.1053/j.seminoncol.2018.12.002 (2019).
36 Tesfaye, A. A. & Philip, P. A. Adjuvant treatment of surgically resectable pancreatic ductal adenocarcinoma. *Clinical advances in hematology & oncology : H&O* **17**, 54-63 (2019).
37 Pauwels, B., Korst, A. E., Lardon, F. & Vermorken, J. B. Combined modality therapy of gemcitabine and radiation. *The oncologist* **10**, 34-51, doi:10.1634/theoncologist.10-1-34 (2005).
38 Lawrence, T. S., Eisbruch, A., McGinn, C. J., Fields, M. T. & Shewach, D. S. Radiosensitization by gemcitabine. *Oncology (Williston Park, N.Y.)* **13**, 55-60 (1999).
39 Lesueur, P. *et al.* Poly-(ADP-ribose)-polymerase inhibitors as radiosensitizers: a systematic review of pre-clinical and clinical human studies. *Oncotarget* **8**, 69105-69124, doi:10.18632/oncotarget.19079 (2017).
40 Garraway, L. A. Genomics-driven oncology: framework for an emerging paradigm. *Journal of clinical oncology : official journal of the American Society of Clinical Oncology* **31**, 1806-1814, doi:10.1200/jco.2012.46.8934 (2013).
41 Bailey, P. *et al.* Genomic analyses identify molecular subtypes of pancreatic cancer. *Nature* **531**, 47-52, doi:10.1038/nature16965 (2016).
42 Fearon, E. R. Molecular genetics of colorectal cancer. *Annual review of pathology* **6**, 479-507, doi:10.1146/annurev-pathol-011110-130235 (2011).
43 Yun, J. *et al.* Glucose deprivation contributes to the development of KRAS pathway mutations in tumor cells. *Science (New York, N.Y.)* **325**, 1555-1559, doi:10.1126/science.1174229 (2009).
44 Hu, J. *et al.* Heterogeneity of tumor-induced gene expression changes in the human metabolic network. *Nature biotechnology* **31**, 522-529, doi:10.1038/nbt.2530 (2013).
45 Hidalgo, M. Pancreatic cancer. *The New England journal of medicine* **362**, 1605-1617, doi:10.1056/NEJMra0901557 (2010).
46 Siegel, R. L., Miller, K. D. & Jemal, A. Cancer statistics, 2019. *CA: a cancer journal for clinicians* **69**, 7-34, doi:10.3322/caac.21551 (2019).

47 Halbrook, C. J. & Lyssiotis, C. A. Employing Metabolism to Improve the Diagnosis and Treatment of Pancreatic Cancer. *Cancer Cell* **31**, 5-19, doi:10.1016/j.ccell.2016.12.006 (2017).
48 Misale, S. *et al.* KRAS G12C NSCLC Models Are Sensitive to Direct Targeting of KRAS in Combination with PI3K Inhibition. *Clin Cancer Res* **25**, 796-807, doi:10.1158/1078-0432.ccr-18-0368 (2019).
49 Halbrook, C. J., Pasca di Magliano, M. & Lyssiotis, C. A. Tumor Crosstalk Networks Promote Growth and Support Immune Evasion in Pancreatic Cancer. *Am J Physiol Gastrointest Liver Physiol*, doi:10.1152/ajpgi.00416.2017 (2018).
50 Brahmer, J. R. *et al.* Safety and activity of anti-PD-L1 antibody in patients with advanced cancer. *N Engl J Med* **366**, 2455-2465, doi:10.1056/NEJMoa1200694 (2012).
51 Badiyan, S. N., Molitoris, J. K., Chuong, M. D., Regine, W. F. & Kaiser, A. The Role of Radiation Therapy for Pancreatic Cancer in the Adjuvant and Neoadjuvant Settings. *Surgical oncology clinics of North America* **26**, 431-453, doi:10.1016/j.soc.2017.01.012 (2017).
52 Herman, J. M. *et al.* Analysis of fluorouracil-based adjuvant chemotherapy and radiation after pancreaticoduodenectomy for ductal adenocarcinoma of the pancreas: results of a large, prospectively collected database at the Johns Hopkins Hospital. *Journal of clinical oncology : official journal of the American Society of Clinical Oncology* **26**, 3503-3510, doi:10.1200/jco.2007.15.8469 (2008).
53 Hsu, C. C. *et al.* Adjuvant chemoradiation for pancreatic adenocarcinoma: the Johns Hopkins Hospital-Mayo Clinic collaborative study. *Annals of surgical oncology* **17**, 981-990, doi:10.1245/s10434-009-0743-7 (2010).
54 Dholakia, A. S. *et al.* Mapping patterns of local recurrence after pancreaticoduodenectomy for pancreatic adenocarcinoma: a new approach to adjuvant radiation field design. *International journal of radiation oncology, biology, physics* **87**, 1007-1015, doi:10.1016/j.ijrobp.2013.09.005 (2013).
55 Loehrer, P. J., Sr. *et al.* Gemcitabine alone versus gemcitabine plus radiotherapy in patients with locally advanced pancreatic cancer: an Eastern Cooperative Oncology Group trial. *Journal of clinical oncology : official journal of the American Society of Clinical Oncology* **29**, 4105-4112, doi:10.1200/jco.2011.34.8904 (2011).
56 Hurt, C. N. *et al.* Long-term results and recurrence patterns from SCALOP: a phase II randomised trial of gemcitabine- or capecitabine-based chemoradiation for locally advanced pancreatic cancer. *British journal of cancer* **116**, 1264-1270, doi:10.1038/bjc.2017.95 (2017).
57 Hammel, P. *et al.* Effect of Chemoradiotherapy vs Chemotherapy on Survival in Patients With Locally Advanced Pancreatic Cancer Controlled After 4 Months of Gemcitabine With or Without Erlotinib: The LAP07 Randomized Clinical Trial. *Jama* **315**, 1844-1853, doi:10.1001/jama.2016.4324 (2016).
58 Wiederschain, D. *et al.* Single-vector inducible lentiviral RNAi system for oncology target validation. *Cell cycle (Georgetown, Tex.)* **8**, 498-504, doi:10.4161/cc.8.3.7701 (2009).

59 Morgan, M. A. *et al.* The combination of epidermal growth factor receptor inhibitors with gemcitabine and radiation in pancreatic cancer. *Clin Cancer Res* **14**, 5142-5149, doi:10.1158/1078-0432.ccr-07-4072 (2008).
60 Wahl, D. R. *et al.* Glioblastoma Therapy Can Be Augmented by Targeting IDH1-Mediated NADPH Biosynthesis. *Cancer Res* **77**, 960-970, doi:10.1158/0008-5472.CAN-16-2008 (2017).
61 Nicolay, B. N. *et al.* Loss of RBF1 changes glutamine catabolism. *Genes Dev* **27**, 182-196, doi:10.1101/gad.206227.112 (2013).
62 Metallo, C. M. *et al.* Reductive glutamine metabolism by IDH1 mediates lipogenesis under hypoxia. *Nature* **481**, 380-384, doi:10.1038/nature10602 (2011).
63 Tomayko, M. M. & Reynolds, C. P. Determination of subcutaneous tumor size in athymic (nude) mice. *Cancer chemotherapy and pharmacology* **24**, 148-154 (1989).
64 Barretina, J. *et al.* The Cancer Cell Line Encyclopedia enables predictive modelling of anticancer drug sensitivity. *Nature* **483**, 603-607, doi:10.1038/nature11003 (2012).
65 Barrett, T. *et al.* NCBI GEO: archive for functional genomics data sets--update. *Nucleic acids research* **41**, D991-995, doi:10.1093/nar/gks1193 (2013).

CHAPTER 4
Extraneous Results

Introduction

Several experimental studies performed during the collection of data from my studies on metabolic changes that occur during ADM or in cancer cells revealed insights that were outside the scope (or opened up new directions) for these projects. The following sections present that data for comprehension and as a future resource for the Lyssiotis lab. Future studies will be required to ascertain their importance and utility.

In vivo oligomycin treatment

Using *in vitro* models of ADM, I found acinar cells are profoundly sensitive to oligomycin, an oxidative phosphorylation inhibitor (**Fig. 2.3**). Previous studies have demonstrated that targeting pathways necessary for ADM *in vitro* also inhibit ADM *in vivo*[1-3]. As such, I hypothesized that oligomycin treatment would inhibit ADM *in vivo*. I used an experimental model of pancreatitis in wild-type mice to stimulate ADM[4]. Pancreatitis can be induced with supraphysiologic concentrations of cerulein, a cholecystokinin ortholog that promotes excessive acinar enzyme production and premature activation resulting in acinar cell damage and ADM[5]. Mice were pretreated with either oligomycin or vehicle followed by treatment with a cerulein regimen that induces acute pancreatitis or saline as a vehicle control (**Fig. 4.1a**). Pancreas mass relative to body mass (% PM/BM) was similar between the groups (**Fig. 4.1b**) and hematoxylin and eosin (H&E) staining of pancreas tissue showed no obvious differences between groups treated with oligomycin (**Fig. 4.1c**). I proceeded with a more severe cerulein treatment that induces chronic pancreatitis in mice[3]. Again, wild-type mice were pretreated with either oligomycin or vehicle; however, a cerulein treatment regimen that induces chronic pancreatitis was used (**Fig. 4.1d**). Unlike induction of acute pancreatitis, there was a slight, but non-statistically significant, increase in relative pancreas mass of mice treated with oligomycin (**Fig. 4.1e**). There also appears to be an increase of ADM lesions and tissue damage in oligomycin-treated mice

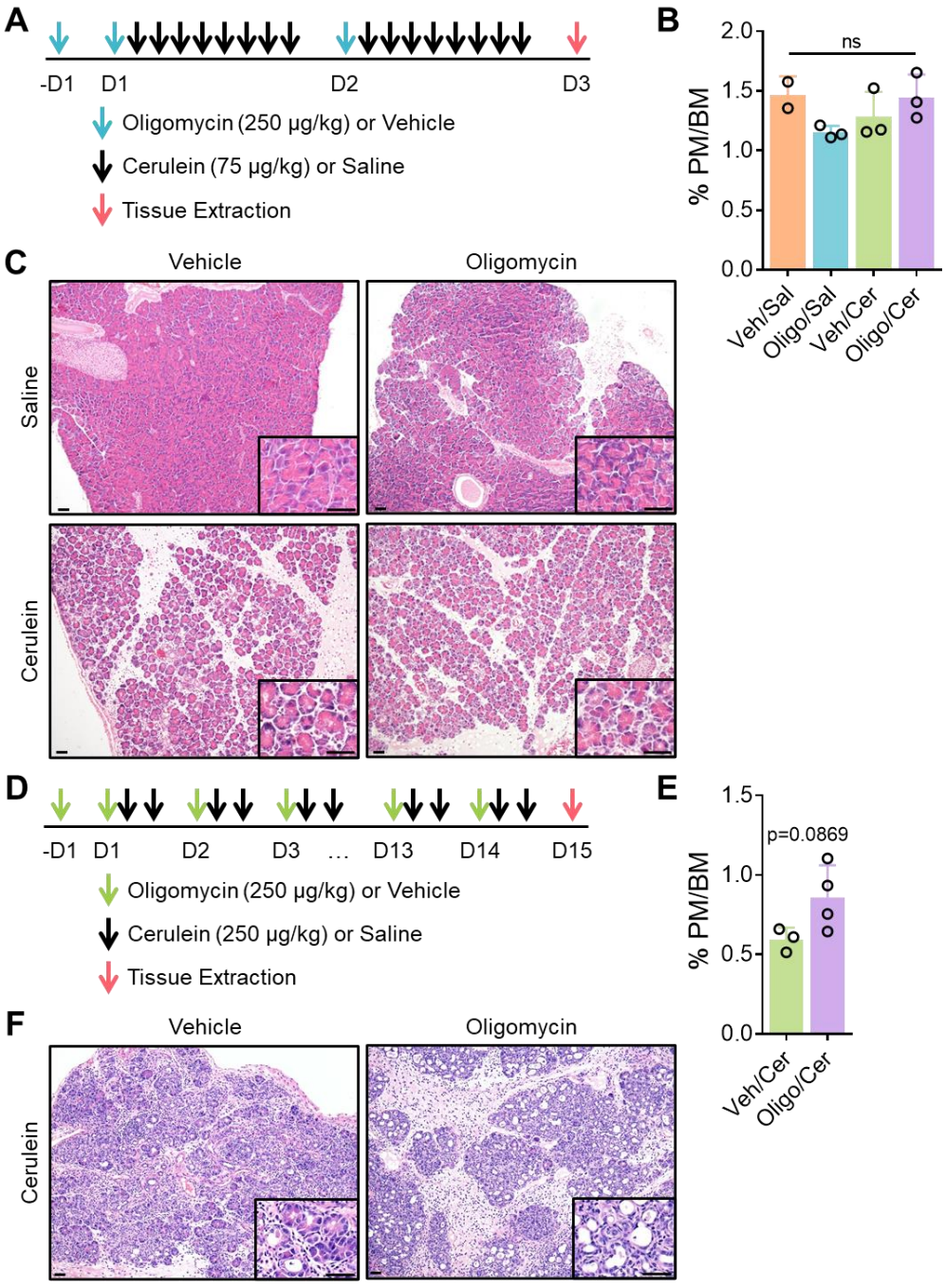

Figure 4.1 Oligomycin treatment during experimental pancreatitis induction. **(A)** Acute pancreatitis protocol with oligomycin pretreatment for wild-type mice. **(B)** Percent ratio of pancreas mass to body mass (% PM/BM) of mice on acute pancreatitis protocol. Error bars represent s.d. from biological replicates (n=2, Veh/Sal; n=3 Oligo/Sal, Veh/Cer, Oligo/Cer). **(C)** Representative H&E staining of pancreas tissue from mice on acute pancreatitis protocol. **(D)** Chronic pancreatitis protocol with oligomycin pretreatment for wild-type mice. Note, cerulein was administered for 14 consecutive days. **(E)** Percent ratio of pancreas mass to body mass (% PM/BM) of mice on chronic pancreatitis protocol. Error bars represent s.d. from biological replicates (n=3 Veh/Cer; n=4, Oligo/Cer). **(F)** Representative H&E staining of pancreas tissue from mice on chronic pancreatitis protocol. Scale bar = 50 µm. Cer, cerulein; Oligo, oligomycin, Sal, saline; Veh, vehicle. One-way ANOVA (**B**); Student's t-test (unpaired, two-tailed) (**E**).

(**Fig. 4.1f**). These data suggest inhibition of oxidative phosphorylation with oligomycin does not prevent chronic pancreatitis-induced ADM, but may accelerate ADM. Since oligomycin treatment is systemic the possible increase in ADM could be a result of oxidative phosphorylation inhibition in other cell types, such as macrophages which not only contribute to pancreatic tumorigenesis, but are also phenotypically altered by oligomycin treatment[6].

Pancreatitis induction in KCG model

Experimental models of pancreatitis accelerate tumor formation in *Kras*^{G12D}-expressing mice[7]. Following the observation that G6PD-deficiency accelerates ADM in *ex vivo* acinar explants (**Fig. 2.5b**), I tested whether induction of pancreatic injury affected *Kras*$^{LSL\text{-}G12D/+}$; *Ptf1a*$^{Cre/+}$ (KC) mice differently depending on G6PD status (KCG^{mut} or KCG^{wt}). Mice were intraperitoneally injected with either cerulein to induce chronic pancreatitis or saline as a vehicle control (**Fig. 4.2a**). Relative pancreas mass significantly increased in cerulein-treated KCG^{mut} mice compared to control mice (*Ptf1a*$^{Cre/+}$; *G6PD*^{mut} [CG^{mut}]) and KCG^{mut} mice injected with saline (**Fig. 4.2b**). Although there is no significant difference between KCG^{mut} and KCG^{wt} mice treated with cerulein, the trend of decreased pancreas mass in KCG^{wt} mice warrants further investigation. Increasing the sample size for the cerulein-treated KCG^{wt} group and including CG^{wt} and KCG^{wt} saline-injected controls are necessary prior to drawing any conclusions. Histological analysis of these pancreas tissue could reveal increased ADM or PanIN formation in cerulein-treated KCG^{mut} mice as inferred from an increase in relative pancreas mass.

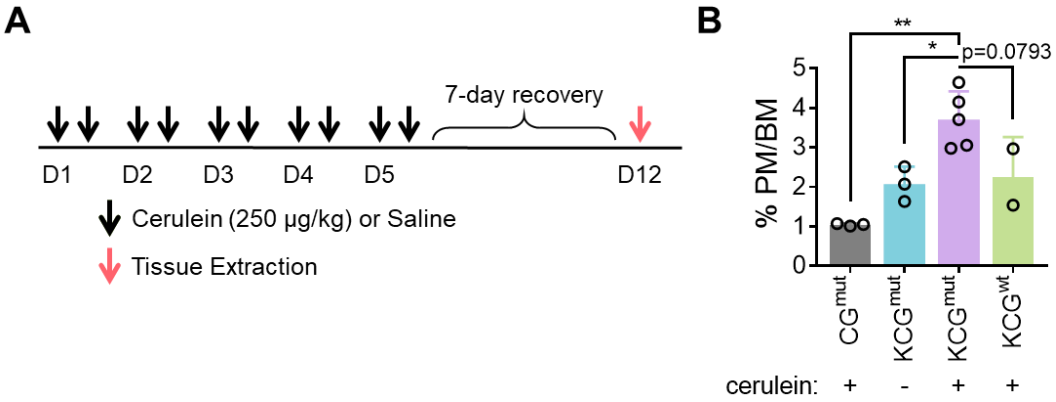

Figure 4.2 Chronic pancreatitis induction in KCG mice. (A) Chronic pancreatitis protocol for KC mice. **(B)** Percent ratio of pancreas mass to body mass (% PM/BM). Error bars represent s.d. from biological replicates (n=3, cerulein-treated CG^{mut}, saline-treated KCG^{mut}; n=5, cerulein-treated KCG^{mut}; n=2, cerulein-treated KCG^{wt}). *, $P < 0.05$; **, $P < 0.01$. One-way ANOVA.

Glutamine dropout in KCG^{mut} acinar explants

It was surprising that KC acinar explants survived and transdifferentiated without exogenous glutamine. This is in stark contrast to glutamine dependency of cultured PDA cells[8]. PDA cells downregulate the oxidative branch of the pentose phosphate pathway (PPP) and rewire glutamine metabolism to generate NADPH. Since G6PD-deficient KC acinar cells presumably generate less NADPH from oxidative PPP, I wanted to determine whether they were sensitive to the absence glutamine in culture. I hypothesized that KCG^{mut} acinar cells rewired glutamine metabolism for NADPH production, like seen in PDA cells. However, there is no difference in transdifferentiation of KCG^{mut} with or without exogenous glutamine (**Fig. 4.3**). This data suggests other NADPH-producing enzymes compensate for G6PD-deficiency and the rewiring of glutamine metabolism seen in PDA cells may not occur in transdifferentiating acinar cells. Future studies will interrogate the roles of NADPH-producing pathways and glutamine metabolism during ADM (**see Chapter 5**).

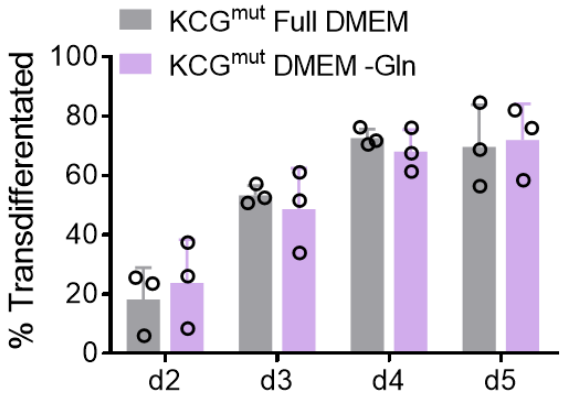

Figure 4.3 KCG^{mut} acinar cells cultured with or without glutamine. Quantification of ductal structures formed in collagen. Each point represents average of 3 technical replicates from independent mice. Error bars represent s.d. Student's t-test (unpaired, two-tailed); no statistical significance between groups.

GOT1 knockout in CRC cell lines

Compared to PDA cell lines, colorectal cancer (CRC) lines are insensitive to GOT1 knockdown by short hairpin RNA (shGOT1) (**Figs. 3.1b, 3.3e**). Although we induced strong knockdown of GOT1 (**Fig. 3.1e**), I hypothesized trace levels of GOT1 may be enough for growth and survival of CRC cells. To address this, I attempted to knock out GOT1 expression via CRISPR-Cas9. Unfortunately, I was not able to completely

knockout GOT1 from HCT116 cells (**Fig. 4.4a**) even after transfecting the cells a second time with the single guide RNA targeting GOT1 (sgGOT1) (**Fig. 4.4b**). DLD1 cells appeared more resistant to GOT1 knockout (**Fig. 4.4c**). Since protein expression was analyzed on the bulk population of CRISPR-Cas9-treated cells, I screened clonal populations for GOT1 knockout. All clones had varying amounts of GOT1 expression (**Fig. 4.4d**) and proliferation was not impaired in any clones (**Fig. 4.4e**). I hypothesize GOT1 is an essential gene in CRC cells, where complete knockout is lethal. Presumably, the cells that grow out are incompletely edited by CRISPR, allowing expression of GOT1.

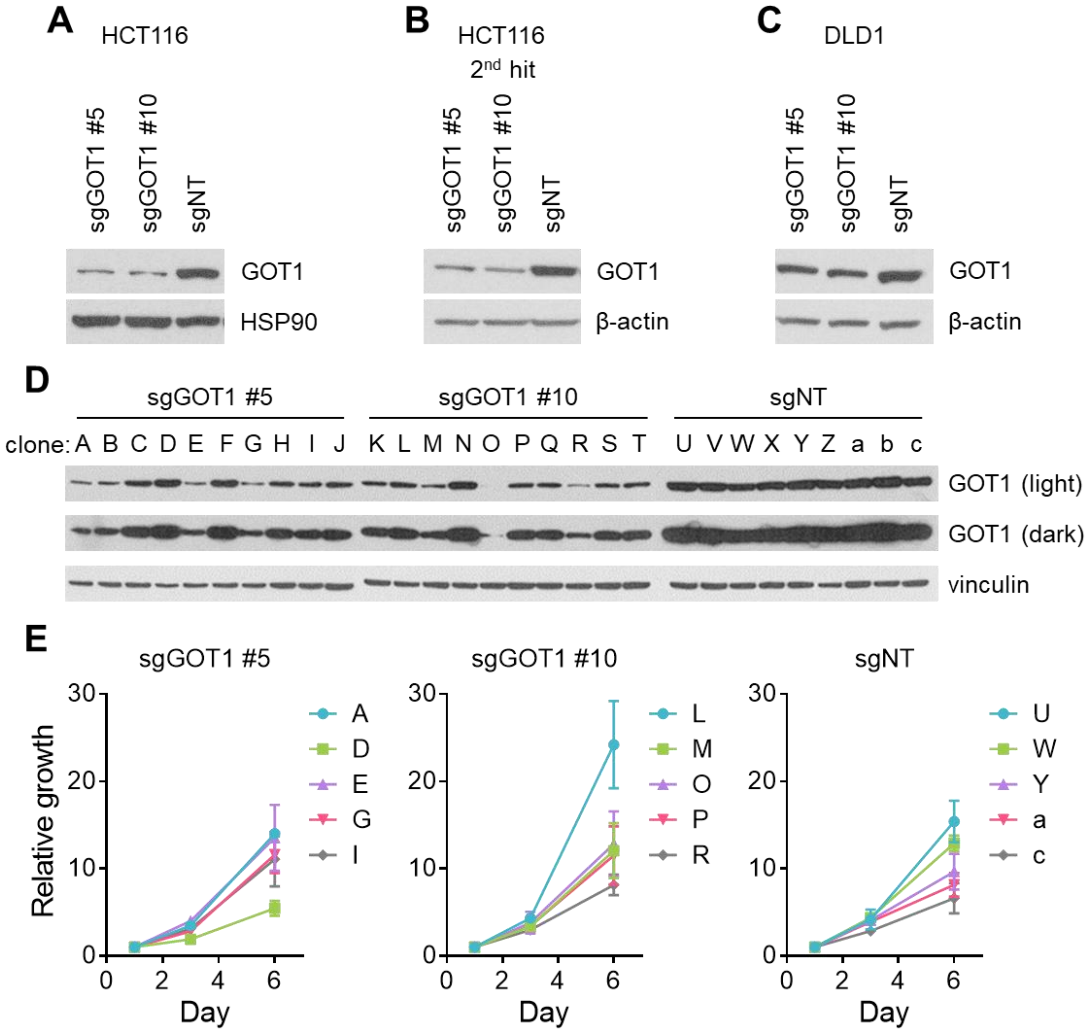

Figure 4.4 CRISPR-Cas9-mediated GOT1 knockout in CRC cells. Western blots for GOT1 and loading controls HSP90 or β-actin from **(A)** HCT116 cells transfected with single guide RNA targeting GOT1 (two independent guides: sgGOT1 #5 and sgGOT1 #10) or non-targeting single guide RNA (sgNT), **(B)** HCT116 cells transfected a second time with sgGOT1 or sgNT, and **(C)** DLD1 cells transfected with sgGOT1 or sgNT. **(D)** Western blots for GOT1 and vinculin loading control from HCT116 clonal populations from the bulk population presented in (**A**). **(E)** Relative growth curves of select HCT116 clones. Error bars represent s.d. from biological replicates (n=3).

Compensation for GOT1 independence in CRC cells

Because CRC cells are insensitive to GOT1 inhibition, I sought to determine how CRC cells compensate for GOT1 independence. Metabolic pathways that could bypass GOT1 include conversion of citrate to oxaloacetate by ATP citrate lyase (ACLY), mitochondrial export of malate via mitochondrial dicarboxylate carrier (SLC25A10), or mitochondrial import of malate or glutamate via mitochondrial 2-oxoglutarate/malate carrier (SLC25A11) and mitochondrial aspartate glutamate carrier (SLC25A12), respectively, to fuel the TCA cycle (**Fig. 4.5a**). Doxycycline (dox)-inducible shACLY was transduced into HCT116 cells expressing dox-inducible shGOT1 or non-targeting control (shNT) (**Fig. 4.5b**). Knockdown of ACLY alone or in combination with GOT1 did not inhibit colony forming potential (**Fig. 4.5c,d**). Dox-inducible expression of shSLC25A10, shSLC25A11, or shSLC25A12 (**Fig. 4.5e**) also did not impair colony forming potential of HCT116 cells (**Fig. 4.5f,g**). The metabolic programs that contribute to GOT1 independence in KRAS-mutated CRC cells remain unknown and could be driven by other genomic or epigenomic events of CRC[9] beyond the scope of my research.

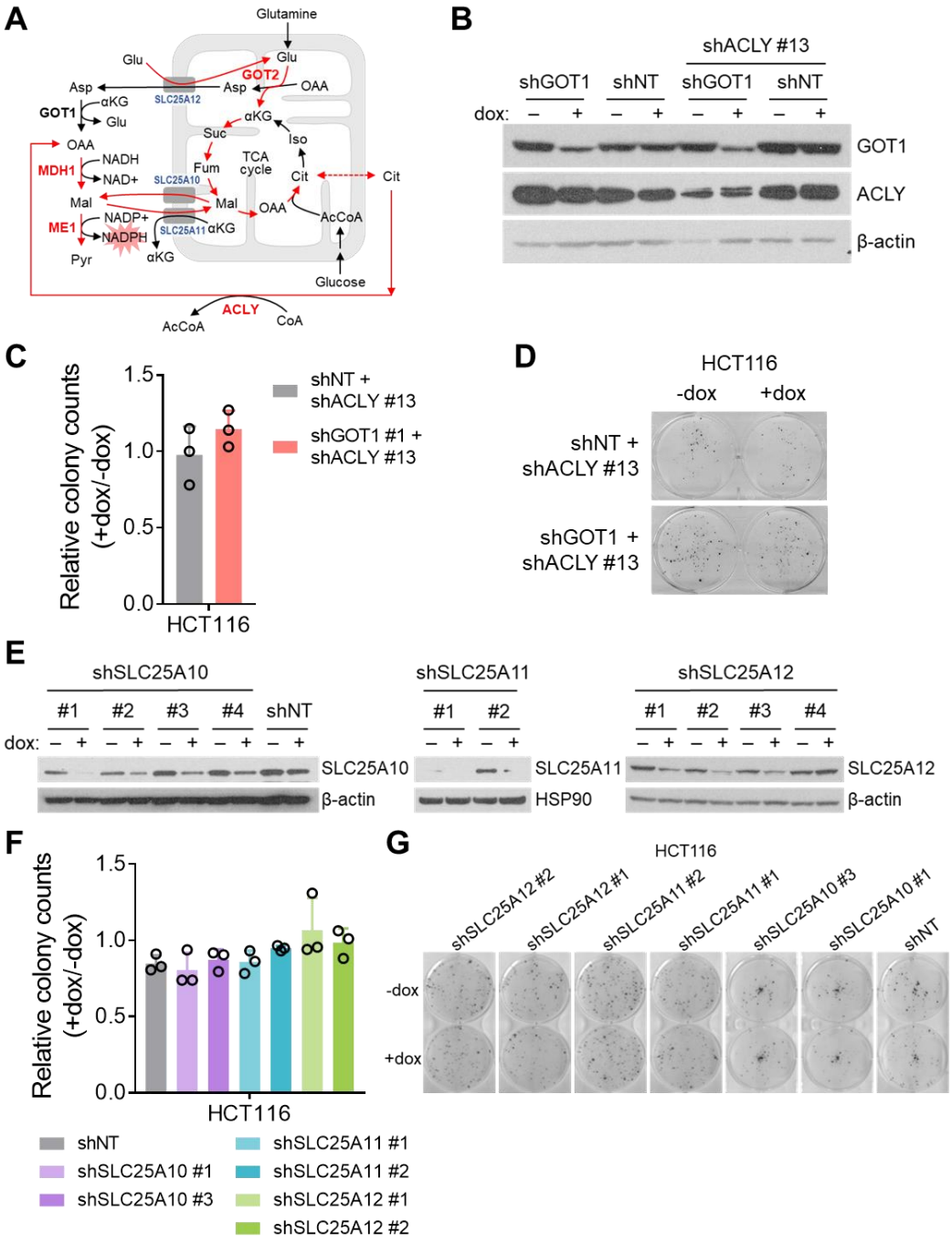

Figure 4.5 Possible mechanisms for bypassing GOT1 in CRC cells. (A) Schematic of mechanisms CRC cells may utilize to bypass GOT1 dependence. **(B)** Western blot for GOT1, ACLY, and β-actin loading control from dox-inducible shGOT1, shACLY, and/or shNT HCT116 cells. **(C)** Relative colony number after dox treatment in HCT116 cells expressing shNT or shGOT1 in combination with shACLY. Error bars represent s.d. from biological replicates (n=3). **(D)** Representative wells from colony forming assays quantified in (**C**). **(E)** Western blots for SLC25A10, SLC25A11, SLC25A12, and β-actin and HSP90 loading controls from HCT116 cells expressing the respective dox-inducible short hairpin RNA. **(F)** Relative colony number after dox treatment in HCT116 cells expressing shNT or two independent hairpins against shSLC25A10, shSLC25A11, or shSLC25A12. **(G)** Representative wells from colony forming assays quantified in (**F**). Error bars represent s.d. from biological replicates (n=3). Student's t-test (unpaired, two-tailed) (**C**); One-way ANOVA (**F**); no statistical significance between groups.

Materials and Methods

Mouse Strains

All animal studies were performed in accordance with the guidelines of Institutional Animal Care and Use Committee (IACUC) and approved protocols. *Kras*$^{LSL\text{-}G12D/+}$, *Ptf1a*$^{Cre/+}$, *Tp53*$^{LSL\text{-}R172H/+}$, and *G6PD*^{mut} mice have been previously described (**see Chapter 2**). *Kras*$^{LSL\text{-}G12D/+}$*; Ptf1a*$^{Cre/+}$ (KC) mice were maintained on a C57BL/6 background. *Kras*$^{LSL\text{-}G12D/+}$*; Ptf1a*$^{Cre/+}$*; G6PD* (KCG) and *Kras*$^{LSL\text{-}G12D/+}$*; Tp53*$^{LSL\text{-}R172H/+}$*; Ptf1a*$^{Cre/+}$*; G6PD* (KPCG) mice were maintained on a mixed background.

Cerulein Treatment

Wild-type mice were generated from the *Kras*$^{LSL\text{-}G12D/+}$*; Ptf1a*$^{Cre/+}$ (KC) colony. Cerulein treatments were performed on mice between 7 and 16 weeks of age. Cerulein (American Peptide Company Inc) was dissolved in sterile saline. For chronic pancreatitis, cerulein was administered to mice twice daily for 14 days at a concentration of 250 mg/kg body weight via intraperitoneal injection. For acute pancreatitis, mice were given hourly injections of cerulein for 8 hours for 2 days at a concentration of 75 mg/kg body weight via intraperitoneal injection. An equal volume of sterile saline was injected as a control. Mice were pretreated with 250 µg/kg oligomycin A (Sigma, 75351) the day prior to starting cerulein injections and 1 hour prior to the first daily cerulein injections.

Histology

Mice were sacrificed by CO_2 asphyxiation then tissue was quickly harvested and fixed overnight at room temperature with zinc formalin fixative (Z-Fix, Anatech LTD, 174). Tissues were processed using a Leica ASP300S Tissue Processor (Leica Microsystems Inc), paraffin embedded, and cut into 5 µm sections. Hematoxylin and eosin (H&E) staining was performed using Mayer's hematoxylin solution and Eosin Y (Thermo Fisher Scientific, HT110116). Slides were scanned with a Pannoramic SCAN scanner (Perkin Elmer).

Three-dimensional Acinar Cell Explant Culture

Pancreas was harvested and rinsed twice in 5 mL cold HBSS (Gibco, 14170112). Tissue was minced with sterile scissors into 1-5 mm sized pieces then centrifuged for 2 minutes at 300 g and 4ºC. Media was aspirated and minced tissue was digested with ~5 mg of

Collagenase P (Roche) in 5 mL cold HBSS for 15-18 minutes, shaking at 100 rpm at 37ºC. Collagenase P was inhibited by addition of 5 mL cold 5% FBS in HBSS. Cells were centrifuged for 2 minutes at 300 g and 4ºC then washed with 5 mL cold 5% FBS in HBSS. This was repeated twice more. Cells were passed through 500 µm polypropylene mesh (Pluriselect, Fisher, NC0822591). Mesh was washed with 5 mL cold 5% FBS in HBSS. Cells were passed through 100 µm polypropylene mesh (Fisherbrand, 22363549) then pelleted through 10 mL of 30% fetal bovine serum gradient. Cells were resuspended in media and incubated at 37ºC for 2-4 hours prior to embedding. All media was supplemented with 0.4 mg/mL soybean trypsin inhibitor (Gibco, 17075-029), 1 ug/mL dexamethasone (Sigma, D4902), and 0.5% gentamicin (Lonza, 17-519L). All media was adjusted to final pH 7.2-7.4 at 37ºC and sterilized through a 0.22 µm PVDF membrane (Millipore, Stericup Filter Unit, SCGVU01RE; Steriflip Filter Unit, SE1M179M6). Unless indicated, cells were cultured in 1x Waymouth's media (Sigma, W1625) supplemented with 2.2 g/L sodium bicarbonate (Sigma, S5761). Glutamine dropout media was prepared from DMEM powder without glucose or glutamine (Sigma, D5030) supplemented with 3.7 g/L sodium bicarbonate and 25 mM D-glucose (Sigma, G7021). Control media was supplemented with 4 mM L-glutamine (Gibco, A2916801). Acinar cells were embedded in bovine collagen (Culturex, 344205001) according to the manufacturer's protocol. Culture media was added on top of solidified matrix and changed on days 1, 3, and 5 after plating.

Cell culture

HCT 116 (RRID:CVCL_0291) cell line was obtained from the American Type Culture Collection. All cell lines were routinely tested for mycoplasma contamination (Lonza MycoAlert Plus, LT07-710). HCT 116 was cultured in DMEM (Gibco, 11965-092) with 10% FBS.

shRNA constructs and iDox-shRNA stable cell lines

The lentiviral vector containing tetracycline inducible system Tet-pLKO-puro (a gift from Dmitri Wiederschain) was engineered to contain the following shRNAs: GOT1 coding region (shGOT1 #1, TRCN0000034784) or GOT1 3'UTR (shGOT1 #3, 5'-CCGGTTGGAGGTCAAAGCAATTAACTCGAGTTAATTTGCTTTGACCTCCAATTTTT-

3’). Oligonucleotides were obtained (Integrated DNA Technologies Inc.), annealed and cloned at AgeI and EcoRI sites in tet-pLKO-puro (Addgene, 21915; http://www.addgene.org/21915, RRID:Addgene_21915) following the Wiederschain Protocol (https://media.addgene.org/data/plasmids/21/21915/21915-attachment_Jws3xzJOO5Cu.pdf). A tet-pLKO non-targeting control vector (shNT, 5’-CCGGCAACAAGATGAAGAGCACCAACTCGAGTTGGTGCTCTTCATCTTGTTGTTTTT-3’; or shLUC, TRCN0000072259) was constructed similarly. Tet-pLKO-shGOT1 and tet-pLKO-shNT lentiviruses were produced by the University of Michigan Vector Core using the purified plasmids. Parental HCT 116 cells were then transduced with optimized viral titers and stable cell lines were established post puromycin selection.

sgRNA constructs and CRISPR-Cas9 cell lines

The lentiviral vector lentiCRISPR v2 (Addgene, 52961) was engineered to contain the following sgRNAs: sgGOT1 #5 (5’-GAGTTGGGTCAATCCCAGTTGGG-3’) or sgGOT1 #10 (5’-GATAGGCTGAGTCAAAGAAG-3’) (gifts from Alec Kimmelman). Cells were transfected via Lipofectamine LTX Reagent with PLUS Reagent (Invitrogen, 15338100) according to the manufacture’s protocol. Stable cell lines were established post puromycin selection.

Colony forming assays

Colony forming assays (CFA) were performed as previously described with slight modifications[8]. Briefly, cells were plated in 6-well plates at 300 cells per well in 2 mL of media. 24 hours after seeding, dox was added at 1 ug/mL and culture medium was changed every 48 hours. After 8-13 days, colonies were fixed with 100% methanol and stained with 0.5% crystal violet solution. Colonies in triplicate wells were counted in ImageJ and graphed. Statistical analyses performed using GraphPad Prism7 software.

Western blot analysis

Protein lysates were collected after five days using RIPA buffer (Sigma, R0278) containing protease inhibitor cocktail (Sigma/Roche, 04 693 132 001). Samples were quantified with Pierce BCA Protein Assay Kit (ThermoFisher, 23225). 10 to 40 µg of protein per sample were resolved on NuPAGE Bis-Tris Gels (Invitrogen, NP0336) and blotted to PVDF membranes (Millipore, IPVH00010). Membranes were blocked in Tris-

buffered saline (Bio-Rad, 170-6435) containing 0.5% of Tween 20 (Sigma, P2287) (TBS-T buffer) and 5% non-fat dry milk (LabScientific, M0841) then incubated with primary antibody overnight at 4ºC. The membranes were then washed with TBS-T buffer followed by exposure to the appropriate horseradish peroxidase-conjugated secondary antibody for 1h and visualized on either Kodak X-ray film (GeneMate, F-9023-8x10) or BioRad ChemiDoc Imaging System using either SuperSignal West Pico Chemiluminescent Substrate (Thermo Scientific, 34080) or ECL Prime Western Blotting Detection Reagent (Amersham, RPN2232). The following antibodies were used: anti-aspartate aminotransferase (anti-GOT1) at a 1:1,000 dilution (Abcam, ab171939), anti-ATP citrate lyase (anti-ACLY) at a 1:500 dilution (ProteinTech, 15421-1-AP), anti-SLC25A10 at 1:250 (Atlas Antibodies, HPP023048), anti-SLC25A11 at 1:250 (Atlas Antibodies, HPA021167), anti-SLC25A12 at 1:250 (Atlas Antibodies, HPA035333), and loading controls β-actin at 1:10,000 (Santa Cruz Biotech, sc-47778) or HSP90 at 1:1,000 (Cell Signaling Technology 4874S). Anti-rabbit IgG, HRP-linked (Cell Signaling Technology, 7074) and anti-mouse IgG, HRP-linked (Cell Signaling Technology, 7076) secondary antibody was used at a 1:10,000 dilution.

Cell Proliferation Assay

Cells were plated in triplicate in 100 µL at 1,000 cells/well in 3 identical plates. At day 1, 3, and 6, media was gently removed from the wells and placed at -80ºC. Cell proliferation was measured using CyQUANT Cell Proliferation Assay (Molecular Probes, C7026) at the same time for all plates. Fluorescence was measured using a SpectraMax M3 Microplate Reader (Molecular Devices).

References

1 Collins, M. A., Yan, W., Sebolt-Leopold, J. S. & Pasca di Magliano, M. MAPK signaling is required for dedifferentiation of acinar cells and development of pancreatic intraepithelial neoplasia in mice. *Gastroenterology* **146**, 822-834.e827, doi:10.1053/j.gastro.2013.11.052 (2014).

2 Ardito, C. M. *et al.* EGF receptor is required for KRAS-induced pancreatic tumorigenesis. *Cancer cell* **22**, 304-317, doi:10.1016/j.ccr.2012.07.024 (2012).

3 Halbrook, C. J. *et al.* Mitogen-activated Protein Kinase Kinase Activity Maintains Acinar-to-Ductal Metaplasia and Is Required for Organ Regeneration in Pancreatitis. *Cellular and molecular gastroenterology and hepatology* **3**, 99-118, doi:10.1016/j.jcmgh.2016.09.009 (2017).

4 Halbrook, C. J. & Lyssiotis, C. A. Employing Metabolism to Improve the Diagnosis and Treatment of Pancreatic Cancer. *Cancer cell* **31**, 5-19, doi:10.1016/j.ccell.2016.12.006 (2017).

5 Lerch, M. M. & Gorelick, F. S. Models of acute and chronic pancreatitis. *Gastroenterology* **144**, 1180-1193, doi:10.1053/j.gastro.2012.12.043 (2013).

6 Chen, W. *et al.* The phenotype of peritoneal mouse macrophages depends on the mitochondria and ATP/ADP homeostasis. *Cellular immunology* **324**, 1-7, doi:10.1016/j.cellimm.2017.11.003 (2018).

7 Guerra, C. *et al.* Pancreatitis-induced inflammation contributes to pancreatic cancer by inhibiting oncogene-induced senescence. *Cancer cell* **19**, 728-739, doi:10.1016/j.ccr.2011.05.011 (2011).

8 Son, J. *et al.* Glutamine supports pancreatic cancer growth through a KRAS-regulated metabolic pathway. *Nature* **496**, 101-105, doi:10.1038/nature12040 (2013).

9 Dienstmann, R. *et al.* Consensus molecular subtypes and the evolution of precision medicine in colorectal cancer. *Nature reviews. Cancer* **17**, 79-92, doi:10.1038/nrc.2016.126 (2017).

CHAPTER 5
Conclusions and Future Directions

Introduction

The incidence of pancreatic ductal adenocarcinoma (PDA) is increasing while some other major cancers are declining[1]. Early detection methods and effective treatments are needed to improve the dismal 10% five-year survival rate. PDA cells extensively reprogram cellular metabolism for growth and survival[2]. Mutations in oncogenic *KRAS* drive metabolic rewiring PDA cells are dependent on to supply biosynthetic precursors and energy. Understanding the metabolic dependencies of tumorigenesis and tumor maintenance could reveal targetable vulnerabilities for disease detection and/or treatment. I determined metabolic requirements, centering on redox homeostasis, that contribute to pancreatic tumorigenesis and could be leveraged for therapeutic strategies against PDA tumors.

Pancreatic Tumorigenesis

Mouse models of pancreatic cancer have revealed that acinar cells, driven by mutations in oncogenic *Kras* in acinar cells can give rise to PDA[3,4]. Tumorigenesis can begin with acinar cells transdifferentiating into ductal progenitor cells, a process termed acinar-to-ductal metaplasia (ADM). Using *ex vivo* models of ADM[5], I determined metabolic requirements for transdifferentiation of primary acinar explants (**Fig. 5.1**). I found acinar cells require subphysiological concentrations of glucose to survive and undergo ADM. Further, I demonstrated that exogenous glutamine or branched-chain amino acids (BCAA) are dispensable for ADM. Mutation of glucose-6-phosphate dehydrogenase (G6PD) impairs the oxidative pentose phosphate pathway (PPP), resulting in an accelerated rate of ADM *in vitro* and tumorigenesis *in vivo*. I also found acinar cells are profoundly sensitive to oxidative phosphorylation inhibition. Future studies will interrogate the role of these processes to determine their therapeutic utility, as outlined below.

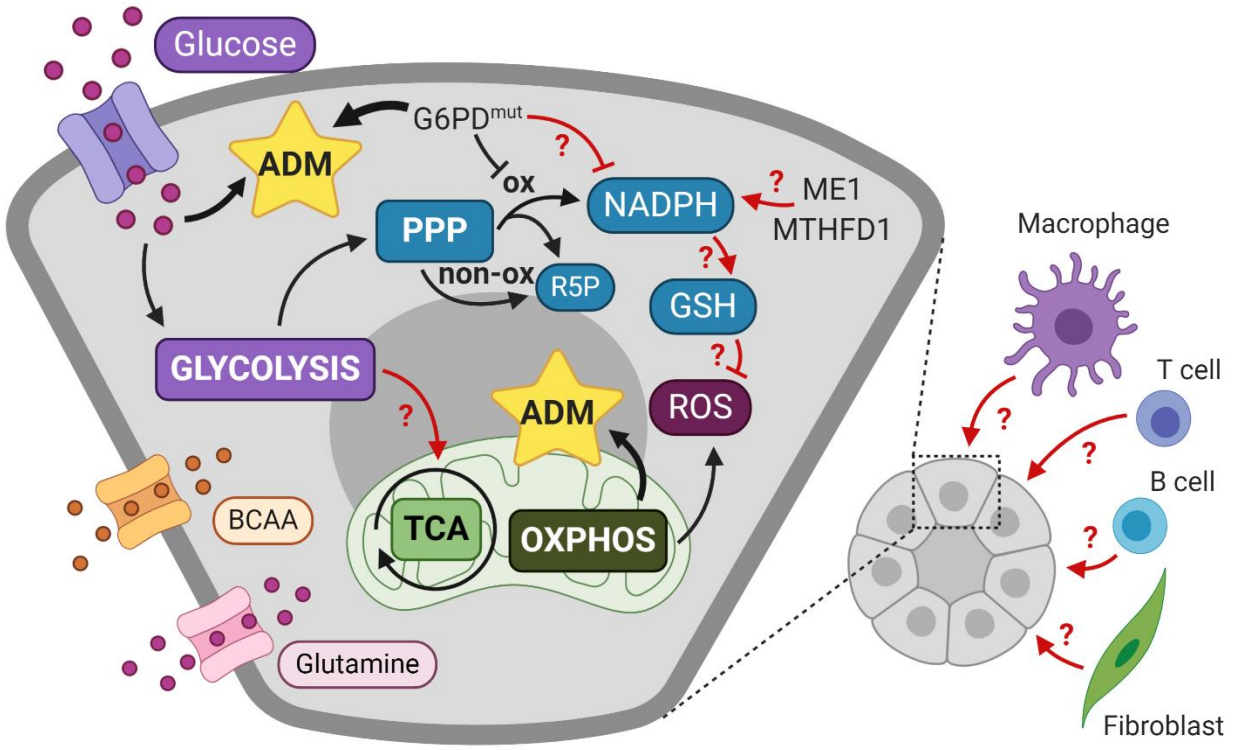

Figure 5.1 Metabolic requirements for ADM and select future directions. Acinar cells require glucose and oxidative phosphorylation to undergo ADM. Exogenous glutamine and branched-chain amino acids (BCAA) are dispensable for ADM, so we hypothesize glucose is a main source feeding mitochondrial metabolism. Mutant G6PD (G6PD^{mut}) impairs the oxidative (ox) pentose phosphate pathway (PPP) and accelerates ADM. We hypothesize G6PD^{mut} causes decreased levels of NADPH, which reduces glutathione (GSH) levels and increases reactive oxygen species (ROS) levels. Other NADPH-producing enzymes, such as malic enzyme 1 (ME1) and methylenetetrahydrofolate dehydrogenase 1 (MTHFD1), may contribute to ADM. Finally, nonautonomous metabolic signals from macrophages, T cells, B cells, and/or fibroblasts are unknown and of interest. Non-ox, non-oxidative; R5P, ribose 5-phosphate; TCA, tricarboxylic acid cycle .Created with BioRender.com

Steady-State and Isotope Tracing Metabolomics

Although aerobic glycolysis during ADM may not be reprogramed to the extent seen in PDA, as demonstrated by lack of glutamine dependency, mutant KRAS does promote oxidative PPP, an anabolic pathway shunting off glycolysis. We hypothesize that *Kras*^{G12D}-expressing acinar cells utilize glucose as a main source feeding into mitochondrial metabolism since ADM is not sensitive to the absence of glutamine or BCAA (**Fig. 5.1**). As a future extension of this work, we will employ steady-state and stable isotope tracing metabolomics, akin to those we performed in PDA and CRC cells. We will characterize metabolism over the course of ADM using the same experimental setup done for transcriptomic analysis. Steady-state analysis will determine changes in metabolite abundance during ADM while isotope tracing will determine how nutrients are

utilized by metabolic pathways. Tracing glucose metabolism with uniformly labeled 13C (U-^{13}C) glucose will reveal the extent of glucose utilization of acinar cells by determining the proportion of glycolytic intermediates dedicated to the TCA cycle and any shifts into anabolic pathways, such as the PPP, hexosamine biosynthetic pathway, and serine/glycine metabolism. It is also of interest to trace glutamine metabolism with U-^{13}C and uniformly labeled 15N (U-^{15}N) glutamine. Since acinar cells do not require glutamine supplementation, metabolic tracing might reveal changes in metabolism that occur during ADM but are not required for transdifferentiation—i.e. neutral metabolic activities that are dispensable for tumor growth[6]. It is important to determine these types of pathways since they are likely not strong therapeutic targets.

Pentose Phosphate Pathway

Further characterization of the *Kras$^{LSL\text{-}G12D/+}$; Ptf1a$^{Cre/+}$; G6PD^{mut}* (KCG^{mut}) and *Kras$^{LSL\text{-}G12D/+}$; Tp53$^{LSL\text{-}R172H/+}$; Ptf1a$^{Cre/+}$; G6PD^{mut}* (KPCG^{mut}) models is needed to determine the consequences G6PD-deficiency has on accelerating tumorigenesis (**Fig. 2.5b,c**). We hypothesize *G6pd* mutation in acinar cells causes decreased production of NADPH, which in turn reduces antioxidant levels (e.g. glutathione [GSH]) and enhances the abundance of reactive oxygen species (ROS) (**Fig. 5.1**). ROS increases in KCG^{mut} mice may be at slightly higher levels that promote accelerated tumorigenesis but still below the levels that initiate senescence. ROS and oxidant stress measurements will be performed on both acinar explants and tissues from KCG^{mut} and KCG^{wt} mice[7]. Levels of NADPH and GSH will be measured with our metabolomics platform and with biochemical assays[8]. Tissue collected from mice at 8, 16, 26, and 52 weeks (**Fig. 2.4e**) will be further analyzed to determine differences in number and grade of ADM and PanIN lesions, presence of carcinoma, proliferation, cell death, and oxidative stress. Tissue analysis will also be performed on 90-day-old KPCG^{mut} and KPCG^{wt} mice (**Fig. 2.6b**). Longitudinal studies are on-going to increase the sample size for survival analysis (**Fig. 2.6c**); pancreas tissue, along with lung and liver tissue—the most common metastatic sites[9]—will be analyzed for differences in tumor differentiation and metastatic burden.

Oxidative Phosphorylation

Mutant KRAS is critical for tumor development, progression, and maintenance[10,11]. However, upon KRAS ablation, a small population of dormant cells survive and contribute to tumor recurrence[12]. The surviving cells have features of tumor-initiating cells and are dependent on oxidative phosphorylation for survival, in contrast to the bulk of glycolytic tumor cells that succumb to oncogene ablation. The surviving cells show profound sensitivity to 200nM oligomycin within 24 hours—like acinar explants at 20nM oligomycin (**Fig. 2.3**)—and are unable increase glycolytic flux to compensate energy production. This suggests metabolic pathways needed for acinar cell transdifferentiation may be relevant in a quiescent, tumor-initiating cell population. We will treat *ex vivo* ADM cysts with oligomycin to determine if these ductal progenitor cells are as sensitive to oxidative phosphorylation inhibition as tumor cells that survive KRAS ablation. Establishing metabolic pathways that drive ADM will not only reveal requirements for tumorigenesis, it may also reveal metabolic dependencies of tumor-initiating populations that survive treatment targeting the bulk tumor and contribute to recurrence. Interestingly, oxidative phosphorylation dependence is also observed in leukemia stem and progenitor cells[13,14].

NADPH-Producing Enzymes

The roles of other NADPH-producing enzymes, such as malic enzyme 1 (ME1) and methylenetetrahydrofolate dehydrogenase 1 (MTHFD1), during ADM are unknown and of interest (**Figs. 2.4b, 5.1**). Not only is NADPH used for maintaining redox balance, large quantities are required in the generation of lipids[15]. Importantly, ADM requires both redox homeostasis and *de novo* lipid synthesis, suggesting an important function for NADPH during ADM[16,17]. Transcription factors nuclear factor erythroid 2-related factor 2 (NRF2) and the family of sterol regulator element-binding proteins (SREBPs)—which regulate expression of genes involved in antioxidant response and lipid homeostasis, respectively—upregulate expression of NADPH-producing enzymes[18,19]. The oxidative PPP, via G6PD, is a major producer of NADPH[20]. Interestingly, serine-driven folate metabolism has been shown to be an almost equal contributor of NADPH via MTHFD1 and oxidative PPP can influence folate metabolism[20,21]. ME1 is of particular interest because it is the enzyme that produces NADPH from rewired glutamine metabolism in PDA[22]. ME1 can compensate for loss of G6PD to maintain redox balance and fatty acid

synthesis[21]. We hypothesize that knockdown or loss of these enzymes in acinar cells will phenocopy the acceleration of ADM seen with G6PD-deficiency due to reduced NADPH production. Also, the role of serine metabolism during ADM is unknown and may reveal metabolic dependencies of tumorigenesis.

ROS Signaling

Maintaining elevated redox homeostasis is important for both tumorigenesis and tumor maintenance[17,23]. ROS is more than a metabolic byproduct that damages cellular components, as traditionally thought. Rather, it plays important roles in cellular signaling that promotes growth and survival[24,25]. Signal induction of receptor tyrosine kinases, such as EGFR, following growth factor binding requires a burst of ROS produced by membrane-bound NADPH oxidases (NOX) and facilitated by RAC1 (ref:[26-30]). This burst of ROS transiently inactivates protein tyrosine phosphatases and dual specific phosphatases that negatively regulate mitogenic signaling[31]. One such phosphatase inactivated by ROS is PTEN, the negative regulator of PI3K–AKT signaling[32,33]. ROS directly inactivates glyceraldehyde-3-phosphate dehydrogenase (GAPDH) and pyruvate kinase muscle isozyme 2 (PKM2), an isoform expressed in proliferating and cancer cells, to promote aerobic glycolysis[34-37]. When oxidative stress levels are too high, ROS inactivates GAPDH and PKM2 to shift glycolysis into the PPP and promote the generation of GSH. Of note, PKM2 can also be inactivated by a lack of serine, causing a backup glycolytic intermediates that can feed into serine biosynthesis[38]. Interestingly, PI3K signaling, activation of RAC1, and increased expression of EGFR and its ligands by nuclear factor kappa B (NF-κB)—a ROS-sensing transcription factor—drive ADM, suggesting membrane-localized ROS likely play a role in promoting signal transduction during ADM[17,39-41].

Hypoxia

Insufficient levels of oxygen decrease the efficiency of the electron transport chain, amplifying mitochondrial-generated ROS (mROS) production[42]. mROS regulates the stabilization of HIF1α and HIF2α, mediating a metabolic shift to maintain redox homeostasis under hypoxic conditions[43-45]. HIF1α promotes a switch from oxidative metabolism to aerobic glycolysis by interacting with coactivator PKM2—a HIF1α target

gene—to induce expression of glycolytic genes and by regulating genes that attenuate oxygen consumption[42,46-48]. HIF2α activates expression of antioxidant genes[49,50]. HIF1α and HIF2α also regulate genes in serine and one-carbon metabolism to increase NADPH generation[51]. Analysis of *Kras*$^{LSL\text{-}G12D/+}$*; Ptf1a*$^{Cre/+}$ (KC) tissue shows ADM and PanIN lesions are hypoxic and express HIF1α and HIF2α[52,53]. Our ADM transcriptomic analysis, in which acinar cells were grown in ambient oxygen, also shows evidence of a hypoxia signature, including increased expression of *Hif1α* and *Epas1* (encodes HIF2α) and their target genes involved in glycolysis, mitochondrial metabolism, and antioxidant defense (**Fig. 5.2**). This response may be from increased oxidative stress required for transdifferentiation. Culturing acinar explants in oxygen tensions observed in the pancreas during ADM will more accurately represent *in vivo* setting and model more relevant metabolic changes. Either way, these results illustrate a provocative role for the HIF pathways and the associated metabolic reprogramming during ADM.

Wild-type p53

Although additional genetic alterations—typically tumor suppressor loss—are required for PDA progression, KRAS mutations drive ADM. As such, wild-type p53 is active during ADM. The p53 transcription factor is a tumor suppressor long known to initiate cell cycle arrest, senescence, and apoptosis[54]. However studies have uncovered a role for p53 regulating cellular metabolism to adapt to metabolic stress and promote survival[55-57]. Although p53 can induce oxidative stress to stimulate cellular senescence or death, it can also limit ROS by inducing expression of antioxidant genes, stabilizing NRF2, and increasing NADPH production through the PPP and serine synthesis pathway[56,58-60]. In mouse embryonic fibroblasts (MEF) and *KRAS*^{G12D}-expressing colorectal cancer (CRC) cell line HCT 116, p53 reduces production of NADPH by binding to and inactivating G6PD and downregulating the expression of *Me1* and *Me2* (ref:[61,62]). This phenotype is likely context and tissue dependent, like we saw with metabolic changes between mutant KRAS PDA and CRC cell lines. During ADM, *TP53*-induced glycolysis and apoptosis regulator (TIGAR), a p53 antioxidant target gene, promotes the generation of NADPH through the oxidative PPP[63]. We also showed that *Me1* expression increases during ADM (**Fig. 2.4b**) and that we can decrease oxidative PPP flux through G6PD-deficiency (**Fig. 2.4e**), suggesting p53 is not negatively regulating *Me1* or G6PD in this context. Since wild-type

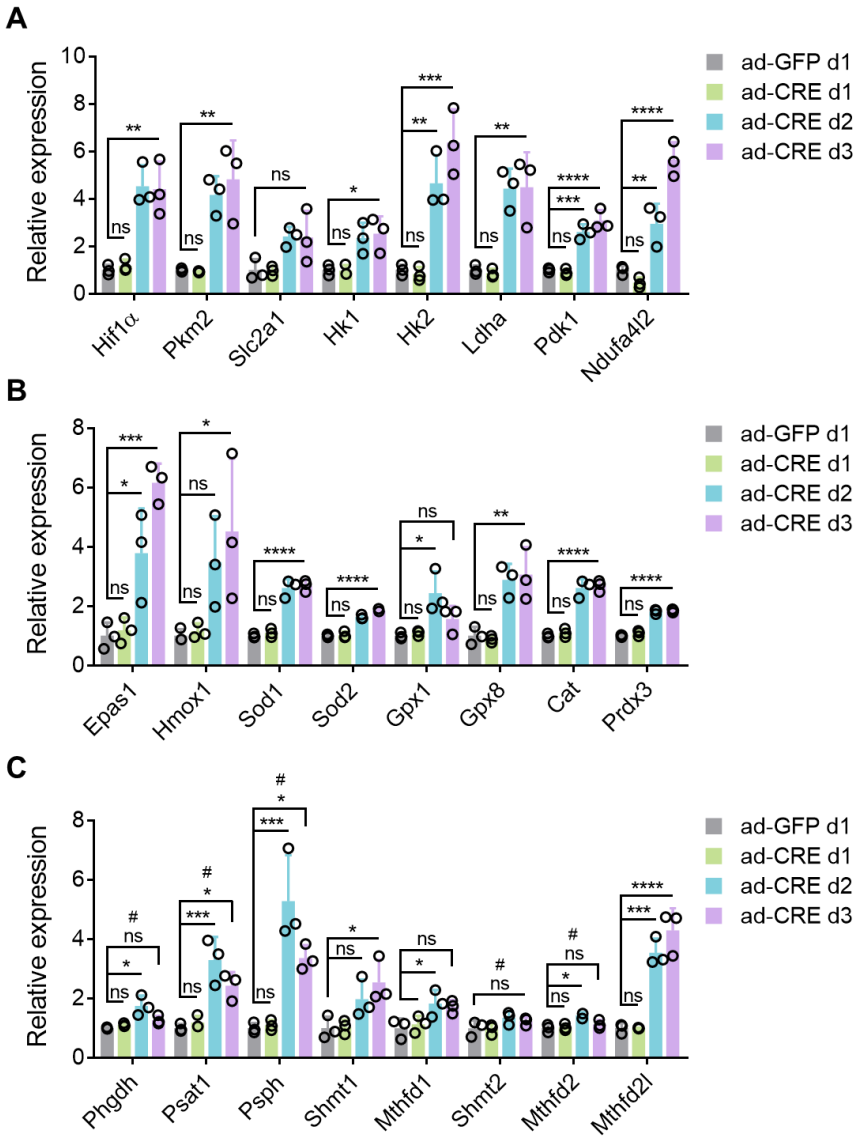

Figure 5.2 Expression of hypoxia target genes. Relative expression of (**A**) Hif1α, glycolytic target genes Pkm2, Slc2a1 (encodes GLUT1), Hk1, Hk2, Ldha, and Pdk1, and mitochondrial complex I inhibitor Ndufa4l2, (**B**) Epas1 (encodes HIF2α) and antioxidant target genes, and (**C**) serine and folate metabolism genes in control (ad-GFP) or *Kras*^{G12D}-expressing (ad-CRE) acinar cells collected days 1-3, n=3. # denotes HIF1α and HIF2α target genes. Cat, catalase; Epas1, endothelial PAS domain protein 1; GLUT1, glucose transporter 1; Gpx1, glutathione peroxidase 1; Gpx8, glutathione peroxidase 8; Hif1α, hypoxia-inducible factor 1 alpha; HIF2α, hypoxia-inducible factor 2 alpha; Hk1, hexokinase 1; Hk2, hexokinase 2; Hmox1, heme oxygenase 1; Ldha, lactate dehydrogenase A; Mthfd1, methylenetetrahydrofolate dehydrogenase, cyclohydrolase and formyltetrahydrofolate synthetase 1; Mthfd2, methylenetetrahydrofolate dehydrogenase (NADP+ dependent) 2, methenyltetrahydrofolate cyclohydrolase; Mthfd2l, methylenetetrahydrofolate dehydrogenase (NADP+ dependent) 2-like;Ndufa4l2, NADH dehydrogenase (ubiquinone) 1 alpha subcomplex, 4-like 2; Pdk1, pyruvate dehydrogenase kinase 1; Phgdh, phosphoglycerate dehydrogenase; Pkm2, pyruvate kinase, muscle isoform M2; Prdx3, thioredoxin-dependent peroxide reductase, mitochondrial; Psat1, phosphoserine aminotransferase 1; Psph, phosphoserine phosphatase; Shmt1, serine hydroxymethyltransferase, cytosolic; Shmt2, serine hydroxymethyltransferase, mitochondrial; Slc2a1, solute carrier family 2 member 1; Sod1, superoxide dismutase 1; Sod2, superoxide dismutase 2. Error bars represent s.d. *, $P < 0.05$; **, $P < 0.01$; ***, $P < 0.001$; ****, $P < 0.0001$; One-way ANOVA.

p53 is inactivated in later stages of tumorigenesis, these data indicate p53 may play a protective role during $Kras^{G12D}$-driven ADM. Inactivating p53 by deletion or mutation in acinar explants will uncover the metabolic effects of wild-type p53 during ADM.

Nonautonomous metabolic crosstalk

PDA tumors are comprised mostly of non-malignant cells that make up the dense fibroinflammatory stroma[2]. Metabolic crosstalk between tumor cells and non-malignant cells in the tumor microenvironment support tumor growth, survival, and metastasis[2,64-67]. Nonautonomous metabolic signals likely influence ADM since mouse models show early immune cell—T cells, B cells, and macrophages—and stromal cell infiltration during and contributing to tumorigenesis[52,68-70]. *In vitro* cell culturing systems can be used to simplify complex *in vivo* crosstalk between different cell types[64,65]. Culturing primary acinar cells alongside immune or stromal cells, or in conditioned media from these cell types[71], could reveal signals or metabolites from these infiltrates that promote ADM and tumorigenesis through metabolic reprograming (**Fig. 5.1**).

Mouse model limitations

The KC mouse was the first to express endogenous levels of mutant $Kras^{G12D}$ in the pancreas and recapitulate tumor progression seen in human PDA[72]. While the KC model is useful for studying pancreatic tumorigenesis, long latency of tumor development and infrequent progression to invasive cancer limits its use. An additional mutation of tumor suppressor *Tp53*, generating the KPC model, increases the penetrance and development of invasive and metastatic PDA[73]. Missense mutations R175H and R273H (corresponding to mouse R172H and R270H) are the most frequent p53 mutations in pancreatic cancer[74]. The KPC mouse is one of the most widely used and studied models of pancreatic cancer. However, this model has its limitations[75]. Expression of Cre recombinase results in recombination of a silencing cassette—“STOP” flanked by two loxP sites (LSL)—which allows expression of the mutant alleles. In KPC mice, due to expression of Cre from pancreas-specific transcription factor promoters, *Ptf1a* or *Pdx1*, mutant *Kras* and *Tp53* alleles are recombined in pancreatic progenitor cells during embryogenesis. Not only does this result in concomitant expression of mutant *Kras* and *Tp53*, but all pancreatic epithelial cells express these mutant alleles. This greatly differs from human PDA

predominantly arising from somatic mutations. Since *Kras*$^{LSL\text{-}G12D}$ and *Tp53*$^{LSL\text{-}R172H}$ are knocked into their respective endogenous loci, the LSL cassette causes all non-recombined cells to be heterozygous knockouts for these genes. Haploinsufficiency of nonautonomous cells (those that do not recombine) could have profound effects on tumorigenesis and disease progression that differ from human PDA. Also, mutant p53 greatly accelerates tumor development and progression leading to a median survival of 5.5 months[73], while human PDA tumors take years to develop. This acceleration could either mask subtle effects or potentiate modest effects that may or may not be important factors in human PDA.

Although KPC mice recapitulate human disease through stepwise progression of premalignant lesions to invasive and metastatic cancer, the embryonic and simultaneous genetic insults do not model the biology of human PDA[9,73]. In PDA, and other cancers with multi-step progression, *Ras* mutations generally occur at early-stages and *Tp53* alterations at mid- or late-stages of tumorigenesis and these genetic insults typically occur in adult tissues[9,76]. Improvements on the KC and KPC models allow temporal expression of mutant *Kras* or *Tp53* to better recapitulate genetic alterations of human pancreatic cancer[77]. Expression of mutant *Kras* and alterations in *Tp53* can be induced in adult acinar cells, however these genetic insults still occur simultaneously[4,10,11,78,79]. Other models that mimic sequential mutations seen in human PDA development can induce *Tp53* alterations in mutant *Kras*-expressing adult acinar cells, however expression of mutant Kras is still activated embryonically in pancreatic progenitor cells[74,80]. Importantly, all of these models still generate heterozygous null mice for Kras and p53. Recently a mouse model was developed that allows tissue-specific conversion of wild-type *Tp53* to mutant *Tp53* while maintaining two alleles of wild-type *Tp53* in the rest of the mouse[81]. Ideally, a mouse model that allows mutant *Kras* expression in adult acinar cells followed by sequential expression of mutant *Tp53* would more closely resemble genetic changes seen in human PDA and model pathways important for tumorigenesis. Utilization of established models that express mutant *Tp53* in adult mutant *Kras*-expressing acinar cells or generating a model that allows separate but temporally controlled expression of mutant Kras then mutant Tp53 mutations in adult acinar cells—all in the G6PD-deficient background—could clarify the discrepancy seen between accelerated tumorigenesis in

KCG mice not causing accelerated mortality in KPCG mice. The metabolic influences of mutant p53, described below, may provide tumorigenic advantages regardless of G6PD status, which would not be a factor if mutant p53 is expressed following transformation of *Kras*^{G12D}-expressing acinar cells.

Oncogenic mutations in *Tp53* possess gain of function activities that promote malignant properties, including metabolic changes[82-85]. Embryonic and simultaneous expression of mutant *Kras* and *Tp53* in the mouse pancreas likely has profound metabolic effects that influence tumorigenesis differently than sequential mutation in adult cells. Mutant p53 enhances glycolysis and anabolic metabolism through transcriptional activation of genes involved in glucose import, the mevalonate pathway, and lipid and nucleotide biosynthesis in cancer cells[86-90]. Positron emission tomography (PET)-computed tomography (CT) with ^{18}F-fluorodeoxyglucose (FDG) (FDG PET-CT) scans of pancreatic cancer patient-derived xenografts (PDX) show elevated glucose uptake in tumors with mutant p53 compared to those with wild-type p53 (ref:[91]). In cancer cell lines, mutant p53 also elevates oxidative phosphorylation, causing increased ROS and oxidative stress levels[87,92,93]. In response to increased oxidative stress, mutant p53 interacts with NRF2 to differentially express select NRF2 target genes that promote cell proliferation and survival and protect from cell death[92-95]. Interestingly, a PDA mouse model with an inducible p53 mutation shows reduced mitochondrial activity and BCAA catabolism[74]. Mutant p53 also protects cancer cells during glucose, glutamine, or oxygen deprivation by inducing activation of pro-survival genes and not pro-death genes[96-98].

Many pathways influenced by mutant p53, such as changes in redox homeostasis and the mevalonate pathway, are important factors for transdifferentiation of oncogenic Kras-expressing acinar cells[16,17,63,99]. Autophagy is another metabolic pathway that plays a role during ADM and is influenced by mutant p53. Impairment of autophagy is required for ADM[100,101], and since mutant p53 inhibits autophagy[102], the mechanism by which autophagy is impaired in mutant *Kras*-expressing acinar cells may be masked by concomitant expression of mutant p53. Mutant p53 increases EGFR and NF-κB signaling pathways—ones required for ADM[70]—in cancer cells. Mutant p53 regulates microRNAs that ultimately lead to increased EGFR expression, enhancing MAPK signaling and

proliferation[103]. Mutant p53 also increases expression of NF-κB and enhances and prolongs its activation by TNFα, promoting chronic inflammation[104,105]. The gain of function activities mutant p53 possess likely contribute to accelerated pancreatic tumorigenesis seen in KPC mice[73], although they may be context dependent.

Pancreatic Tumor Maintenance

PDA cells reprogram cellular metabolism to support growth and proliferation[2]. Mutant KRAS diverts glucose-derived carbon into anabolic pathways that branch off glycolysis and enhances utilization of glutamine-derived carbon in mitochondrial metabolism[10,22]. Since oncogenic KRAS enhances glycolytic flux into the non-oxidative PPP pathway and not the NADPH-generating oxidative PPP, the malate-aspartate shuttle is rewired to generate NADPH and maintain redox homeostasis. We found that inhibition of this pathway decreases PDA cell and tumor growth and sensitizes cells to oxidative stress via radiation treatment, revealing a potential therapeutic strategy.

GOT1 Inhibitors and Targeted Radiotherapy

Genetic knockdown of glutamate oxaloacetate transaminase 1 (GOT1) with short hairpin RNA (shGOT1) impedes the growth of PDA cell lines and primary cells *in vitro* and subcutaneous and orthotopic xenograft tumors *in vivo* (**Figs. 3.1b,c, 3.3b-d**)[106]. GOT1 knockdown induces redox imbalance and sensitizes PDA to radiation therapy (**Figs. 3.19-3.21**). Since cell lines were genetically manipulated prior to implantation, GOT1 knockdown only occurs in the cancer cells. However, most treatments are systemic, affecting the entire body. We recently developed novel small molecule inhibitors (SMI) targeting GOT1 that will enable us to treat xenograft or autochthonous PDA mouse models in a more clinically relevant manner[107-109]. We will be able to determine if these SMI are a viable therapeutic option not only for the effect on tumors, but also the effect on normal tissues throughout the body. We will also use the GOT1 SMI in conjunction with Small Animal Radiation Research Platform (SARRP) (Xstrahl) to treat orthotopic xenografts. SARRP accurately identifies tumor tissue with cone beam-CT and bioluminescent imaging and delivers targeted radiation in a manner that mimics treatment of human tumors. This new technology will allow us to improve upon our results treating subcutaneous shGOT1 xenografts with radiotherapy (**Fig. 3.21**).

GOT1 Pathway

Mutant KRAS mediates metabolic rewiring of the malate-aspartate shuttle to generate NADPH and maintain redox homeostasis in PDA cells (**Fig. 3.1a**). Knockdown of GOT1, malate dehydrogenase 1 (MDH1), or malic enzyme 1 (ME1) impair PDA cell line proliferation and tumor growth[22]. We developed mouse models that allows conditional deletion of GOT1, MDH1, or ME1 (*Got1*$^{f/f}$, *Mdh1*$^{f/f}$, and *Me1*$^{f/f}$, respectively). These alleles are being introduced into the KC model for concomitant expression of Kras^{G12D} and deletion of GOT1/MDH1/ME1 in the pancreas to determine how these enzymes affect tumorigenesis and tumor progression.

Conclusions

KRAS mutations are found in over 90% of PDA tumors and is the driving mutation for tumor development and maintenance[110]. Unfortunately, KRAS has proven notoriously difficult to target pharmacologically, so KRAS-dependent pathways remain promising targets for the development of new therapeutics[111-113]. PDA, mediated by oncogenic KRAS, extensively rewire cellular metabolism; as such present as metabolic vulnerabilities for therapeutic targets[2]. I found acinar cells require subphysiological levels of glucose to survive and undergo ADM, presumably to maintain flux through anabolic pathways that contribute to preserving redox homeostasis during heightened oxidative stress. Perturbing the oxidative PPP during ADM likely decreases NADPH production used to generate antioxidants, raising ROS levels to accelerate tumorigenesis. Redox balance is tightly regulated in PDA cells by reprogramming glutamine metabolism to generate NADPH[22]. I found inhibition of GOT1, a key enzyme in this pathway, disrupts GSH levels and sensitizes cells to oxidative stress induced by radiotherapy. Radiotherapy is a standard of care in many institutions and the addition of GOT1 inhibition could overcome radiation resistance seen in PDA patients and improve therapeutic outcomes[114]. Understanding the metabolic pathways that contribute to pancreatic tumorigenesis and tumor maintenance, such as redox homeostasis, could provide biomarkers for diagnosis of early disease or development of better therapeutics for treating PDA.

References

1 Siegel, R. L., Miller, K. D. & Jemal, A. Cancer statistics, 2020. *CA: a cancer journal for clinicians* **70**, 7-30, doi:10.3322/caac.21590 (2020).

2 Halbrook, C. J. & Lyssiotis, C. A. Employing Metabolism to Improve the Diagnosis and Treatment of Pancreatic Cancer. *Cancer cell* **31**, 5-19, doi:10.1016/j.ccell.2016.12.006 (2017).

3 Kopp, J. L. *et al.* Identification of Sox9-dependent acinar-to-ductal reprogramming as the principal mechanism for initiation of pancreatic ductal adenocarcinoma. *Cancer cell* **22**, 737-750, doi:10.1016/j.ccr.2012.10.025 (2012).

4 Bailey, J. M. *et al.* p53 mutations cooperate with oncogenic Kras to promote adenocarcinoma from pancreatic ductal cells. *Oncogene* **35**, 4282-4288, doi:10.1038/onc.2015.441 (2016).

5 Means, A. L. & Leach, S. D. Lineage commitment and cellular differentiation in exocrine pancreas. *Pancreatology : official journal of the International Association of Pancreatology (IAP) ... [et al.]* **1**, 587-596, doi:10.1159/000055868 (2001).

6 Vander Heiden, M. G. & DeBerardinis, R. J. Understanding the Intersections between Metabolism and Cancer Biology. *Cell* **168**, 657-669, doi:10.1016/j.cell.2016.12.039 (2017).

7 Liou, G. Y. & Storz, P. Detecting reactive oxygen species by immunohistochemistry. *Methods in molecular biology (Clifton, N.J.)* **1292**, 97-104, doi:10.1007/978-1-4939-2522-3_7 (2015).

8 Lee, H. J., Kremer, D. M., Sajjakulnukit, P., Zhang, L. & Lyssiotis, C. A. A large-scale analysis of targeted metabolomics data from heterogeneous biological samples provides insights into metabolite dynamics. *Metabolomics : Official journal of the Metabolomic Society* **15**, 103, doi:10.1007/s11306-019-1564-8 (2019).

9 Hezel, A. F., Kimmelman, A. C., Stanger, B. Z., Bardeesy, N. & Depinho, R. A. Genetics and biology of pancreatic ductal adenocarcinoma. *Genes Dev* **20**, 1218-1249, doi:10.1101/gad.1415606 (2006).

10 Ying, H. *et al.* Oncogenic Kras maintains pancreatic tumors through regulation of anabolic glucose metabolism. *Cell* **149**, 656-670, doi:10.1016/j.cell.2012.01.058 (2012).

11 Collins, M. A. *et al.* Oncogenic Kras is required for both the initiation and maintenance of pancreatic cancer in mice. *J Clin Invest* **122**, 639-653, doi:10.1172/jci59227 (2012).

12 Viale, A. *et al.* Oncogene ablation-resistant pancreatic cancer cells depend on mitochondrial function. *Nature* **514**, 628-632, doi:10.1038/nature13611 (2014).

13 Skrtić, M. *et al.* Inhibition of mitochondrial translation as a therapeutic strategy for human acute myeloid leukemia. *Cancer cell* **20**, 674-688, doi:10.1016/j.ccr.2011.10.015 (2011).

14 Lagadinou, E. D. *et al.* BCL-2 inhibition targets oxidative phosphorylation and selectively eradicates quiescent human leukemia stem cells. *Cell stem cell* **12**, 329-341, doi:10.1016/j.stem.2012.12.013 (2013).

15 Lunt, S. Y. & Vander Heiden, M. G. Aerobic glycolysis: meeting the metabolic requirements of cell proliferation. *Annual review of cell and developmental biology* **27**, 441-464, doi:10.1146/annurev-cellbio-092910-154237 (2011).
16 Carrer, A. *et al.* Acetyl-CoA Metabolism Supports Multistep Pancreatic Tumorigenesis. *Cancer discovery* **9**, 416-435, doi:10.1158/2159-8290.cd-18-0567 (2019).
17 Liou, G. Y. *et al.* Mutant KRas-Induced Mitochondrial Oxidative Stress in Acinar Cells Upregulates EGFR Signaling to Drive Formation of Pancreatic Precancerous Lesions. *Cell reports* **14**, 2325-2336, doi:10.1016/j.celrep.2016.02.029 (2016).
18 Mitsuishi, Y. *et al.* Nrf2 redirects glucose and glutamine into anabolic pathways in metabolic reprogramming. *Cancer cell* **22**, 66-79, doi:10.1016/j.ccr.2012.05.016 (2012).
19 Horton, J. D. Sterol regulatory element-binding proteins: transcriptional activators of lipid synthesis. *Biochemical Society transactions* **30**, 1091-1095, doi:10.1042/bst0301091 (2002).
20 Fan, J. *et al.* Quantitative flux analysis reveals folate-dependent NADPH production. *Nature* **510**, 298-302, doi:10.1038/nature13236 (2014).
21 Chen, L. *et al.* NADPH production by the oxidative pentose-phosphate pathway supports folate metabolism. *Nature metabolism* **1**, 404-415 (2019).
22 Son, J. *et al.* Glutamine supports pancreatic cancer growth through a KRAS-regulated metabolic pathway. *Nature* **496**, 101-105, doi:10.1038/nature12040 (2013).
23 Nelson, B. S. *et al.* Tissue of origin dictates GOT1 dependence and confers synthetic lethality to radiotherapy. *Cancer & metabolism* **8**, 1, doi:10.1186/s40170-019-0202-2 (2020).
24 Finkel, T. Signal transduction by reactive oxygen species. *The Journal of cell biology* **194**, 7-15, doi:10.1083/jcb.201102095 (2011).
25 Holmström, K. M. & Finkel, T. Cellular mechanisms and physiological consequences of redox-dependent signalling. *Nature reviews. Molecular cell biology* **15**, 411-421, doi:10.1038/nrm3801 (2014).
26 Bae, Y. S. *et al.* Epidermal growth factor (EGF)-induced generation of hydrogen peroxide. Role in EGF receptor-mediated tyrosine phosphorylation. *J Biol Chem* **272**, 217-221 (1997).
27 Sundaresan, M., Yu, Z. X., Ferrans, V. J., Irani, K. & Finkel, T. Requirement for generation of H2O2 for platelet-derived growth factor signal transduction. *Science (New York, N.Y.)* **270**, 296-299, doi:10.1126/science.270.5234.296 (1995).
28 Truong, T. H. & Carroll, K. S. Redox regulation of epidermal growth factor receptor signaling through cysteine oxidation. *Biochemistry* **51**, 9954-9965, doi:10.1021/bi301441e (2012).
29 Sundaresan, M. *et al.* Regulation of reactive-oxygen-species generation in fibroblasts by Rac1. *The Biochemical journal* **318 (Pt 2)**, 379-382, doi:10.1042/bj3180379 (1996).
30 Ushio-Fukai, M., Zafari, A. M., Fukui, T., Ishizaka, N. & Griendling, K. K. p22phox is a critical component of the superoxide-generating NADH/NADPH oxidase

system and regulates angiotensin II-induced hypertrophy in vascular smooth muscle cells. *J Biol Chem* **271**, 23317-23321, doi:10.1074/jbc.271.38.23317 (1996).
31 Wang, X., Martindale, J. L., Liu, Y. & Holbrook, N. J. The cellular response to oxidative stress: influences of mitogen-activated protein kinase signalling pathways on cell survival. *The Biochemical journal* **333 (Pt 2)**, 291-300, doi:10.1042/bj3330291 (1998).
32 Leslie, N. R. *et al.* Redox regulation of PI 3-kinase signalling via inactivation of PTEN. *The EMBO journal* **22**, 5501-5510, doi:10.1093/emboj/cdg513 (2003).
33 Kwon, J. *et al.* Reversible oxidation and inactivation of the tumor suppressor PTEN in cells stimulated with peptide growth factors. *Proc Natl Acad Sci U S A* **101**, 16419-16424, doi:10.1073/pnas.0407396101 (2004).
34 Anastasiou, D. *et al.* Inhibition of pyruvate kinase M2 by reactive oxygen species contributes to cellular antioxidant responses. *Science (New York, N.Y.)* **334**, 1278-1283, doi:10.1126/science.1211485 (2011).
35 Christofk, H. R. *et al.* The M2 splice isoform of pyruvate kinase is important for cancer metabolism and tumour growth. *Nature* **452**, 230-233, doi:10.1038/nature06734 (2008).
36 Hwang, N. R. *et al.* Oxidative modifications of glyceraldehyde-3-phosphate dehydrogenase play a key role in its multiple cellular functions. *The Biochemical journal* **423**, 253-264, doi:10.1042/bj20090854 (2009).
37 Shestov, A. A. *et al.* Quantitative determinants of aerobic glycolysis identify flux through the enzyme GAPDH as a limiting step. *eLife* **3**, doi:10.7554/eLife.03342 (2014).
38 Ye, J. *et al.* Pyruvate kinase M2 promotes de novo serine synthesis to sustain mTORC1 activity and cell proliferation. *Proc Natl Acad Sci U S A* **109**, 6904-6909, doi:10.1073/pnas.1204176109 (2012).
39 Eser, S. *et al.* Selective requirement of PI3K/PDK1 signaling for Kras oncogene-driven pancreatic cell plasticity and cancer. *Cancer cell* **23**, 406-420, doi:10.1016/j.ccr.2013.01.023 (2013).
40 Heid, I. *et al.* Early requirement of Rac1 in a mouse model of pancreatic cancer. *Gastroenterology* **141**, 719-730, 730.e711-717, doi:10.1053/j.gastro.2011.04.043 (2011).
41 Wu, C. Y. *et al.* PI3K regulation of RAC1 is required for KRAS-induced pancreatic tumorigenesis in mice. *Gastroenterology* **147**, 1405-1416.e1407, doi:10.1053/j.gastro.2014.08.032 (2014).
42 Schito, L. & Semenza, G. L. Hypoxia-Inducible Factors: Master Regulators of Cancer Progression. *Trends in cancer* **2**, 758-770, doi:10.1016/j.trecan.2016.10.016 (2016).
43 Brunelle, J. K. *et al.* Oxygen sensing requires mitochondrial ROS but not oxidative phosphorylation. *Cell Metab* **1**, 409-414, doi:10.1016/j.cmet.2005.05.002 (2005).
44 Guzy, R. D. *et al.* Mitochondrial complex III is required for hypoxia-induced ROS production and cellular oxygen sensing. *Cell Metab* **1**, 401-408, doi:10.1016/j.cmet.2005.05.001 (2005).

45 Mansfield, K. D. *et al.* Mitochondrial dysfunction resulting from loss of cytochrome c impairs cellular oxygen sensing and hypoxic HIF-alpha activation. *Cell Metab* **1**, 393-399, doi:10.1016/j.cmet.2005.05.003 (2005).
46 Luo, W. *et al.* Pyruvate kinase M2 is a PHD3-stimulated coactivator for hypoxia-inducible factor 1. *Cell* **145**, 732-744, doi:10.1016/j.cell.2011.03.054 (2011).
47 Iyer, N. V. *et al.* Cellular and developmental control of O2 homeostasis by hypoxia-inducible factor 1 alpha. *Genes Dev* **12**, 149-162, doi:10.1101/gad.12.2.149 (1998).
48 Tello, D. *et al.* Induction of the mitochondrial NDUFA4L2 protein by HIF-1α decreases oxygen consumption by inhibiting Complex I activity. *Cell Metab* **14**, 768-779, doi:10.1016/j.cmet.2011.10.008 (2011).
49 Scortegagna, M. *et al.* Multiple organ pathology, metabolic abnormalities and impaired homeostasis of reactive oxygen species in Epas1-/- mice. *Nat Genet* **35**, 331-340, doi:10.1038/ng1266 (2003).
50 Bertout, J. A. *et al.* HIF2alpha inhibition promotes p53 pathway activity, tumor cell death, and radiation responses. *Proc Natl Acad Sci U S A* **106**, 14391-14396, doi:10.1073/pnas.0907357106 (2009).
51 Samanta, D. *et al.* PHGDH Expression Is Required for Mitochondrial Redox Homeostasis, Breast Cancer Stem Cell Maintenance, and Lung Metastasis. *Cancer research* **76**, 4430-4442, doi:10.1158/0008-5472.can-16-0530 (2016).
52 Lee, K. E. *et al.* Hif1a Deletion Reveals Pro-Neoplastic Function of B Cells in Pancreatic Neoplasia. *Cancer discovery* **6**, 256-269, doi:10.1158/2159-8290.cd-15-0822 (2016).
53 Criscimanna, A. *et al.* PanIN-specific regulation of Wnt signaling by HIF2α during early pancreatic tumorigenesis. *Cancer research* **73**, 4781-4790, doi:10.1158/0008-5472.can-13-0566 (2013).
54 Levine, A. J. & Oren, M. The first 30 years of p53: growing ever more complex. *Nature reviews. Cancer* **9**, 749-758, doi:10.1038/nrc2723 (2009).
55 Vousden, K. H. & Ryan, K. M. p53 and metabolism. *Nature reviews. Cancer* **9**, 691-700, doi:10.1038/nrc2715 (2009).
56 Liang, Y., Liu, J. & Feng, Z. The regulation of cellular metabolism by tumor suppressor p53. *Cell & bioscience* **3**, 9, doi:10.1186/2045-3701-3-9 (2013).
57 Sablina, A. A. *et al.* The antioxidant function of the p53 tumor suppressor. *Nature medicine* **11**, 1306-1313, doi:10.1038/nm1320 (2005).
58 Bensaad, K. *et al.* TIGAR, a p53-inducible regulator of glycolysis and apoptosis. *Cell* **126**, 107-120, doi:10.1016/j.cell.2006.05.036 (2006).
59 Chen, W. *et al.* Direct interaction between Nrf2 and p21(Cip1/WAF1) upregulates the Nrf2-mediated antioxidant response. *Mol Cell* **34**, 663-673, doi:10.1016/j.molcel.2009.04.029 (2009).
60 Maddocks, O. D. *et al.* Serine starvation induces stress and p53-dependent metabolic remodelling in cancer cells. *Nature* **493**, 542-546, doi:10.1038/nature11743 (2013).
61 Jiang, P. *et al.* p53 regulates biosynthesis through direct inactivation of glucose-6-phosphate dehydrogenase. *Nature cell biology* **13**, 310-316, doi:10.1038/ncb2172 (2011).

62 Jiang, P., Du, W., Mancuso, A., Wellen, K. E. & Yang, X. Reciprocal regulation of p53 and malic enzymes modulates metabolism and senescence. *Nature* **493**, 689-693, doi:10.1038/nature11776 (2013).
63 Cheung, E. C. *et al.* Dynamic ROS Control by TIGAR Regulates the Initiation and Progression of Pancreatic Cancer. *Cancer cell* **37**, 168-182.e164, doi:10.1016/j.ccell.2019.12.012 (2020).
64 Halbrook, C. J. *et al.* Macrophage-Released Pyrimidines Inhibit Gemcitabine Therapy in Pancreatic Cancer. *Cell Metab*, doi:10.1016/j.cmet.2019.02.001 (2019).
65 Sousa, C. M. *et al.* Pancreatic stellate cells support tumour metabolism through autophagic alanine secretion. *Nature* **536**, 479-483, doi:10.1038/nature19084 (2016).
66 Dalin, S. *et al.* Deoxycytidine Release from Pancreatic Stellate Cells Promotes Gemcitabine Resistance. *Cancer research* **79**, 5723-5733, doi:10.1158/0008-5472.can-19-0960 (2019).
67 Auciello, F. R. *et al.* A Stromal Lysolipid-Autotaxin Signaling Axis Promotes Pancreatic Tumor Progression. *Cancer discovery* **9**, 617-627, doi:10.1158/2159-8290.cd-18-1212 (2019).
68 Zhang, Y. *et al.* Epithelial-Myeloid cell crosstalk regulates acinar cell plasticity and pancreatic remodeling in mice. *eLife* **6**, doi:10.7554/eLife.27388 (2017).
69 Liou, G. Y. & Storz, P. Inflammatory macrophages in pancreatic acinar cell metaplasia and initiation of pancreatic cancer. *Oncoscience* **2**, 247-251, doi:10.18632/oncoscience.151 (2015).
70 Storz, P. & Crawford, H. C. Carcinogenesis of Pancreatic Ductal Adenocarcinoma. *Gastroenterology* **158**, 2072-2081, doi:10.1053/j.gastro.2020.02.059 (2020).
71 Liou, G. Y. *et al.* Macrophage-secreted cytokines drive pancreatic acinar-to-ductal metaplasia through NF-κB and MMPs. *The Journal of cell biology* **202**, 563-577, doi:10.1083/jcb.201301001 (2013).
72 Hingorani, S. R. *et al.* Preinvasive and invasive ductal pancreatic cancer and its early detection in the mouse. *Cancer cell* **4**, 437-450, doi:10.1016/s1535-6108(03)00309-x (2003).
73 Hingorani, S. R. *et al.* Trp53R172H and KrasG12D cooperate to promote chromosomal instability and widely metastatic pancreatic ductal adenocarcinoma in mice. *Cancer cell* **7**, 469-483, doi:10.1016/j.ccr.2005.04.023 (2005).
74 Schofield, H. K. *et al.* Mutant p53R270H drives altered metabolism and increased invasion in pancreatic ductal adenocarcinoma. *JCI insight* **3**, doi:10.1172/jci.insight.97422 (2018).
75 Westphalen, C. B. & Olive, K. P. Genetically engineered mouse models of pancreatic cancer. *Cancer journal (Sudbury, Mass.)* **18**, 502-510, doi:10.1097/PPO.0b013e31827ab4c4 (2012).
76 Fearon, E. R. Molecular genetics of colorectal cancer. *Annual review of pathology* **6**, 479-507, doi:10.1146/annurev-pathol-011110-130235 (2011).
77 DeCant, B. T., Principe, D. R., Guerra, C., Pasca di Magliano, M. & Grippo, P. J. Utilizing past and present mouse systems to engineer more relevant pancreatic

cancer models. *Frontiers in physiology* **5**, 464, doi:10.3389/fphys.2014.00464 (2014).
78 Lee, A. Y. L. *et al.* Cell of origin affects tumour development and phenotype in pancreatic ductal adenocarcinoma. *Gut* **68**, 487-498, doi:10.1136/gutjnl-2017-314426 (2019).
79 Collins, M. A. *et al.* Metastatic pancreatic cancer is dependent on oncogenic Kras in mice. *PLoS One* **7**, e49707, doi:10.1371/journal.pone.0049707 (2012).
80 Schönhuber, N. *et al.* A next-generation dual-recombinase system for time- and host-specific targeting of pancreatic cancer. *Nature medicine* **20**, 1340-1347, doi:10.1038/nm.3646 (2014).
81 Zhang, Y. *et al.* Somatic Trp53 mutations differentially drive breast cancer and evolution of metastases. *Nature communications* **9**, 3953, doi:10.1038/s41467-018-06146-9 (2018).
82 Shaulsky, G., Goldfinger, N. & Rotter, V. Alterations in tumor development in vivo mediated by expression of wild type or mutant p53 proteins. *Cancer research* **51**, 5232-5237 (1991).
83 Dittmer, D. *et al.* Gain of function mutations in p53. *Nat Genet* **4**, 42-46, doi:10.1038/ng0593-42 (1993).
84 Hsiao, M. *et al.* Gain-of-function mutations of the p53 gene induce lymphohematopoietic metastatic potential and tissue invasiveness. *Am J Pathol* **145**, 702-714 (1994).
85 Stein, Y., Rotter, V. & Aloni-Grinstein, R. Gain-of-Function Mutant p53: All the Roads Lead to Tumorigenesis. *International journal of molecular sciences* **20**, doi:10.3390/ijms20246197 (2019).
86 Zhang, C. *et al.* Tumour-associated mutant p53 drives the Warburg effect. *Nature communications* **4**, 2935, doi:10.1038/ncomms3935 (2013).
87 Eriksson, M. *et al.* Effect of Mutant p53 Proteins on Glycolysis and Mitochondrial Metabolism. *Molecular and cellular biology* **37**, doi:10.1128/mcb.00328-17 (2017).
88 Freed-Pastor, W. A. *et al.* Mutant p53 disrupts mammary tissue architecture via the mevalonate pathway. *Cell* **148**, 244-258, doi:10.1016/j.cell.2011.12.017 (2012).
89 Zhou, G. *et al.* Gain-of-function mutant p53 promotes cell growth and cancer cell metabolism via inhibition of AMPK activation. *Mol Cell* **54**, 960-974, doi:10.1016/j.molcel.2014.04.024 (2014).
90 Kollareddy, M. *et al.* Regulation of nucleotide metabolism by mutant p53 contributes to its gain-of-function activities. *Nature communications* **6**, 7389, doi:10.1038/ncomms8389 (2015).
91 Rajeshkumar, N. V. *et al.* Therapeutic Targeting of the Warburg Effect in Pancreatic Cancer Relies on an Absence of p53 Function. *Cancer research* **75**, 3355-3364, doi:10.1158/0008-5472.can-15-0108 (2015).
92 Kalo, E. *et al.* Mutant p53R273H attenuates the expression of phase 2 detoxifying enzymes and promotes the survival of cells with high levels of reactive oxygen species. *Journal of cell science* **125**, 5578-5586, doi:10.1242/jcs.106815 (2012).

93 Liu, D. S. *et al.* Inhibiting the system x(C)(-)/glutathione axis selectively targets cancers with mutant-p53 accumulation. *Nature communications* **8**, 14844, doi:10.1038/ncomms14844 (2017).
94 Lisek, K., Campaner, E., Ciani, Y., Walerych, D. & Del Sal, G. Mutant p53 tunes the NRF2-dependent antioxidant response to support survival of cancer cells. *Oncotarget* **9**, 20508-20523, doi:10.18632/oncotarget.24974 (2018).
95 Walerych, D. *et al.* Proteasome machinery is instrumental in a common gain-of-function program of the p53 missense mutants in cancer. *Nature cell biology* **18**, 897-909, doi:10.1038/ncb3380 (2016).
96 Chavez-Perez, V. A., Strasberg-Rieber, M. & Rieber, M. Metabolic utilization of exogenous pyruvate by mutant p53 (R175H) human melanoma cells promotes survival under glucose depletion. *Cancer biology & therapy* **12**, 647-656, doi:10.4161/cbt.12.7.16566 (2011).
97 Tran, T. Q. *et al.* Tumor-associated mutant p53 promotes cancer cell survival upon glutamine deprivation through p21 induction. *Oncogene* **36**, 1991-2001, doi:10.1038/onc.2016.360 (2017).
98 Kamat, C. D. *et al.* Mutant p53 facilitates pro-angiogenic, hyperproliferative phenotype in response to chronic relative hypoxia. *Cancer letters* **249**, 209-219, doi:10.1016/j.canlet.2006.08.017 (2007).
99 DeNicola, G. M. *et al.* Oncogene-induced Nrf2 transcription promotes ROS detoxification and tumorigenesis. *Nature* **475**, 106-109, doi:10.1038/nature10189 (2011).
100 Rosenfeldt, M. T. *et al.* p53 status determines the role of autophagy in pancreatic tumour development. *Nature* **504**, 296-300, doi:10.1038/nature12865 (2013).
101 Yang, A. *et al.* Autophagy is critical for pancreatic tumor growth and progression in tumors with p53 alterations. *Cancer discovery* **4**, 905-913, doi:10.1158/2159-8290.cd-14-0362 (2014).
102 Morselli, E. *et al.* Mutant p53 protein localized in the cytoplasm inhibits autophagy. *Cell cycle (Georgetown, Tex.)* **7**, 3056-3061, doi:10.4161/cc.7.19.6751 (2008).
103 Neilsen, P. M. *et al.* Mutant p53 drives invasion in breast tumors through up-regulation of miR-155. *Oncogene* **32**, 2992-3000, doi:10.1038/onc.2012.305 (2013).
104 Scian, M. J. *et al.* Tumor-derived p53 mutants induce NF-kappaB2 gene expression. *Molecular and cellular biology* **25**, 10097-10110, doi:10.1128/mcb.25.22.10097-10110.2005 (2005).
105 Weisz, L. *et al.* Mutant p53 enhances nuclear factor kappaB activation by tumor necrosis factor alpha in cancer cells. *Cancer research* **67**, 2396-2401, doi:10.1158/0008-5472.can-06-2425 (2007).
106 Kremer, D. M. *et al.* GOT1 Inhibition Primes Pancreatic Cancer for Ferroptosis through the Autophagic Release of Labile Iron. *bioRxiv*, 2020.2002.2028.970228, doi:10.1101/2020.02.28.970228 (2020).
107 Anglin, J. *et al.* Discovery and optimization of aspartate aminotransferase 1 inhibitors to target redox balance in pancreatic ductal adenocarcinoma. *Bioorganic & medicinal chemistry letters* **28**, 2675-2678, doi:10.1016/j.bmcl.2018.04.061 (2018).

108 Holt, M. C. *et al.* Biochemical Characterization and Structure-Based Mutational Analysis Provide Insight into the Binding and Mechanism of Action of Novel Aspartate Aminotransferase Inhibitors. *Biochemistry* **57**, 6604-6614, doi:10.1021/acs.biochem.8b00914 (2018).
109 Yoshida, T. *et al.* A covalent small molecule inhibitor of glutamate-oxaloacetate transaminase 1 impairs pancreatic cancer growth. *Biochemical and biophysical research communications* **522**, 633-638, doi:10.1016/j.bbrc.2019.11.130 (2020).
110 Shi, C. *et al.* KRAS2 mutations in human pancreatic acinar-ductal metaplastic lesions are limited to those with PanIN: implications for the human pancreatic cancer cell of origin. *Molecular cancer research : MCR* **7**, 230-236, doi:10.1158/1541-7786.mcr-08-0206 (2009).
111 Cox, A. D., Fesik, S. W., Kimmelman, A. C., Luo, J. & Der, C. J. Drugging the undruggable RAS: Mission possible? *Nature reviews. Drug discovery* **13**, 828-851, doi:10.1038/nrd4389 (2014).
112 Kempf, E., Rousseau, B., Besse, B. & Paz-Ares, L. KRAS oncogene in lung cancer: focus on molecularly driven clinical trials. *European respiratory review : an official journal of the European Respiratory Society* **25**, 71-76, doi:10.1183/16000617.0071-2015 (2016).
113 Bryant, K. L. & Der, C. J. Blocking autophagy to starve pancreatic cancer. *Nature reviews. Molecular cell biology* **20**, 265, doi:10.1038/s41580-019-0120-8 (2019).
114 Badiyan, S. N., Molitoris, J. K., Chuong, M. D., Regine, W. F. & Kaiser, A. The Role of Radiation Therapy for Pancreatic Cancer in the Adjuvant and Neoadjuvant Settings. *Surgical oncology clinics of North America* **26**, 431-453, doi:10.1016/j.soc.2017.01.012 (2017).

Appendix: Author Contributions

CHAPTER 2

Barbara S. Nelson[1], Christopher J. Halbrook[1], Howard C. Crawford[1,2,3], Costas A. Lyssiotis[1,2,3]

[1]Department of Molecular and Integrative Physiology, University of Michigan Medical School, Ann Arbor, MI, USA 48109
[2]Rogel Cancer Center, University of Michigan Medical School, Ann Arbor, MI, USA 48109
[3]Department of Internal Medicine, Division of Gastroenterology and Hepatology, University of Michigan Medical School, Ann Arbor, MI, USA 48109

CHAPTER 3

Barbara S. Nelson[1,*], Lin Lin[1,*], Daniel M. Kremer[1], Cristovão M. Sousa[2,#], Cecilia Cotta-Ramusino[3], Amy Myers[1], Johanna Ramos[1], Tina Gao[1], Ilya Kovalenko[1], Kari Wilder-Romans[4], Joseph Dresser[4], Mary Davis[4], Ho-Joon Lee[1], Zeribe C. Nwosu[1], Scott Campit[5], Oksana Mashadova[6], Brandon N. Nicolay[7], Zachary P. Tolstyka[1], Christopher J. Halbrook[1], Sriram Chandrasekaran[5,9,10], John M. Asara[8], Howard C. Crawford[1,10,11], Lewis C. Cantley[6], Alec C. Kimmelman[2,12], Daniel R. Wahl[4,10], Costas A. Lyssiotis[1,10,11]

[1]Department of Molecular and Integrative Physiology, University of Michigan Medical School, Ann Arbor, MI, USA 48109
[2]Division of Genomic Stability and DNA Repair, Department of Radiation Oncology, Dana-Farber Cancer Institute, Harvard Medical School, Boston, MA, USA 02215
[3]Experimental Therapeutics Core and Belfer Center for Applied Cancer Science, Dana-Farber Cancer Institute, Harvard Medical School, Boston, MA, USA 02215
[4]Department of Radiation Oncology, University of Michigan Medical School, Ann Arbor, MI, USA 48109
[5]Department of Biomedical Engineering, University of Michigan Medical School, Ann Arbor, MI, USA 48109
[6]Meyer Cancer Center, Weill Cornell Medicine, New York City, NY, USA 10065
[7]Agios Pharmaceuticals, Inc, Cambridge, MA, USA 02139
[8]Beth Israel Deaconess Medical Center and Harvard Medical School, Boston, MA, USA 02115
[9]Center for Computational Medicine and Bioinformatics, University of Michigan Medical School, Ann Arbor, MI, USA 48109
[10]Rogel Cancer Center, University of Michigan Medical School, Ann Arbor, MI, USA 48109
[11]Department of Internal Medicine, Division of Gastroenterology and Hepatology, University of Michigan Medical School, Ann Arbor, MI, USA 48109
[12]Department of Radiation Oncology, Perlmutter Cancer Center, NYU Langone Medical Center, New York, NY 10016
*equal contribution
[#]current address, Agios Pharmaceuticals, Inc, Cambridge, MA, USA 02139